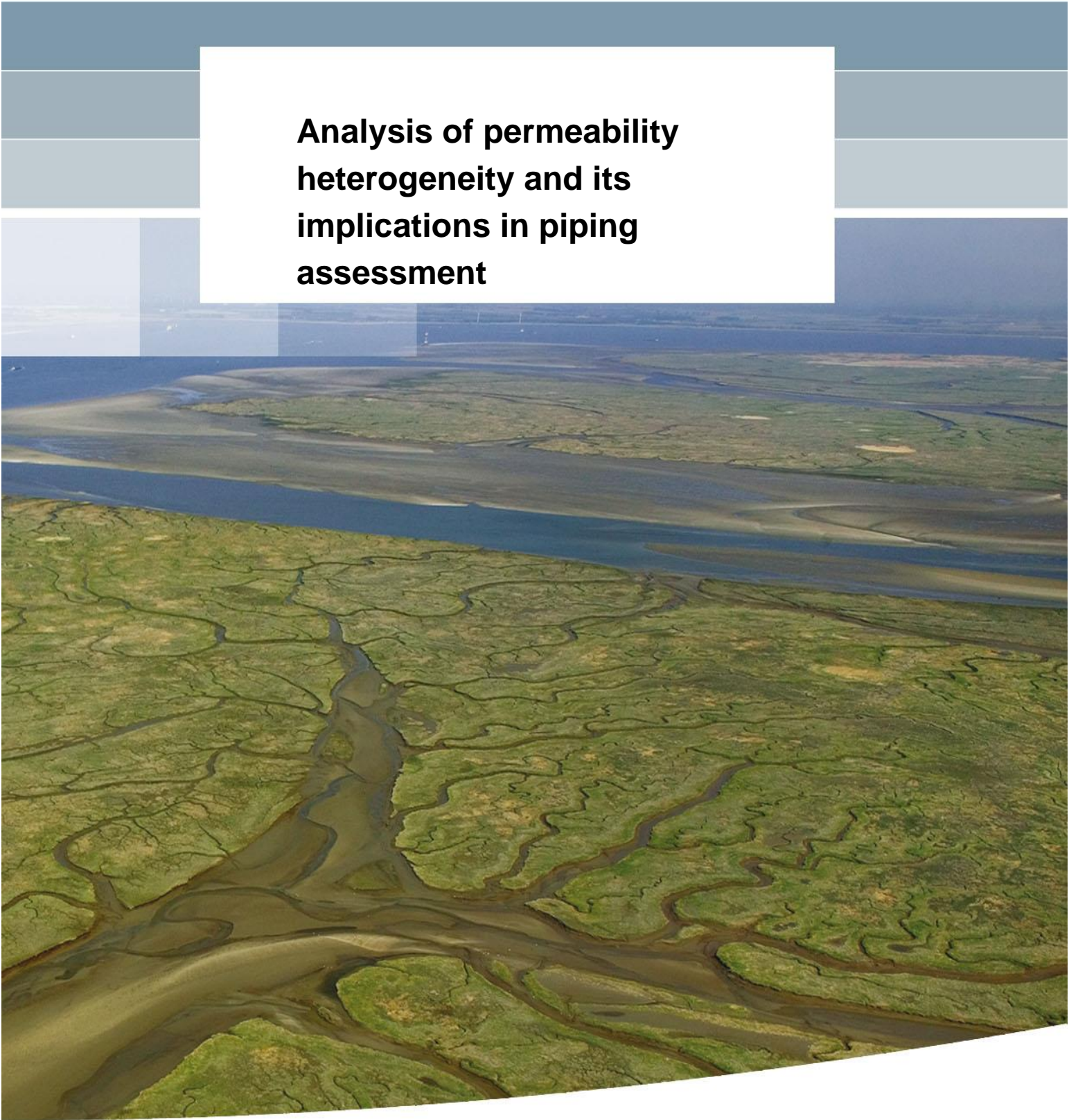


**Analysis of permeability  
heterogeneity and its  
implications in piping  
assessment**





**Analysis of permeability  
heterogeneity and its implications  
in piping assessment**

PoV Piping HPT

Maximilian Huber  
Mark van der Krogt

1209637-000



**Title**

Analysis of permeability heterogeneity and its implications in piping assessment

Client	Project	Reference	Pages
Waterschap Aa en Maas	1209637-000	1209637-000-GEO-0008- m	36

**Keywords**

Piping, HPT sonde, sampling theory, probabilistic analysis, spatial correlation, piping safety assessment

**Summary**

Piping is an important failure mechanism of dikes, in which water flows under the dike result in erosion and failure if this erosion occurs sufficiently long. Measures against this failure mechanism are relatively expensive using traditional measures such as construction of berms. Moreover, the piping mechanism is surrounded by many uncertainties; e.g. with respect to subsoil conditions.

Within the "POV Piping HPT" project, the partners (Waterboard Aa en Maas, Fugro and Deltares) investigated subsoil permeability using different methods in combination with the Hydraulic Profiling Tool (HPT). This report provides a statistical data analysis of permeability measurements. Using a large number of test results, statistical methods are employed to quantify the uncertainty of the permeability measurements. Moreover, a framework for the quantification of spatial correlation between permeability measurements is developed and used for the analysis of the measurements. Additionally, these findings are translated to piping safety assessment considering the spatial variability within the semi-probabilistic approach.

From the results it can be concluded that the scaling of the permeability measurements, i.e. the larger the affected soil volume, the larger the conductivity seems to be, is a valuable step in order to estimate the permeability of the aquifer. The Maximum Likelihood method can be employed as versatile tool for the quantification of the horizontal correlation length of the aquifer permeability. The resulting estimated horizontal correlation lengths are in the order of 10 m to 680 m, but also show high variability.

The correlation lengths derived from the different permeability measurements are used within a local averaging approach in a framework for piping safety assessment. It can be seen that the additional required berm lengths are significantly reduced by taking the measured spatial correlation into account. However, the uncertainty in the estimate of the correlation length is very high, which makes firm conclusions from this study impossible. Nevertheless, this study shows the importance of the scale effect, and gives a to be validated example of the concept of averaging measurement data due to heterogeneity in the piping safety assessment.

Version	Date	Author	Initials	Review	Initials	Approval	Initials
2	Oct. 2015	Dr.-Ing. M. Huber ir. M. van der Krogt		Dr.ir. W. Kanning		Dr.ir. M. Sule	
3	Jan. 2016	Dr.-Ing. M. Huber ir. M. van der Krogt		Dr.ir. W. Kanning		Dr.ir. M. Sule	

**State**  
final

**Title**

Analysis of permeability heterogeneity and its implications in piping assessment

**Client**

Waterschap Aa en Maas

**Project**

1209637-000

**Reference**

1209637-000-GEO-0008-  
m

**Pages**

36

## Contents

<b>1</b>	<b>Introduction</b>	<b>3</b>
1.1	Scope of the project	3
1.2	Goal of this report	4
1.3	Structure of the report	4
<b>2</b>	<b>Statistical analysis of the permeability measurement methods used in this project</b>	<b>5</b>
2.1	Introduction	5
2.2	Statistical analysis	6
2.3	Parameter selection from the measurement results	7
<b>3</b>	<b>Quantification of spatially correlated field data</b>	<b>11</b>
3.1	Scales of spatial correlation	11
3.2	Methods for the quantifying spatial correlation	12
3.3	Sampling theory	13
3.3.1	Introduction	13
3.3.2	Description of the sampling design in this case	14
3.4	Horizontal spatial correlation of the permeability	14
3.5	Vertical spatial correlation of the permeability	16
3.6	Summary	18
<b>4</b>	<b>Quantifying the effects of spatially correlated permeability</b>	<b>19</b>
4.1	Introduction	19
4.2	Theoretical background on spatial averaging	19
4.3	Consideration of the horizontal correlation length in the semi-probabilistic piping safety assessment	20
4.4	Piping safety assessment	21
4.4.1	Variables	21
4.4.2	Semi-probabilistic assessment	22
4.4.3	Interpretation of the results	24
4.4.4	Sensitivity study on the influence of the uncertainty of the horizontal correlation length	25
4.5	Bayesian Updating of the VNK-dataset with the measurement values	26
<b>5</b>	<b>Summary and recommendations</b>	<b>29</b>
<b>6</b>	<b>References</b>	<b>33</b>
<b>Appendices</b>		
<b>A</b>	<b>Introduction to statistics</b>	<b>A-1</b>
A.1	Moments of a distribution function	A-1
A.2	Distribution functions	A-1
A.2.1	Normal distribution function	A-2
A.2.2	Lognormal distribution function	A-2
A.3	Multivariate normal distribution	A-3

<b>B Mathematical description of spatial correlation</b>	<b>B-1</b>
B.1 Introduction	B-1
B.2 Variogram approach	B-2
B.2.1 Variogram calculation	B-2
B.2.2 Theoretical variogram	B-4
B.2.3 Model selection using the AKAIKE Information criterion	B-5
B.3 Maximum likelihood method	B-6
B.4 On the correlation length	B-7
B.5 Uncertainty of the correlation length	B-8
B.6 Anisotropy of the correlation length	B-8
<b>C Theoretical background on the evaluation of the vertical spatial correlation</b>	<b>C-1</b>
C.1 Intra-class correlation coefficient	C-2
C.2 Bartlett statistics	C-2
C.3 Comparison of the intra-class correlation coefficient and the Bartlett statistics	C-3
C.4 Bayesian model averaging	C-3
<b>D Sampling plans</b>	<b>D-1</b>
D.1 Introduction	D-1
D.2 Common spatial sampling plans	D-1
<b>E Statistical properties and correlation length of the permeability measurements</b>	<b>E-1</b>
E.1 Introduction	E-1
E.2 Empirical correlations from 20 sieve curves	E-1
E.3 HPT results	E-4
E.4 MPT	E-7
E.5 Dissipation test	E-9
E.6 Slugtests	E-11
E.7 Falling Head Test	E-13
<b>F Background on Piping</b>	<b>F-1</b>
<b>G Bayesian evaluation procedure for characteristic values</b>	<b>G-1</b>
G.1 Calculation of the characteristic values for normal and lognormal distributed data	G-1
G.1.1 Variables with Normal distribution	G-1
G.1.2 Variables with Log-normal distribution	G-1
G.2 Theoretical background on Bayesian updating	G-1
G.3 Calculation of the characteristic values using Bayesian Updating	G-2
<b>H Extract Handreiking ontwerpen met overstromingskansen</b>	<b>H-1</b>

# 1 Introduction

Groundwater flow is the driving force behind the process that can lead to piping and thus to instability of a dike. The permeability of piping sensitive sand layers is an important parameter in the detailed safety assessment of dikes on piping. In current practice, the permeability of these layers is determined on the basis of grain distributions and/ or a number of in-situ permeability measurements in the sand layer. In this manner, the calculated permeability strongly depends on the used methods and formulas, which offer limited insight into the permeability of the entire water-bearing (sand) layer.

To evaluate the risk of piping better, it is important to get insight in the variation of the permeability in the piping sensitive layer. Together with the thickness of the sand layer this determines the ability to let water through. It is difficult and costly task to evaluate the representative permeability of an aquifer due to several reasons: the heterogeneity of the subsoil, the limitations of current measurement techniques and the high costs for the conduction of permeability measurements and thus the limited amount of measurements.

The cooperating partners (Waterboard Aa en Maas, Fugro and Deltares) investigated the subsoil permeability using different methods in combination with the Hydraulic Profiling Tool (HPT). This HPT-cone penetration was developed for the field environment in order to determine a continuous profile of the in-situ permeability. The application of this technique provides in-depth understanding of the permeability and structure of the soil. This may contribute to a more cost-efficient and better schematization (less uncertainty) of permeability in the piping safety assessment.

In order to be able to make a comparison between HPT and more commonly used methods, the following methods will be used to determine the permeability of the piping sensitive sand layer for a specific case study:

- Empirical correlations of the permeability derived from sieve curves.
- Slug tests.
- HPT test.
- MPT test.
- Permeability determination in laboratory (constant head tests).
- Data available in DINO / REGIS.
- Correlations based on soil description and literature.

Given the relatively high cost and potential impact on the environment, conducting a pumping test is not part of the investigations.

## 1.1 Scope of the project

This pilot project roughly consists of three basic steps namely site selection, data collection and data analysis, which is carried out by Fugro in collaboration with Deltares and Waterboard Aa en Maas. After selecting a suitable dike section, Deltares developed the sampling scheme in order to analyze the spatial variability of the permeability considering prior knowledge of a literature study. The second step of the data collection is performed by Fugro, which consists of performing HPT tests, collecting available information on the expected permeability (including information on the permeability based DINO / REGIS and literature). Then there are analyses of the grain size distributions of the aquifer and slug tests in boreholes performed. Additionally, permeability measurements and classification tests in

laboratory are carried out. Next to these investigations, the HPT technology is used in order to set up a correlation between the various test methods.

This report describes how to use these results in a detailed analysis of the heterogeneity, using different geostatistical and statistical approaches. This helps to translate the HPT measurements into a representative permeability for a piping assessment.

The next two work packages are performed by Deltares and are described in this report.

- **Analysis of heterogeneity effects:** The purpose of the heterogeneity analysis is to translate permeability measurements to a (for piping) representative permeability. In these analyses uncertainty and spatial variability play an important role.
- **Influence on the schematization and flood safety assessment regarding piping:** This analysis quantifies the effects of considering the spatial uncertainty of subsoil permeability on the assessment of the risk of piping. The assessments are carried out at a detailed level using existing and the new piping rule Sellmeijer (2011). Herein, only the permeability of the sand pack as a parameter is varied.

## 1.2 Goal of this report

The goal of this report is to investigate the heterogeneity of the subsoil permeability based on various test methods for the permeability, compare the methods, and investigate how these findings can be translated to piping safety assessment.

## 1.3 Structure of the report

The structure of this report is as follows. First, it is focussed on the statistical analysis of the permeability measurement. The next chapter is on the quantification of spatial correlation of permeability measurements, including a brief explanation of the methods for quantifying the correlation length, the explanation of the sampling concept and the results for the vertical and horizontal correlation of the permeability. The next chapter covers the quantification of the effects of spatially correlated permeability measurements in the safety assessment regarding piping failure using semi-probabilistic and probabilistic methods. This report ends with a summary and conclusions.

## 2 Statistical analysis of the permeability measurement methods used in this project

### 2.1 Introduction

In this report the following different permeability measurement methods are used, which are described in detail in the report of Fugro [25].

For the sake of completeness, we briefly state the difference in the hydraulic conductivity and the intrinsic permeability. Within this report we only investigate the hydraulic conductivity referred to as permeability in this document. The anisotropy of the permeability is not in the focus of the sequel investigations.

- Empirical correlations of the permeability derived from sieving curves
  - Den Rooijen.
  - Ernst.
  - Hazen.
  - Kozeny-Carman.
  - Seelheim.
  - Seelheim (2).
- Slug tests in mechanical borings
  - Bouwer-Rice lijn 1&3.
  - Hvorslev.
- HPT test
 

HPT stands for hydraulic profiling tool (HPT) and is based on a cone penetration test, which allows determine a continuous profile of the in-situ permeability. The relation of injected water ( $Q$ ) during the penetration process of the HPT sonde and the pressure  $P$  are measured. The ratio of  $Q$  and  $P$  gives a measure of the permeability and the permeability differences. Fugro [25] derive a site specific transformation, in which  $C$  is given as  $C_{hpt}=0.46$  for the top aquifer layer at the investigated site. This site specific, empirical relation in equation (0.1) is used to derive for each HPT test the permeability profile, from which the top and bottom is visually identified and used for the calculation of the corresponding mean value and standard deviation as described in Appendix E.3. Note that the mean value of each profile is interpreted as representative values for each HPT measurement, which are used for the analysis of the spatial correlation.

$$k = \frac{1}{C_{hpt}} \frac{Q}{P} \quad (0.1)$$

Note that the HPT tests and the corresponding relation in equation (0.1) results are made in a geologically coarse grained formation, which is not necessarily applicable in fine grained sediments. This site specific, empirical relation is not fully clear and asks for more investigation to underpin the outcomes.

- MPT tests:
 

MPT stands for mini-pumping test. It is the same principal as a pumping test, for which the HPT tool is used. A detailed description can be found in the report of Fugro [25].

2.2 Statistical analysis

All of the above described methods are statistically analysed. The values for permeability are plotted in histograms. The best fit for the lognormal distribution for four common methods (Hvorslev, Bouwer&Rice1, Hazen, Den Rooijen) is plotted by a red line, see Figure 2.1. The results for the HPT are shown in Figure 2.2. The mean value and standard deviations for four common methods (Hvorslev, Bouwer&Rice1, Hazen, Den Rooijen) are shown in the Figure 2.1. The mean values and standard deviations of the permeability measurements show a big spread for the employed testing methods. The reasons for this are probably the test procedures and the limited size of the tested soil volume. The explanation of differences and background on the measurement results can be found in the corresponding report by Fugro [25]]. The results of all analyses are given in Appendix E.

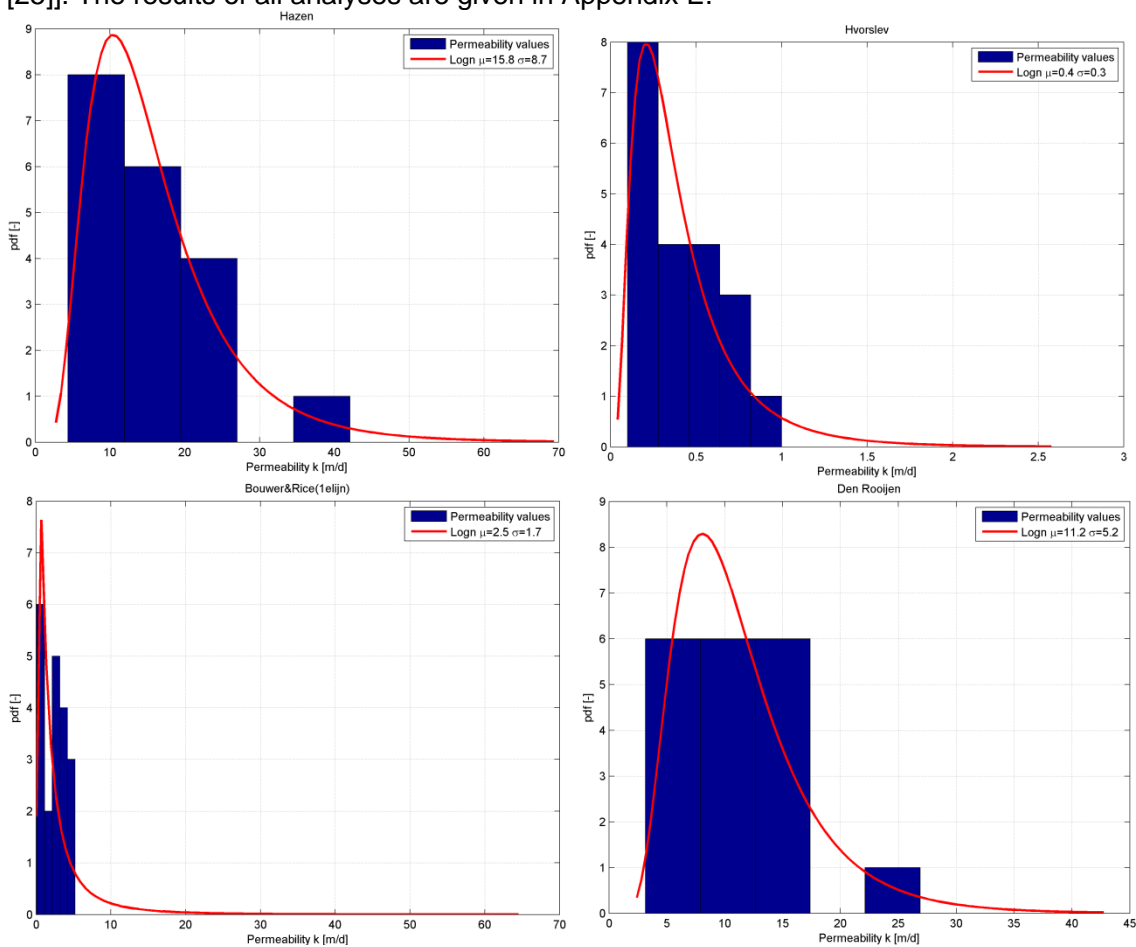


Figure 2.1 Histograms and fitted lognormal distribution for four common methods to determine permeability

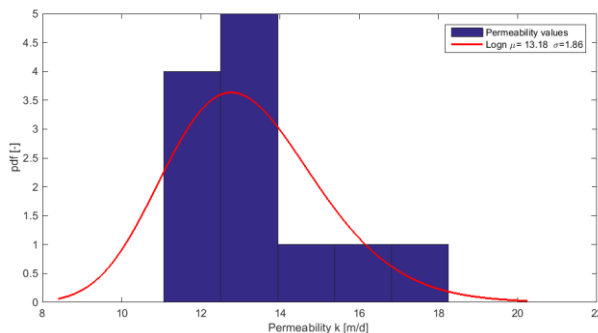


Figure 2.2 Histograms and fitted lognormal distribution for the HPT permeability values

### 2.3 Parameter selection from the measurement results

When selecting the parameters from the measurement results, one has to consider the different testing conditions of the measurement methods.

It is assumed that the soil volume, which is being tested by the different methods, is one of the main sources for the different permeability measurement results. Therefore, the measurement values have to be scaled to the same level. Fugro [25] proposes a scaling approach from [57], which is used to scale the measurement values. This approach is given in Figure 2.3. One can see that it is assumed that the permeability values of measurement methods, using only a small soil volume, results in a smaller permeability value than tests using a bigger soil volume. It can be also seen that the REGIS results are being influenced by a very large soil volume. This is logical because the values of REGIS are derived from pumping test and expert judgement.

The derived relationship between the soil volume and the permeability can be described in equation (0.2).

$$k = \begin{cases} k_p \left( \frac{V_R}{V_p} \right)^m & \text{for } V_p \leq V_R \\ k_p & \text{for } V_p > V_R \end{cases} \quad (0.2)$$

Herein, the permeability  $k$  is describing the reference volume  $V_R$ , and  $k_p$  is describing the measurement volume  $V_p$ . This correlation has been derived by Fugro [25] and is underpinned by published approaches [57]. Fugro derived the [25] the exponent  $m$  by fitting  $m = 2.31$ .

Using this empirical scaling relation, one implicitly assumes that the differences of the permeability measurement relates mainly on the soil volume being tested. If the volume is small (like case of the falling head test in the laboratory), the measured permeability is smaller compared to a method (e.g. a large scale pumping test), which is measuring a larger volume of soil. This can be related to the presence of heterogeneous parts with a higher permeability. Note that this used upscaling approach is an empirical relation between the permeability and the measured soil volume. It is not clear how this upscaling approach [25] is influencing the uncertainty of the upscaled permeability values.

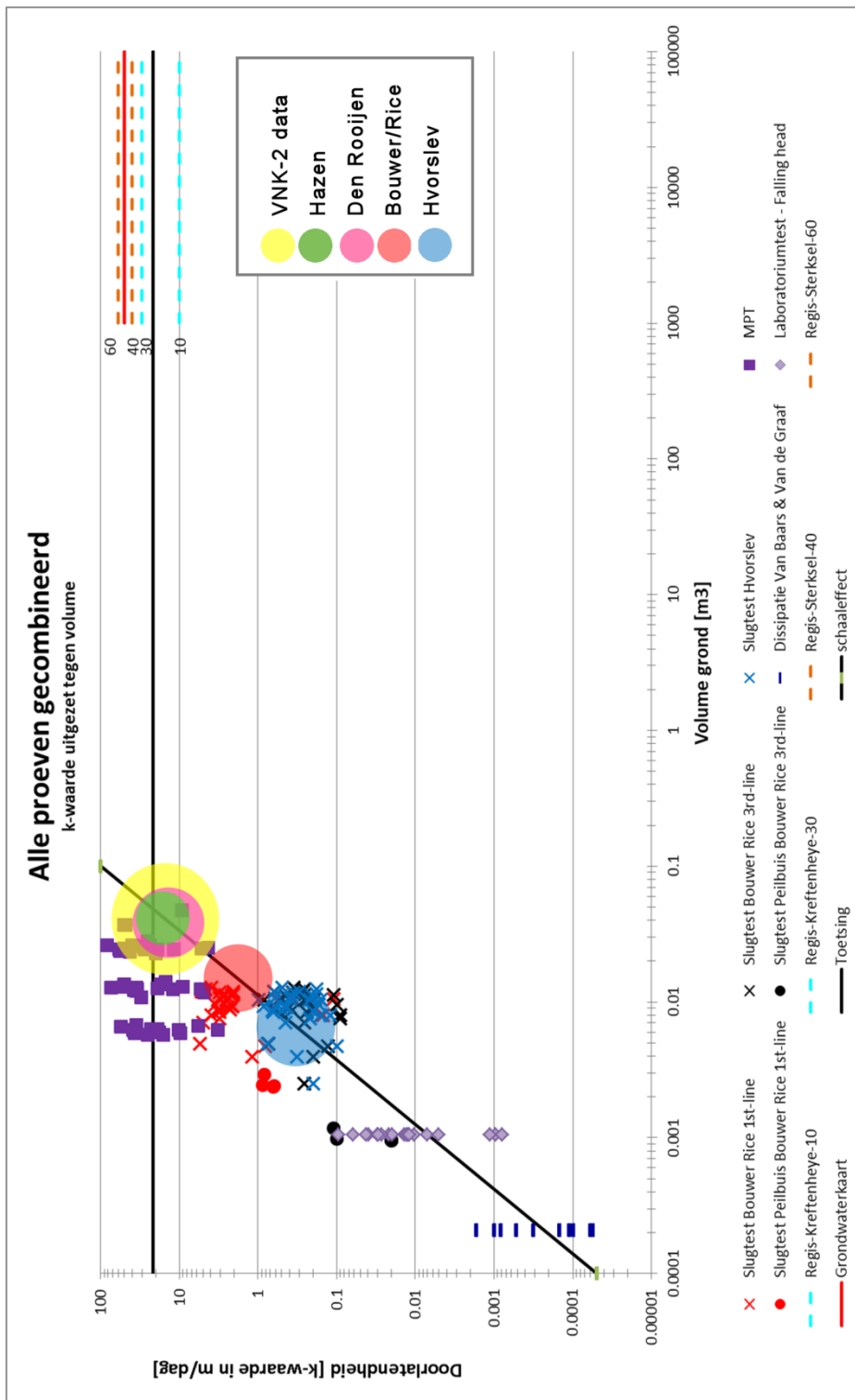


Figure 2.3 Permeability (vertical axis) related to the volume of soil (horizontal axis) for each method from Fugro [25]

Table 2.1 provides a summary of the measurement results including mean value, standard deviation and measurement volume  $V_p$ . The scaling rule described above is used to scale the measurement data and to derive from this the corresponding mean value and standard deviation, which are referring to the reference volume  $V_R$ .

Table 2.1. Raw measurement data and scaled permeability

	Number of tests	raw data			$V_p$	scaled permeabilities			$V_R$
		$\mu_{raw}$	$\sigma_{raw}$	COV	volume being tested	$\mu_{scaled}$	$\sigma_{scaled}$	COV	Reference volume being scaled up to
		[m/day]	[m/day]	[%]	$m^3$	[m/day]	[m/day]	[%]	$m^3$
<b>falling head test</b>	20	0.0228	0.0231	101%	0.0015	15.5	15.7	101%	1000
<b>Bouwer Rice 3 lijn</b>	20	0.3	0.2	67%	0.015	12.3	8.7	71%	1000
<b>Bouwer Rice 1 lijn</b>	20	2.5	1.7	67%	0.015	97.3	71.5	73%	1000
<b>Hvorslev</b>	20	0.4	0.3	64%	0.015	15.9	11.3	71%	1000
<b>Den Rooijen</b>	20	11.2	5.2	47%	1000	11.2	5.2	47%	1000
<b>Ernst</b>	20	21.5	10	47%	1000	21.5	10	47%	1000
<b>Hazen</b>	20	15.8	8.7	55%	1000	15.8	8.7	55%	1000
<b>Kozeny-Carman</b>	20	1.3	0.4	31%	1000	1.3	0.4	31%	1000
<b>Seelheim</b>	20	16.5	6.1	37%	1000	16.5	6.1	37%	1000
<b>Seelheim2</b>	20	18.8	8.4	45%	1000	18.8	8.4	45%	1000
<b>Parez Fauriel *</b>	6	0.1	0.1	116%	0.0002	(4168)*	(4170)*		1000
<b>VanBaars VanDeGraaf *</b>	6	0.01	0.1	116%	0.0002	(417)*	(417)*		1000
<b>MPT - Meetreeks1</b>	19	29.8	19.3	65%	0.02	29.8	19.3	65%	1000
<b>MPT - Meetreeks2</b>	19	30	20.1	67%	0.02	30.0	20.1	67%	1000
<b>MPT - Meetreeks3</b>	19	29.6	17.3	59%	0.02	29.6	17.3	59%	1000
<b>HPT data</b>	12	13.18	1.86	14%	1000	13.18	1.86	14%	1000

\* These test results are significantly (bigger than a factor of 100!) lower than the other results of the permeability measurements.



### 3 Quantification of spatially correlated field data

The measurement data of the permeability given in section 2.1 (are obtained by FUGRO [30]. It is described in detail in the corresponding report [30] how the different measurements are carried out and how the permeability is derived from the results. In this chapter the results of this are analysed with respect to their spatial correlation.

At first, a brief introduction to spatial correlation including a description and explanation of the sampling scheme is provided. Then, the workflow for evaluating the vertical and horizontal correlation length of the permeability is explained.

#### 3.1 Scales of spatial correlation

Many scientists have investigated the spatial variability of soil properties in different fields ranging from hydrology, soil sciences, reservoir engineering up to geotechnical engineering.

It can be clearly seen in Figure 3.1 that there are different scales of variability, ranging from the micro level at the grain size scale to the geological scale of several tens and hundreds of meters. In this context, heterogeneity can be defined as the opposite of homogeneity and is further used as a synonym of spatial variability. The geotechnical level is between the specimen scale and the geological scale; therefore, it is important to keep in mind that there is not a single spatial scale, but multiple spatial scales contributing to soil variability. Of course, this plays a role in the evaluation of spatial variability of soil properties as well in the evaluation of the effects of soil variability.

The visualisation of spatial correlation in horizontal ( $\theta_h$ ) and vertical direction ( $\theta_v$ ) are shown in Figure 3.2 for no spatial correlation ( $\theta_h, \theta_v \gg \lambda$ ), an isotropic correlation  $\theta_h = \theta_v$  and anisotropic correlation structure ( $\theta_h > \theta_v$ ).

Within a piping safety assessment, one distinguishes between primary piping erosion and secondary piping erosion. Simplified speaking, primary piping erosion process describes the starting of the piping erosion process, which is not covered by the Sellmeijer formulas (2006 and 2011); secondary piping erosion is the erosion process in a given pipe, which is described by the Sellmeijer formulas (2006 and 2011). Small scale heterogeneity effects in permeability have less effect for secondary piping erosion process because the total flow that enters the pipe is the main driving force in the Sellmeijer method. Therefore, one is interested in the aquifer permeability, with dimension and spatial correlation ranging from  $\theta_h = 10$  to 100 m in the horizontal direction within a piping safety assessment. Using the Sellmeijer formulas (2006 and 2011), large scales ( $\theta_h > 100$  m) and the vertical spatial correlation of the permeability is captured via a schematisation into different layers and therefore not considered.

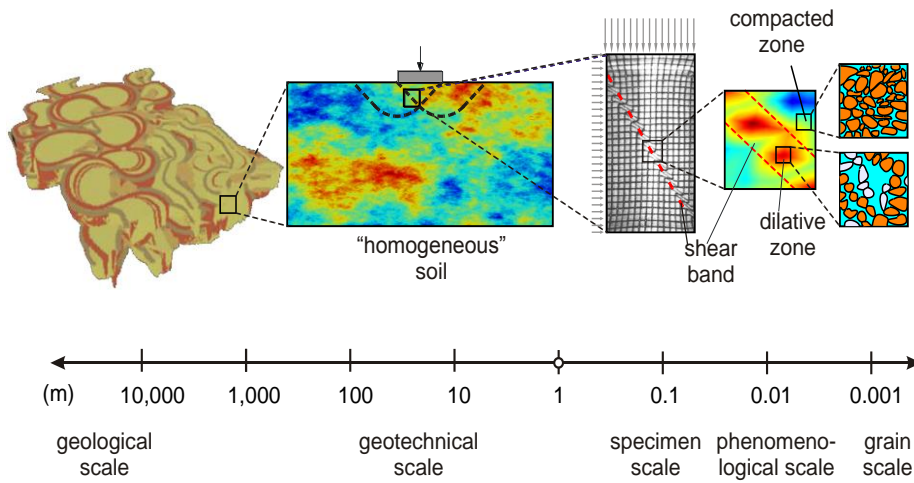


Figure 3.1 Illustration of the multi-scale nature of soil after Huber [34]

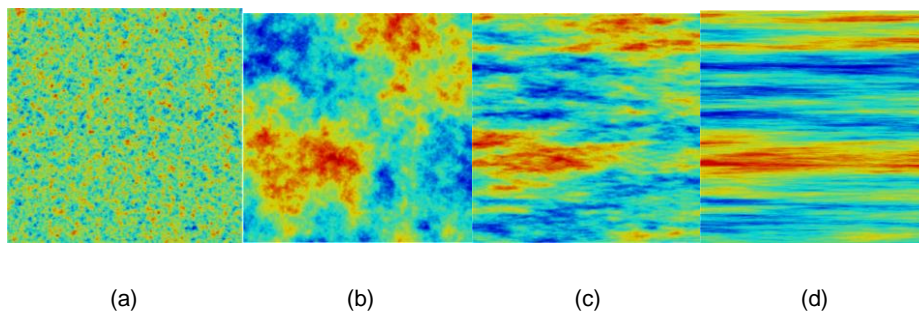


Figure 3.2 Examples for a very small (a), an isotropic (b), an anisotropic (c) and a strong anisotropic correlation structure (d)

### 3.2 Methods for the quantifying spatial correlation

The spatial correlation of e.g. measurements can be mathematically described by means of geostatistics. Herein, one uses the mean value, the standard deviation and the correlation length to describe the spatial variability of e.g. measurement data. The correlation length is a measure to quantify the spatial dependence. The correlation length can be evaluated by various methods, of which two are applied in this study (variogram methodology and maximum likelihood method), which are given in the Appendix B including their mathematical background.

The *variogram methodology* is a robust approach to quantify the correlation length. As derived in detail in Appendix B.2, the variogram  $\gamma(\tau)$  of a random function  $Z(X)$  can be computed using equation (0.3). The lag vector  $\tau$  is generally a vector describing the mutual distance between the points and  $m(\tau)$  is the number of points for a given mutual distance  $\tau$ .

$$\hat{\gamma}(\tau) \equiv \frac{1}{2} E \left[ (Z(\mathbf{X}) - Z(\mathbf{X} + \tau))^2 \right] \approx \frac{1}{2 m(\tau)} \sum_{i=1}^{m(\tau)} (Z(\mathbf{X}_i) - Z(\mathbf{X}_i + \tau))^2 \quad (0.3)$$

The variogram does not require the knowledge of the mean of the random function  $Z(X)$  because the squared difference in equation (0.3) eliminates the mean value. The variogram approach is a robust approach to quantify the spatial correlation. Due to its simple mathematical definition it is also easy to apply it to measurement data without big

programming effort. The variogram approach needs more or less equally spaced measurement data. In case of arbitrary or random samples this approach gives limited results.

The *Maximum Likelihood method* (ML) of estimating the unknown autocorrelation parameter  $\Theta$  is a parametric method assuming that the distribution of the data is known. ML takes the value of  $\Theta$  as an estimate of the unknown parameters  $\Theta$  that provides the greatest probability of having measurements  $Z$ , as calculated from the joint probability distribution of the observations conditioned on  $\Theta$ . The possible outcomes  $z(X)$  of the random function  $Z(X)$  with mean value  $\bar{Z}$  and covariance matrix  $\mathbf{C}_{ZZ}$  are assumed to be described by a  $n$ -dimensional multivariate normal distribution in equation (0.3).

$$f_z(\mathbf{z}) = \frac{1}{\sqrt{(2\pi)^n |\mathbf{C}_{ZZ}|}} \exp\left[-\frac{1}{2}(\mathbf{z} - \bar{Z})^T \mathbf{C}_{ZZ}^{-1} (\mathbf{z} - \bar{Z})\right] \quad (0.3)$$

The covariance matrix  $\mathbf{C}_{ZZ}$  contains the values of the auto-covariance function  $C(\mathbf{Z}_i, \mathbf{Z}_j)$  of each possible pair of measurements. Selecting the unknown parameters in a vector  $\Theta = [\bar{Z}, \sigma_r, \theta_h, \theta_v]^T$  the log-likelihood for  $\Theta$  is given in equation (0.3).

$$L(\Theta | \mathbf{z}) = -\frac{n}{2} \ln(2\pi) - \frac{1}{2} \ln |\mathbf{C}_{ZZ}| - \frac{1}{2} (\mathbf{z} - \bar{Z})^T \mathbf{C}_{ZZ}^{-1} (\mathbf{z} - \bar{Z}) \quad (0.3)$$

By maximizing the likelihood, the optimal parameter set  $\Theta$  can be obtained by standard optimization strategies, for example the simplex method. The advantage of the simplex algorithm is that the results are independent of the initial parameters, hence only depending on data.

The ML method is also a robust approach in estimating the mean value, standard deviation and spatial correlation at once. Moreover, it is not dependent on the sampling scheme as the variogram approach. Therefore, it is well suited for the nested sampling plan, as described in the sequel.

### 3.3 Sampling theory

#### 3.3.1 Introduction

If one evaluates the spatial correlation, one has to have an idea of the spatial variability in order to set up the design of experiments. If the grid of experiments is larger than the spatial correlation, the variogram methodology does not detect a spatial correlation. This drawback can be overcome by using the Maximum Likelihood method (ML). ML is a robust method, which can be employed to analyse the spatial correlation of arbitrary distributed variables. Via this, it is possible to analyse also nested or clustered data, which is favourable for the investigation of multiple scales of spatial variability. This also enables one to analyse the spatial correlation without knowing its quantity on beforehand. However, even though ML will give results, if the grid spacing is larger than the spatial correlation, the uncertainty around the estimate will be very large and results are less usable.

According to Baecher & Christian [4], a sampling plan is a program of action for collecting data from a sampled population. Common plans are grouped into many types: for example,

simple random, systematic, stratified random, cluster, traverse, line intersects, and so on as summarized in Appendix D.2.

The purpose of sampling is to obtain estimates of population parameters (e.g. mean value, standard deviation and correlation length). Without knowing the spatial correlation of measurement values beforehand, it is very difficult to design a sampling plan. If the sampling distance is too small, big correlation lengths will not be captured and vice versa. Therefore, we selected the nested sampling strategy in combination with the Maximum Likelihood method, as described in detail in Appendix B.3. This enables the identification of spatial correlation at multiple scales.

### 3.3.2 Description of the sampling design in this case

Within this project, a nested sampling plan is designed. Herein, the soil investigations have different distance classes ranging from few meters to more several hundreds of meters. The mutual distances are chosen in a simple way, following an arithmetic sequence of numbers using the following recursive definition.

$$((n-1) \cdot 2) \approx 2, 4, \dots \quad (0.3)$$

Starting from a mutual distance of 2 m, the spacing is doubled. By employing this strategy, one can estimate the horizontal spatial variability efficiently. One has to be aware that this sampling scheme is influencing the results significantly. If the sampling scheme is too coarse, the derived correlation will be too big, if the sampling is too small, the larger spatial correlation might be overseen.

In Figure 3.3 *HPT* stands for the HPT measurement together with MPT tests, *DKMP* for CPT measurement with pore pressure measurements and used for dissipation tests. *MB* stands for a mechanical boring.

## 3.4 Horizontal spatial correlation of the permeability

The results from the conducted test on the permeability (empirical correlations from the grain size distributions, slug test, piezo-cones and laboratory test) are used for the analysis of the horizontal variability. This sampling scheme is given in Figure 3.3.

The analysis of the horizontal correlation length of the permeability for all measurement results is carried out using the Maximum Likelihood approach, which can handle also arbitrary spaced samples as obtained with the nested sampling approach. The variogram approach is not applicable for the chosen sampling scheme.

The summary of the results of the ML analysis are given in Table 3.1 and in the Appendix E. The variability of the different permeability measurement techniques ranges from  $COV = 14\%$  to  $-116\%$ . From the results in Table 2.1 and Table 3.1 one cannot derive a reason for the different ranges of the spatial variability. The correlation length is different for each permeability measurement, except for the HPT results, method and ranges from 31 m to 684 m. Note that for the HPT results, the  $COV = 14\%$  and the  $\theta_h = 18.8$  m are much smaller in comparison to the other methods. A reason for this could be the calculation of the permeability from the Q/P profile, which is basically an averaging over the Q/P measurements as briefly described in section 2. However, the  $COV_{\theta_h}$  of the HPT measurement results is comparable to the other approaches.

However, the uncertainty in the estimate of the correlation length is also very high with  $COV_{\theta_h}$ . The reason for the high  $COV_{\theta_h}$  can possibly be attributed to both the COV and to the

sampling scheme. However, due to the scarcity of investigations on  $COV_{\theta_h}$  in literature [14], it is difficult to draw conclusions from this.

Table 3.1 Coefficient of variation (COV) of the variability and horizontal correlation lengths  $\theta_h$  and COV of the correlation length  $COV_{\theta_h}$  of the subsoil based on all methods

	Number of tests	raw data		
		COV [%]	Horizontal correlation length Mean value $\theta_h$ in m	$COV_{\theta_h}$
<b>falling head test</b>	20	101%	31	102%
<b>Bouwer Rice 3 lijn</b>	20	67%	81	101%
<b>Bouwer Rice 1 lijn</b>	20	67%	69	102%
<b>Hvorslev</b>	20	64%	79	101%
<b>Den Rooijen</b>	20	47%	137	101%
<b>Ernst</b>	20	47%	105	102%
<b>Hazen</b>	20	55%	119	99%
<b>Kozeny-Carman</b>	20	31%	684	103%
<b>Seelheim</b>	20	37%	149	101%
<b>Seelheim2</b>	20	45%	113	99%
<b>Parez Fauriel *</b>	6	116%	41	99%
<b>VanBaars VanDeGraaf *</b>	6	116%	36	99%
<b>MPT - Meetreeks1</b>	19	65%	225	97%
<b>MPT - Meetreeks2</b>	19	67%	322	101%
<b>MPT - Meetreeks3</b>	19	59%	216	99%
<b>HPT data</b>	12	14%	18.8	101%

\* These test results are significantly (bigger than a factor of 100!) lower than the other results of the permeability measurements.

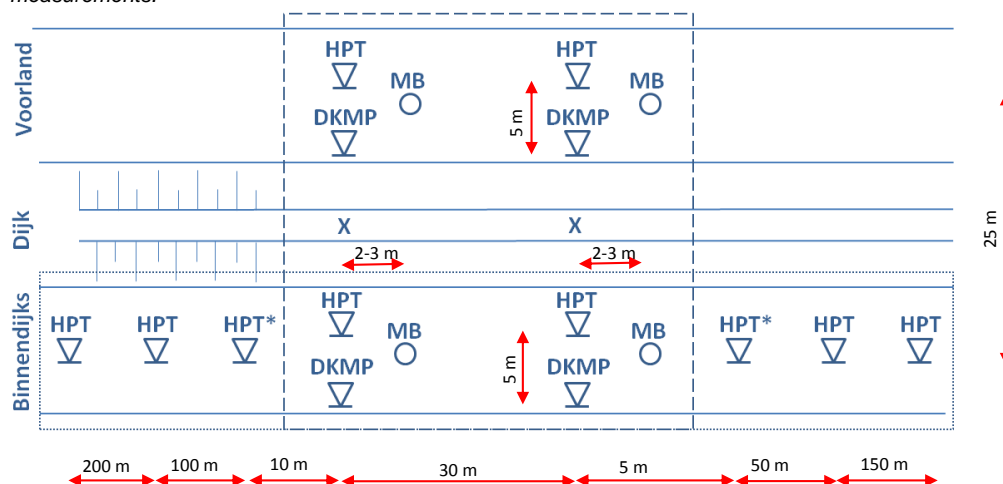


Figure 3.3. Sketch of the used sampling scheme for HPT test (HPT), mechanical borings (MP) and HPT test with MPT measurements at different depths (DKMP).

### 3.5 Vertical spatial correlation of the permeability

The vertical spatial variability of the permeability is derived from the HPT test. Herein, the relation of injected water ( $Q$ ) during the penetration process of the HPT sonde with the pressure  $P$  is employed as relative measure of the permeability. These results are compared to the analysis of the cone resistance values (CPT), which are analysed in the same manner. As described in the accompanying report of Fugro [30, 62], the  $Q/P$  relation represents the vertical changes in the permeability. Fugro [30, 62] translate the  $Q/P$  measurements into permeability of the soil layers. This has not been considered in the sequel. The  $Q/P$  relation is analysed in order to get the corresponding correlation length. Due to the fact that  $Q$  and  $P$  are continuously measured, Maximum Likelihood method and variogram approach are employed for the analysis of the spatial correlation.

The basic steps of the analysis of the vertical correlation length are summarized in Figure 3.4. The first step is the engineering judgement on soil layering and setting up of preliminary boundaries. After this, the measurement data have to fulfil the homogeneity and stationarity criteria. Both criteria are verified by statistical tests such as the Bartlett statistics  $B_{stat}$  and intra-class correlation coefficient  $RI$ . In the presence of a significant trend of the data one cannot derive the spatial correlation. Therefore, one has to detrend the measurements inside each layer. Now each layer is analysed by the variogram approach and the Maximum Likelihood method (ML) to evaluate the correlation lengths. Of course, one has to check now the sensitivity of the correlation length inside each layer to the small changes of the layer boundaries. This is important because the subdivision of a soil profile into layers and the detrending inside each layer has a significant impact on the correlation length. Using this scheme, one can separate different scales of spatial variability (Figure 3.1) the large geologically based spatial variability are separated from the meso-scale phenomena, which can be investigated without injuring the basic assumptions of the theory described in detail in the appendix C.

By looking at the measurement data  $Q/P$  in Figure 3.5, one can clearly indicate a trend of the measurements with depth, which can be described by equation (2.1), where  $m(z)$  is a deterministic function giving the mean measurement value at a depth  $z$  below the surface level; and  $\varepsilon(z)$  are the random residuals.

$$Q/P(z) = m(z) + \varepsilon(z) \quad (0.4)$$

In Figure 3.5 one can see the results of this analysis of the vertical spatial correlation length in the aquifer. The vertical correlation length is analysed by the variogram and the ML approach. Herein, we evaluated also the uncertainty of the vertical correlation length using both approaches, which is given in Figure 3.5. The uncertainty of the correlation length for the variogram approach and for the ML approach is described by a lognormal probability distribution function. By employing the Bayesian Model Averaging approach, we combine these two probability distribution functions, which are describing the uncertainty of the vertical correlation length. The result of this and the corresponding 68% confidence interval is visualized in Figure 3.5. The resulting vertical correlation length is  $\theta_{ver} = 0.59$  m. This is in line with values often mentioned in literature.

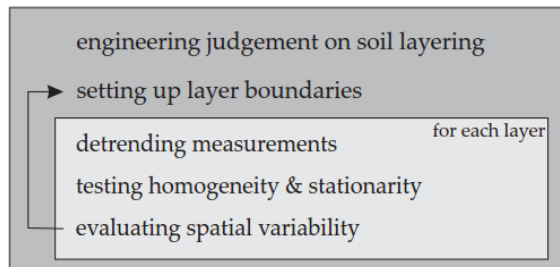


Figure 3.4 Steps of evaluating the vertical correlation length, Huber [34]

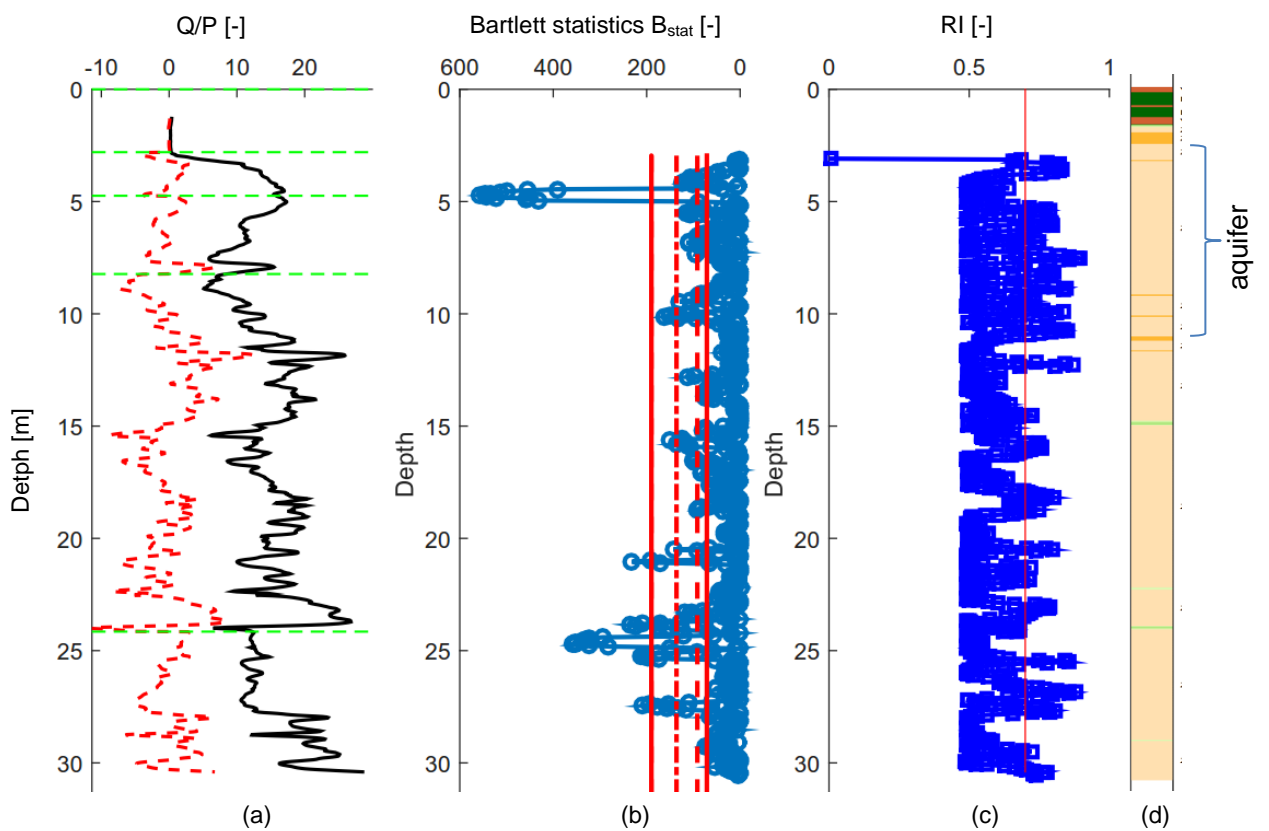


Figure 3.5 Analysis of the cone resistance of CPT 12 including the original data of the Q/P relation in black, the detrended data (dotted red) and layer boundaries (green) in (a), the Bartlett statistics in (b) and the intra-class correlation index in (c) and an indicative soil description derived from CPT (yellow = sand, green = clay, red = peat)

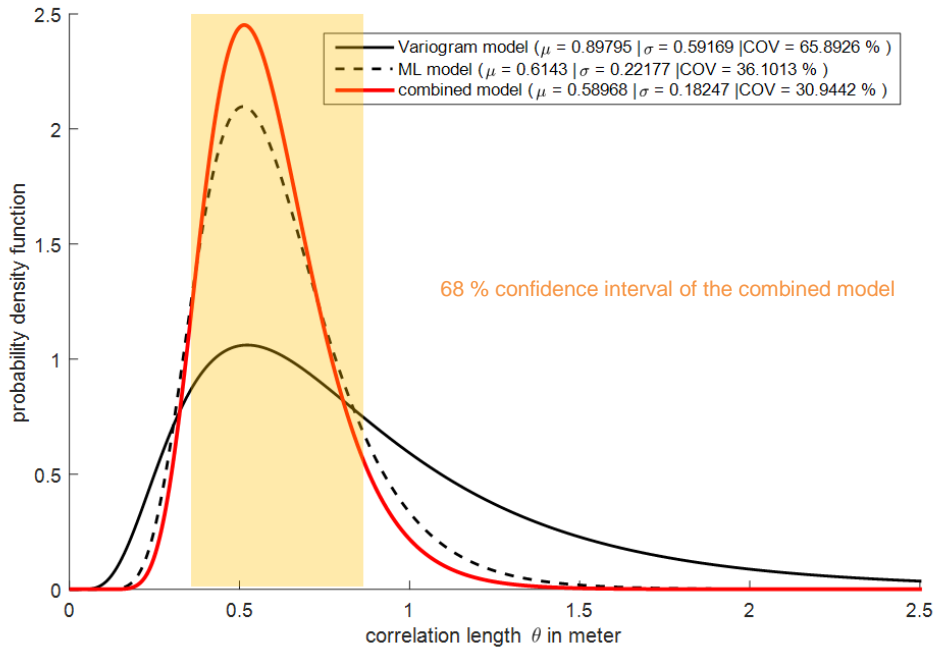


Figure 3.6 Vertical correlation length of the Q/P relation from the HPT using the variogram and ML together with the combined results

### 3.6 Summary

The different test results of the permeability of the aquifer are investigated by means of the variogram and the ML approach. The analysis results give a diverse picture. The horizontal correlation length show large differences for the different test types. The evaluated horizontal correlation lengths  $\theta$  also show a large coefficient of variation  $COV_{\theta,h}$ . The vertical correlation length for the permeability is only derived from HPT tests.

Note that the results of the horizontal correlation length are dependent on the sampling scheme, which is used in this study. Due to the design of experiments given in section Sampling theory 3.3, it is not possible to find smaller correlation lengths than the minimum mutual distance between the samples.

## 4 Quantifying the effects of spatially correlated permeability

### 4.1 Introduction

This chapter describes the steps to quantify the effects of the evaluated horizontal spatial correlation of the permeability using a semi-probabilistic and probabilistic safety assessment. The employed piping approaches do not consider the vertical spatial variability of the permeability. The effects of the vertical correlation length of the permeability are assumed to be taken into account within the subsoil schematisation. Only the effects of the horizontal spatial correlation are investigated in this chapter.

At first, the theoretical introduction for the quantification of effects the spatial correlation of soil properties is given. To analyse the effect of the different measures of permeability on the safety assessment, detailed safety assessments are elaborated for the failure mechanism piping. The permeability is varied on basis of the different test results and the analysis of heterogeneity. Firstly, the safety assessment method and failure mechanism are described, and then applied in a case study.

If the horizontal correlation of soil properties is considered to evaluate the probability of failure of a dike, one has to be aware that only the combination of a large variance in combination with a relatively low spatial correlation will result in large length effects, shown in Figure 4.1.

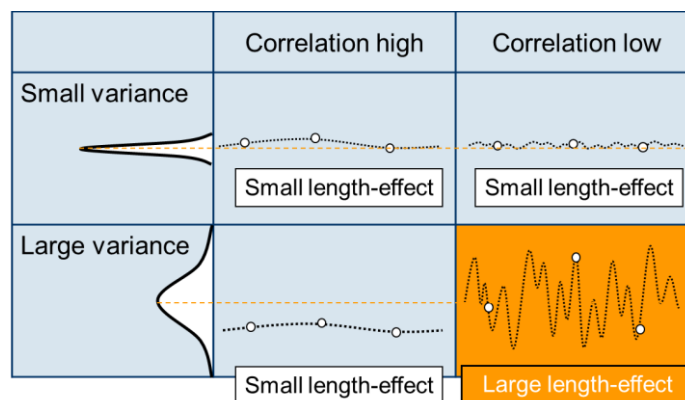


Figure 4.1 Concept of the small and large length effects

### 4.2 Theoretical background on spatial averaging

Amongst others, Vanmarcke [64] shows the relationship between small volume tests and large volume tests. Small volume tests show a higher scatter than large volume tests. Vanmarcke [64] explains this using spatial averaging. Therefore, the measured scatter has to be averaged over the soil volume, which is influenced by the mechanism (e.g. piping). Vanmarcke [64] presented simple relationships for the variance reduction using the correlation length in combination with different variance functions. Herein, he assumes that the variability of a soil property  $u$  is measured by the standard deviation  $\sigma_i$  and the standard deviation of the spatial average property  $u_T$  is measured by  $\sigma_T$ . The standard deviation of the spatially averaged property is inversely proportional to the size of the averaging length or volume  $T$ , and the standard deviation reduction factor  $\Gamma_u(T)$  due to spatial averaging is defined in equation (0.5). Vanmarcke [64] derived the following relationship for the reduction

factor  $\Gamma_u(T)$  for a squared exponential correlation function. Herein is  $\varrho$  the correlation length.

$$\Gamma_u(T) = \frac{\sigma_T}{\sigma_i} = 2 \cdot \left(\frac{\varrho}{T}\right)^2 \cdot \left[\frac{T}{\varrho} + \exp\left(-\frac{T^2}{\varrho}\right) - 1\right] \tag{0.5}$$

The reduction factors for different correlation functions (triangular, exponential, second-order autoregressive and squared exponential) are given in [63]. One can clearly see in Figure 4.2 that the reduction factors for different correlation functions are comparable.

From Equation (0.5) and Figure 4.2 (where  $\Gamma_u(T)$  is depicted as  $\gamma(T)$ ) one can clearly derive that the bigger the volume  $T$ , over which the property is averaged, the larger is the variance reduction factor  $\Gamma_u(T)$ . Estimating the volume  $T$  is dependent on the piping mechanism. In the sequel case study, it is assumed that the whole aquifer has an impact on the piping phenomenon, which is assumed to be in the order  $T=1.000 \text{ m}^3$  ( $1.000 \text{ m}^3=250 \text{ m} * 3.5 \text{ m} * 1\text{m}=\text{required seepage length} * \text{depth of the aquifer} * 1\text{m-slice}$ ). Note that in case of a larger volume  $T$ , the reduction of due to spatial averaging is bigger.

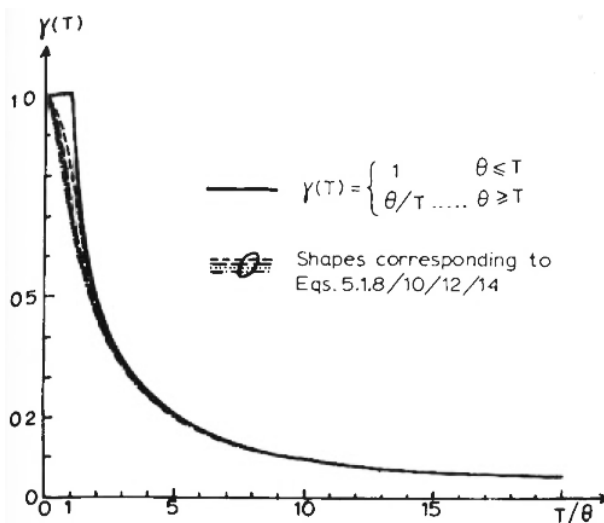


Figure 4.2 Different correlation factors for correlation function from [64]

### 4.3 Consideration of the horizontal correlation length in the semi-probabilistic piping safety assessment

Although it is not clear how uncertainty of the permeability values is influenced by the upscaling approach, it is assumed in this report that the upscaling approach is not influencing the uncertainty. Moreover, it is assumed that the upscaling approach of the permeability's does not include the spatial averaging. These two assumptions need further investigation.

In the semi-probabilistic safety approach the horizontal correlation length is considered by the variance reduction factor  $\Gamma_u(T)$ . After upscaling, the measurement values, the variance reduction factor  $\Gamma_u(T)$  is used for each testing method to calculate an updated standard deviation. Note that the reference volume is assumed as  $V_R=1000 \text{ m}^3$  ( $1.000 \text{ m}^3=250 \text{ m} * 3.5$

$m \cdot 1m$  = required seepage length \* depth of the aquifer \* 1m-slice) as given in 4.2. Finally, these updated standard deviation values are used to calculate the characteristic values for the each permeability testing methods. It can be clearly seen in Table 4.1 that the standard deviation is reduced through the spatial averaging approach, which leads to a smaller characteristic value of the permeability. Note that a low correlation length, such as for the HPT data, leads to spatial averaging, which reduces the corresponding standard deviation. As a consequence, a smaller standard deviation leads to a lower characteristic values and vice versa. Since it is not fully understood how upscaling, spatial averaging and the HPT permeability relate to each other, it could be that a full spatial averaging is not justified. Due to a lack of knowledge, full spatial averaging is applied as first step.

Table 4.1 Horizontal correlation length, corresponding variance reduction factor and corrected permeabilities per method

	raw data				$V_p$ volume being tested	scaled permeabilities			$V_R=T$ volume being scaled up to	horizontal correlation length $\theta$	Variance reductio n function $\Gamma(T)$	corrected permeabilities	
	$\mu_{raw}$ [m/day]	$\sigma_{raw}$ [m/day]	COV [%]	$m^3$		$\mu_{scaled}$ [m/day]	$\sigma_{scaled}$ [m/day]	CO V [%]				$m^3$	$\mu_{corr}$ [m/day]
<b>Bouwer Rice 3 lijn</b>	0.3	0.2	67	0.015	12.3	8.7	71	1000	81.00	15%	12.3	1.3	
<b>Hvorslev</b>	0.4	0.3	64	0.015	15.9	11.3	71	1000	79.00	15%	15.9	1.6	
<b>Den Rooijen</b>	11.2	5.2	47	1000	11.2	5.2	47	1000	137.00	24%	11.2	1.2	
<b>Hazen MPT - Meetreeks1</b>	15.8	8.7	55	1000	15.8	8.7	55	1000	119.00	21%	15.8	1.8	
<b>HPT data</b>	29.8	19.3	65	0.02	29.8	19.3	65	1000	225.00	35%	29.8	6.8	
	13.18	1.86	14	1000	13.18	1.9	14	1000	18.80	4%	13.2	0.1	

#### 4.4 Piping safety assessment

The piping safety assessment is done for segment 36-5 where the measurements were carried out. The total length measures 17.6 km and the safety standard  $P_T$  of the segment is 1/10,000. According to the VNK approach, the considered (cross) section 36003003 has a length of 893 m and counts 4 “bodenvakken”, in which it is assumed that the sub-soil is similar. Per “bodenvak” there are 3 sub-soil schematizations scenarios with the corresponding probabilities of occurrence (scenarios 302, 303 and 305).

For the semi-probabilistic calculations both the piping rule Sellmeijer (2006) rule and the Sellmeijer (2011) rule are employed in combination with VNK2-project data for sub-soil schematizations and soil parameters. The piping failure mechanism and the parameters (according to the VNK-2 project [65]) are included in Appendix F.

##### 4.4.1 Variables

The measured permeability  $k$  (FUGRO [30]) and the  $d_{70}$  value, which is derived from the grain size distributions for this given site, are used in combination with the VNK2-data set. The  $d_{70}$  value is lognormally distributed with a mean value of  $3.1e-4$  m and a standard deviation of  $6.9e-4$  m. For the sake of completeness, it shall be stated that in the VNK2-data set has a lognormally distributed permeability with a mean value of 19.96m/d, a standard deviation of 21.16 m/d and a correlation length of  $\theta=600$  m. These values represent the aquifer permeability and includes spatial averaging.

## 4.4.2 Semi-probabilistic assessment

Semi-probabilistic calculations are made in accordance with “Ontwerpinstrumentarium 2014 v3” [54], which is in line with the anticipated WT12017 approaches for Dutch safety assessment method for checking the reliability of flood defences [54].

In this novel approach the semi-probabilistic safety assessment considers multiple subsoil scenarios. The scenarios have to be combined through their probabilities. For this reason the safety factor is transformed to a probability as given in Figure 4.3.

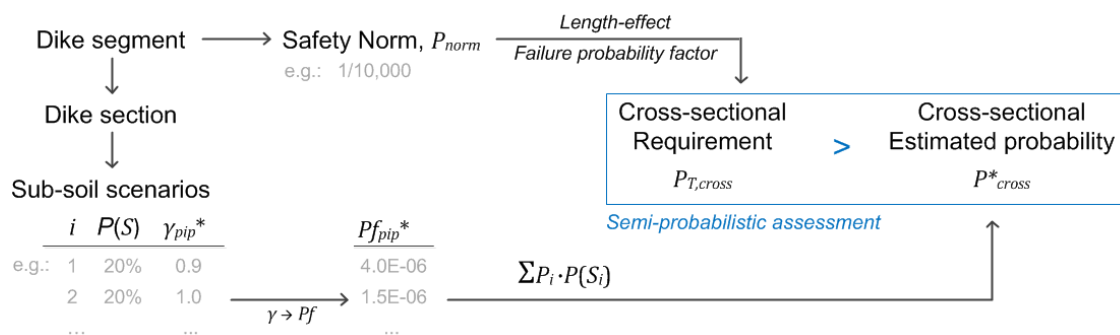


Figure 4.3. Scheme for combining subsoil scenarios in the semi-probabilistic safety assessment for piping

For each random variable, a characteristic value is used (Table F.1). For each possible subsoil scenario (according to VNK2, shown in Figure 4.4) the safety factor is determined [71]. The results of the various semi-probabilistic calculations are different due to different measurements of the permeability; see Table 4.2. The possible sub-soil scenarios for the investigated site are shown in Figure 4.4. The results of semi-probabilistic calculations are different due to different measurements of the permeability; see and Table 4.2.

Using the piping rule Sellmeijer (2011), the scenarios are combined per “bodenvak” that represents a length of 250 m according to the VNK2-project. First, the factor of safety is transformed into a probability by a reliability index  $\beta$  per scenario, according to OI2014 v3 [54]. The schematisation theory [23] allows summing the probabilities of the scenarios with respect to the probability of the scenario given in equation (0.7)

$$SF(\beta) = 0.8\beta_i - 2.4, \quad P_{f,i} = \Phi(-\beta) \quad (0.6)$$

$$P_{f,bodenvak} = \sum_{i=1}^n P_{f,i} \cdot P(i) \quad (0.7)$$

The weight of a sub-soil scenario differs per bodenvak, so the summation differs per bodenvak. The weights can be seen in Table 4.3. After taking the weighted sum of the probabilities, the failure probabilities are re-converted to a safety factor again.

From the results in and it can be deduced that that the factor of safety is higher using the results from the given tests in combination with the VNK dataset. Since the lowest permeability is obtained using the Hvorslev method, the safety factor is the highest for this method.

To put the results in context, the required safety factor per cross-section ( $SF_{T,cross}$   $T=target$ ,  $cross=cross\ section$ ) is calculated according to OI2014 v3 [54]. This is shown in equation (0.8). The target reliability per cross-section (including length-effect) is determined by the target reliability of the segment ( $P_T$ ), the failure probability budget for piping ( $\omega=0.24$ ) and a

factor for the length-effect. Herein,  $a$  represents the part of the segment, which is sensitive for piping, and  $b$  is the length of an independent equivalent cross-section.

$$P_{T,cross} = \frac{P_T \cdot \omega}{\left(1 + \frac{a \cdot L_{segment}}{b}\right)} = \frac{10^{-4} \cdot 0.24}{\left(1 + \frac{0.9 \cdot 17600}{300}\right)} = 4.65 \cdot 10^{-7}$$

$$\beta_{T,cross} = \Phi^{-1}\left(4.65 \cdot 10^{-7}\right) = 4.91 \tag{0.8}$$

$$SF_{T,cross} = 0.80 \cdot \beta_{req.} - 2.4 = 1.53$$

Table 4.2 shows the calculated safety factors ( $SF_{cross}$ ) for each subsoil scenario, which are given in Figure 4.4. It can be concluded from the results in Table 4.2 that the safety factors for the segment 36-5 increase in all cases due to the lower characteristic values of the permeability. It can also be seen that the results using the Piping 2011 rule offers lower safety factors compared to the Piping 2006 rule.

The subsoil scenario safety factors are combined using equation (0.8) and the weights for each “bodenvak” given in Table 4.3. Again, one can see that the combined safety factors for each “bodenvak” is higher when using the permeability measurement values compared to the VNK-2 data set.

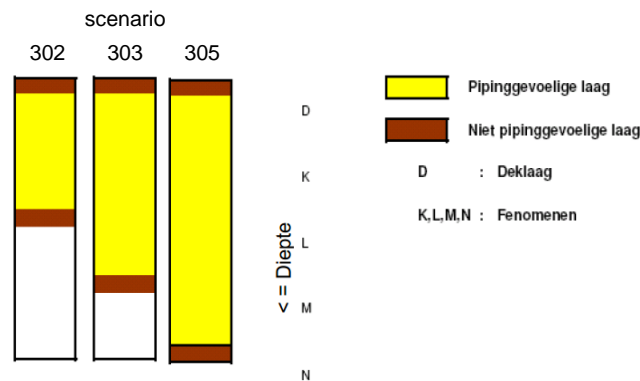


Figure 4.4 Schematic view of sub-soil scenarios for piping

Table 4.2 Calculated safety factors for the subsoil scenarios from the semi-probabilistic piping safety assessment using the scaled measurement values for permeability in combination with the VNK dataset

	SF <sub>cross</sub> Piping 2006							SF <sub>cross</sub> Piping 2011						
	VNK2 data *	Hazen	Hvorslev	Bouwer/ Rice	Den Rooijen	MPT Meetreeks	HPT	VNK2 data*	Hazen	Hvorslev	Bouwer/ Rice	Den Rooijen	MPT Meetreeks	HPT
Scenario 302	1.20	2.02	2.03	2.19	2.25	1.59	2.25	0.85	1.34	1.34	1.46	1.51	1.02	1.50
Scenario 303	0.62	1.29	1.30	1.40	1.44	1.02	1.44	0.46	0.91	0.92	1.00	1.03	0.70	1.03
Scenario 305	0.64	1.10	1.10	1.19	1.22	0.86	1.22	0.50	0.80	0.80	0.87	0.90	0.61	0.90

\* The VNK2 data set is used without any upscaling and without averaging.

Table 4.3 Combined safety factors from the semi-probabilistic piping safety assessment for each "bodenvak" in segment 36-5

		bodenvak 1 - 250 m			bodenvak 2 - 250 m			bodenvak 3 - 250 m			bodenvak 4 - 250 m		
Scenario		302	303	305	302	303	305	302	303	305	302	303	305
<b>weights</b>	<b>P(i)</b>	17%	20%	63%	26%	33%	41%	26%	42%	32%	12%	33%	55%
VNK2-data set*		0.52			0.53			0.53			0.51		
VNK + test data		0.85			0.89			0.91			0.86		
Hazen		0.85			0.89			0.91			0.86		
Hvorslev		0.86			0.90			0.91			0.86		
Bouwer/Rice		0.93			0.97			0.98			0.93		
Den Rooijen		0.96			1.00			1.01			0.96		
MPT-Meetreeks1		0.66			0.70			0.71			0.66		
HPT		0.95			1.00			1.01			0.96		

\* The VNK2 data set is used without any upscaling and without averaging.

#### 4.4.3 Interpretation of the results

The results have to be seen as preliminary results with oversimplifications to show the applicability of the presented approach. Note that these results are derived on upscaled and locally averaged permeability values, which needs further investigation especially for small scale tests. Note that the estimates of the horizontal correlation length are very uncertain ( $COV_{\theta} \sim 100\%$ ). This study is a successful proof-of-concept, however the results should be interpreted only relatively to each other and not in an absolute way.

To support the interpretation relative to each other, the different results are compared by the required seepage length. This is closely related to the required length of the piping berm. This required seepage length is calculated both semi-probabilistically for each scenario. Herein, the piping rule Sellmeijer (2011) [58] is employed to analyse VNK-2 data and the measured  $d_{70}$  (mean value and standard deviation) and permeability (mean value, standard deviation and correlation length). These results are shown in Table 4.4 .

The semi-probabilistic approach results in relatively more or less the same required seepage length, given in Figure 4.5 and Table 4.4 . Note that the required seepage lengths are defined as additional seepage length, which considers the given geometry with a berm of 69 meter. The MPT Meetreeks 1 results are higher compared to the other measurement values. By revisiting the corrected permeability values in Figure 4.1, one can see that the mean values and standard deviations show comparable values of the COV, but not the MPT meetreeks1 results, which are higher. It can be concluded from these results that for all investigated permeability measurement results a significant reduction of the required seepage length can be derived.

If there is no local averaging, there standard deviation is not reduced and therefore, the characteristic value of the permeability will be significantly higher. This will result in higher required additional berm length compared to the results given in Table 4.4 and Figure 4.5.

Table 4.4 Semi-probabilistic piping safety assessment for bodemvak 1: additional required seepage length [m] to comply to a safety threshold

		Scenario 302	Scenario 303	Scenario 305
VNK-2 data set*		129	261	248
VNK2 + test data	Hazen	79	121	147
	Hvorslev	78	121	146
	Brouwer/Rice	71	110	133
	Den Rooijen	69	106	128
	MPT – Meetreeks 1	105	163	199
	HPT	69	107	128

\* The VNK2 data set is used without any upscaling and without averaging.

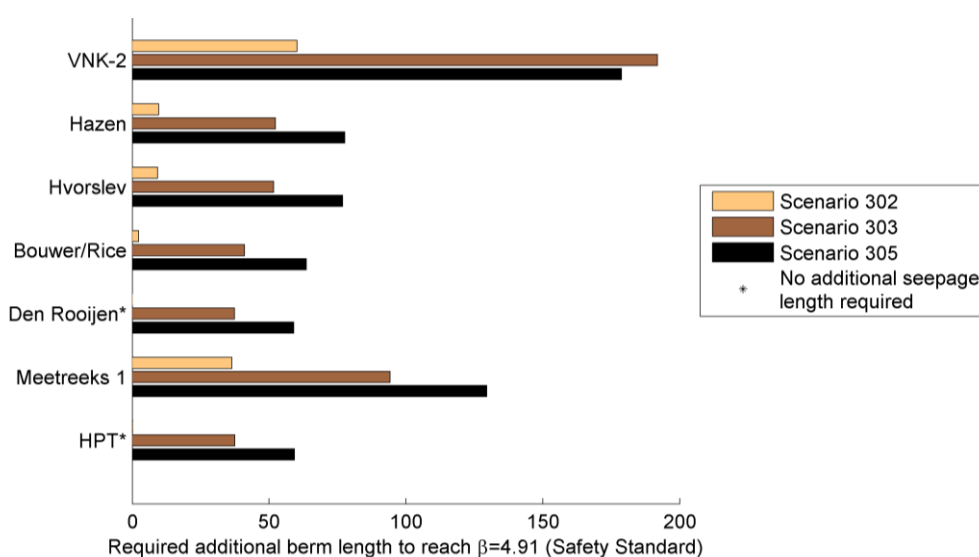


Figure 4.5 Semi-probabilistic safety assessment of bodemvak 1: Required additional berm lengths to meet the safety standards. (Note that the VNK2 data set is used without any upscaling and without averaging.)

4.4.4 Sensitivity study on the influence of the uncertainty of the horizontal correlation length

Additionally, the influence of the uncertainty of the horizontal correlation length of the upscaled and locally averaged permeability values is investigated. For this reason we vary the lognormally distributed correlation length ( $\theta_h$ ) between the lower and upper bound of a 68 % confidence interval and evaluate the required additional berm length. The lower bound is defined by the 16 percentile value of the lognormally distributed correlation length and the upper bound the 84 percentile value. One can see in Figure 4.6 and Table 4.5 the effects of the uncertainty of the correlation length on the required additional berm length. Note that in a lognormal distribution with a high COV, the lower bound (16 percentile value) is closer to the mean value than the upper bound (84 percentile value). This is related to the skewness of the distribution function. As a consequence, the differences of the additional required berm length using the lower bound and mean value of  $\theta_h$  are smaller compared to the differences of the additional required berm lengths using the mean value and the 84 percentile value of  $\theta_h$ . All investigated cases result in required additional berm lengths, which are smaller than the VNK-2 results. Moreover, the sensitivity of the calculation results on the uncertainty of the spatial correlation can be derived. Note that the low COV for the HPT leads to a very small sensitivity of the additional required berm lengths, although the COV of the correlation length is high. This may be linked to the evaluation of the HPT permeabilities, as described in section 2.

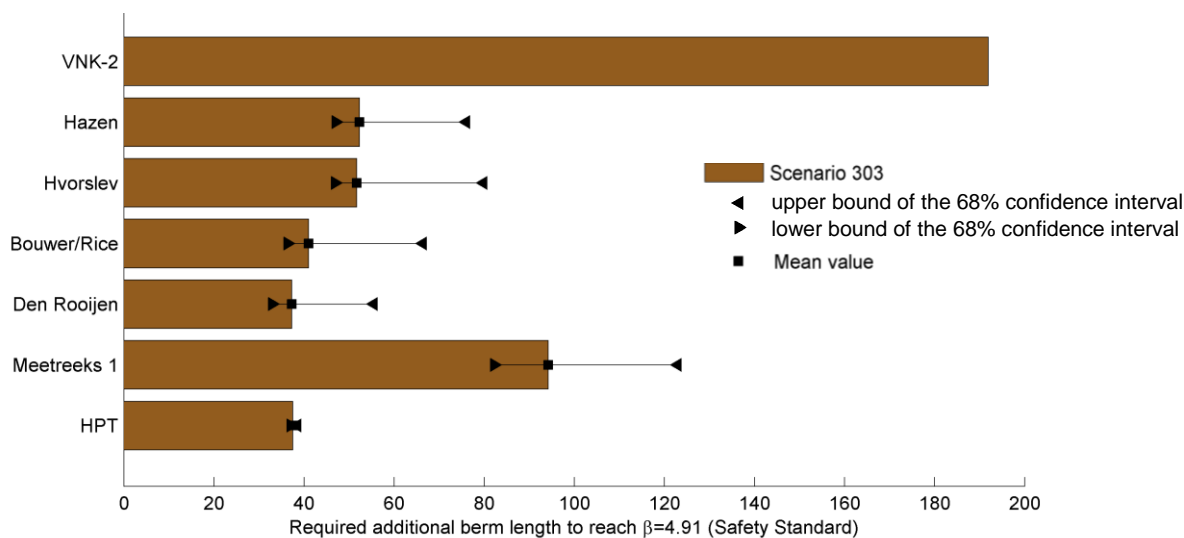


Figure 4.6 Semi-probabilistic safety assessment of bodemvak 1: Influence of the horizontal correlation length of the permeability for the lower and upper bound of the 68 % confidence interval of the lognormally distributed horizontal on the required additional berm lengths. (The VNK2 data set is used without any upscaling and without averaging.)

Table 4.5 Sensitivity study on the influence of the uncertainty of the horizontal correlation length on the required additional berm lengths for scenario 303 and for bodemvak 1

Horizontal correlation length is	Required additional berm lengths for			Correlation length		
	Lower bound 16 percentile value [m]	Mean value [m]	Upper bound 84 percentile value [m]	Lower bound 16 percentile value [m]	Mean value [m]	Upper bound 84 percentile value [m]
<b>VNK-2 data set*</b>	-	194	-	600		
Hazen	116	121	145	37	119	192
Hvorslev	116	121	149	24	79	127
Brouwer/Rice	105	110	135	25	81	131
Den Rooijen	102	106	124	42	137	221
Meetreeks	151	163	192	72	225	365
HPT	106	107	108	6	18.8	174

\* The VNK2 data set is used without any upscaling and without averaging.

#### 4.5 Bayesian Updating of the VNK-dataset with the measurement values

In order to investigate the effects of the spatial correlation, an additional case study is carried out. Herein we update the probability density function (pdf) of the VNK-2 data set with the pdf of the measurement results using the Bayesian theorem. Note that we use the upscaled permeability values in Table 2.1. In this context, the VNK-2 data set is called prior distribution of parameters, which is updated with measurement data using a so-called likelihood function. The resulting pdf is called posterior distribution. The single steps of Bayesian updating are given in Appendix G. The basic idea of the Bayesian principle is the combination of two

probability density functions. This combination is leading to a significant reduction of the standard deviation. Note that we only updated the mean value and the standard deviation of the permeability using upscaled permeability values and not the correlation length.

Appendix G provides all steps in updating the VNK-2 data set with the mean value and standard deviation of the test results from Hazen Hvorslev, Bower-Rice-lijn1, Den Rooijen MPT and HPT. The characteristic values of the prior pdfs and of the likelihood pdfs are given in Table 4.6. In Table 4.7 one can see the effects of the Bayesian updating. Comparing the characteristic values in Table 4.6 and Table 4.7, one can see that the Bayesian Updating is resulting in lower values of the permeability. However, the characteristic value of the MPT test is much higher than for the other methods.

The effects of these lower characteristic values are depicted in in Figure 4.7. Herein we show the required berm lengths. Assuming the same spatial correlation as the VNK dataset, the permeability's from the Hazen, Hvorslev, Bouwer/Rice-lijn 1, Den Rooijen and HPT results comparable required additional berm lengths, which are significantly lower than the berm length resulting from the VNK2 data set. Additionally, one can see that the MPT-Meetreeks1 test is resulting in a slightly higher required additional berm length due to its higher permeability value given in Table 4.7.

Comparing the results in Figure 4.6 and Figure 4.7, one can see that the results of both approaches are nearly the same. The Bayesian updating approach offers slightly longer required additional berm length than the spatial averaging approach for this investigated case.

From this it can be deduced that Bayesian updating of the mean value and standard deviation of the permeability has a major effect on the characteristic permeability and as a consequence also on the resulting design of required berm length compared to an improved estimation of the permeability using one method including also the spatial correlation of the parameters. The investigated cases show that also the testing method has a less significant approach. However, it is not clear how this can be related to the findings in section 4.4. Therefore it is recommended to study this in additional case studies.

Table 4.6 Lognormal distribution (mean value  $m$ , standard deviation  $s$ ) and corresponding characteristic values of the upscaled permeability of the prior distributions (VNK) in m/day and of the pdfs of the likelihood functions (Hazen, Hvorslev, Bouwer/rice-lijn1, Den Rooijen and MPT Meetreeks 1) in m/day

	VNK2 data*	Hazen	Hvorslev	Bouwer/Rice-lijn 3	Den Rooijen	MPT Meetreeks 1	HPT
m in m/day	19.96	15.8	15.9	12.3	11.2	29.8	13.8
s in m/day	21.16	8.7	11.3	8.7	5.2	19.3	1.86
COV	106%	55%	71%	71%	46%	65%	13 %
95%-quantile in m/day	57.3	32.4	37.2	28.7	21.1	66.4	17.1

\* The VNK2 data set is used without any upscaling and without averaging.

Table 4.7 Lognormal distribution (mean value  $m$ , standard deviation  $s$ ) and corresponding characteristic values of the posterior distributions of the permeability (Hazen, Hvorslev, Bouwer/rice-lijn1, Den Rooijen and MPT Meetreeks 1) in after Bayesian updating in m/day

	Hazen	Hvorslev	Bouwer/Rice-lijn 3	Den Rooijen	MPT Meetreeks 1	HPT
m in m/day	13.8	12.98	10.1	10.2	24.7	13.7
s in m/day	1.6	2.1	1.4	1.0	4.7	0.5
COV	12%	16%	14%	10%	19%	4%
95%-quantile in m/day	<b>16.8</b>	<b>16.8</b>	<b>12.8</b>	<b>12.0</b>	<b>30.8</b>	<b>14.6</b>

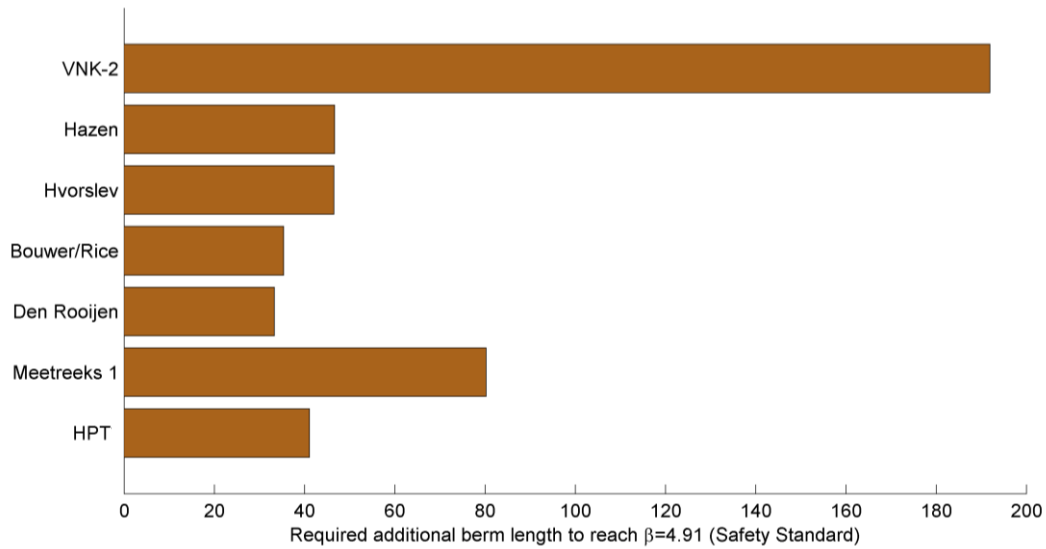


Figure 4.7 Required additional berm length for scenario 303 to meet the safety standards using semi-probabilistic piping safety assessment using Bayesian updating of the VNK data with measurement values

## 5 Summary and recommendations

In this report various permeability measurement results are analysed by means of statistical analysis. Additionally, the spatial correlation of the measurement data is quantified in vertical and horizontal direction. These findings are used to evaluate the effects in the piping safety assessment using the semi-probabilistic approach.

The findings are as follows:

- This study results in important insight into the interpretation of permeability measurements. Within this, the HPT sonde results are found to be a useful tool to measure aquifer permeability's.
- **Parameter selection from permeability measurements**  
It is necessary to relate the results of permeability measurements to the corresponding soil volume being investigated. These results have to be scaled to the volume of the aquifer, which is used in a piping safety assessment. This scaling can be done using simple approaches, as proposed by Fugro [25]. However, this upscaling approach needs further investigation and analysis of its effects on the derived parameter uncertainty.  
Using the upscaling approach of Fugro [25], the upscaled permeabilities of a given soil type can be related to each other. Within this, the HPT and MPT methods show good agreement with the other investigated permeability measurements.
- **Quantification of spatial correlated permeability:**  
The Maximum Likelihood methodology is found to be effective and versatile tool for the calculation of the correlation length, which is a measure of the spatial correlation of measurement data. Therefore, the Maximum Likelihood method is used to evaluate the horizontal spatial variability of the permeability measurements, which are used for a case study.

The resulting spatial correlation lengths vary for the different approaches. Empirical correlations of the permeability derived from sieving curves (Den Rooijen, Ernst, Hazen, Kozeny-Carman and Seelheim) show correlation lengths that are bigger than a factor of 2 compared to the slug test in mechanical borings (Bouwer-Rice lijn 1 & 3 and Hvorslev) and compared to the falling head test. The correlation lengths of the permeability's derived from HPT test data have the smaller correlation length, whereas the MPT test results show the largest correlation length. However, there is large uncertainty in the correlation length estimate, indicating a weak spatial correlation, which limits the applicability of the results.

- **Quantification of the effects of spatially correlated permeability**  
The semi-probabilistic approach is employed to quantify the effects of the permeability measurements in the piping safety assessment. The spatial correlations of the upscaled measurement data are considered by using spatial averaging theory, which is reducing the standard deviation of the measurement data. These updated data are used for the piping safety assessment of a given cross section and the results are compared to those of the VNK-2 dataset. The results show that the improved knowledge of the spatial variability of the permeability leads to smaller additional required berm length compared to the VNK-2 data. However, the upscaling and spatial averaging seem to be related to each other. Because of this possible relation, full spatial averaging is not necessarily justified. Therefore, the positive effect of smaller additional required berm lengths might be smaller than in the investigated case. Additionally, it is also not fully clear why the correlation length, which has a high variability (COV ~ 100 %), has only limited effects on the additional required berm lengths. The large COVs of the correlation length leave room for interpretation.
- **Bayesian Updating of the VNK-dataset with measurement results**  
Additionally, the Bayesian approach is used to update mean value and standard deviation of the VNK-2 permeability with the mean value and standard deviation of the different permeability measurements. Note, that the spatial correlation length of the permeability from the VNK-2 data set is used. Using this updated mean value and updated standard deviation of the permeability shows a big effect on the additional required berm lengths. However, this Bayesian approach is not incorporating the available knowledge and measurement on geology and heterogeneity. It has to be determined, if this approach is justified.

The following **recommendations** for next further investigations can be made on basis of this report:

- Additional investigations are recommended in order to understand in detail **how to interpret locally average permeability measurements**. It would be very interesting to gain more insight, if the employed approach for **upscaling of measurements is including a local averaging**.
- Additional investigations are recommended to **investigate**, if the **spatial averaging is justified** for methods.
- **Additional test sites** are required to underpin the **upscaling approach** of the permeability measurements with permeability of an aquifer. Herein, the anisotropy of the permeability should be addressed. These investigations shall also contribute to quantify also the **uncertainty of this upscaling approach**, as well as spatial averaging, which is not yet completely understood.
- **Additional field test using the HPT sonde** in combination with other testing methods are necessary to derive the **correlation between the Q/P measurements and the permeability for different sites**. Additionally, also the **model uncertainty** should be investigated in this context. Moreover, this should also be used to study the spatial correlation of the derived permeability.
- Additional tests should be employed to study the **combination of different measurement methods for the statistical description of the permeability at one**

**given site.** This contributes to a more effective use of the measurement data and can possibly lead to a more cost effective design of measures against piping failure.

- The **effectiveness of different sampling schemes** for permeability measurements should be investigated in order to reduce the uncertainty of the correlation length.
- Moreover, it is recommended to **validate the effectiveness of the Bayesian approach** in an additional study, given in section 4.5, which is updating the mean value and standard deviation of the VNK-2 set with measurement results.



## 6 References

- [1] M. Abramovich and I.A. Stegun. *Handbook of Mathematical Functions, Graphs and Mathematical Tables*. National Bureau of Standards Applied Mathematics, Washington, 1964.
- [2] H. Akaike. Information theory and an extension of the maximum likelihood principle. In *Proceedings of Second International Symposium on Information Theory*, volume 1, pages 267–281. Springer Verlag, 1973.
- [3] H. Akaike. A Bayesian analysis of the minimum AIC procedure. *Ann. Inst. Statist. Math.*, 30:9–14, 1978.
- [4] G.B. Baecher and J.T. Christian. *Reliability and statistics in geotechnical engineering*. John Wiley & Sons Inc., 2003.
- [5] S. Bakhtiari. *Stochastic Finite Element Slope Stability Analysis*. PhD thesis, Manchester Centre for Civil and Construction Engineering, University of Manchester, England, 2011.
- [6] A. Bárdossy, U. Haberlandt, and J. Grimm-Strele. Interpolation of groundwater quality parameters using additional information. In A. Soares, editor, *Proceedings of geoENV I-Geostatistics for Environmental Applications*. Kluwer Academic Publishers, 1997.
- [7] A. Bárdossy and Z.W. Kundzewicz. Geostatistical methods for detection of outliers in groundwater quality spatial fields. *Journal of Hydrology*, 115(1-4):343–359, 1990.
- [8] J.S. Bendat and A.G. Piersol. *Random data analysis and measurement procedures*, volume 11. IOP Publishing, 2000.
- [9] R. J. Bennett. *Spatial Time Series*. Pion Ltd., London, 1979.
- [10] G.E.P. Box and G.M. Jenkins, editors. *Time Series Analysis: Forecasting and Control*. Holden-Day, San Francisco, 1970.
- [11] H. Bozdogan. Model selection and akaike's information criterium: The general theory and its analytical extensions. *Psychometrika*, 52:345–370, 1987.
- [12] R.G. Campanella, D.S. Wickremesinghe, and P.K. Robertson. Statistical treatment of cone penetration test data. In *Proceedings of the 5th International Conference on Reliability and Risk Analysis in Civil Engineering*, 1987.
- [13] R. Caspeele. *Probabilistic evaluation of conformity control and the use of the Bayesian updating techniques in the framework of safety analyses of concrete structures*. PhD thesis, University Gent, 2009.
- [14] J.P. Chiles and P. Delfiner. *Geostatistics—modeling spatial uncertainty*. Wiley-Interscience, 1999.
- [15] G. Christakos. *Random field models in earth sciences*. Academic Press, 1992.
- [16] A. D. Cliff and J.K. Ord. *Spatial processes: models & applications*, volume 44. Pion London, 1981.
- [17] W. G. Cochran, editor. *Sampling techniques*. New York: John Wiley and Sons, 1977.

- [18] N. Cressie. Fitting variogram models by weighted least squares. *Mathematical Geology*, 17(5):563–586, 1985.
- [19] N. Cressie. *Statistics for spatial data*. John Wiley & Sons, 2015.
- [20] C.V. Deutsch. *Geostatistical Reservoir Modeling*. Oxford University Press, New York, USA, 2002.
- [21] C.V. Deutsch and A.G. Journel. *GSLIB - Geostatistical Software Library and Users's Guide*. Oxford University Press, 1998.
- [22] Roscoe K. Lopez de la Cruz J. Steenbergen H. Vrouwenvelder T. Diermanse, F. Hydra Ring Scientific Documentation, Deltares Report 1206006-004. Technical report, Deltares, 2013.
- [23] ENW. Technisch rapport grondmechanisch schematiseren bij dijken. Technical report, Rijkswaterstaat, 2012.
- [24] G.A. Fenton and D.V. Griffiths. *Risk assessment in geotechnical engineering*. John Wiley & Sons, 2008.
- [25] B. Van der Meer M. FUGRO Geoservices, Berbee. Presentation pov-piping doorlatendheden. July 2nd, 2015.
- [26] C. Gascuel-Oudoux and P. Boivin. Variability of variograms and spatial estimates due to soil sampling: a case study. *Geoderma*, 62(1-3):165–182, 1994.
- [27] A. Gelman, J.B. Carlin, H.S. Stern, and D.B. Rubin. *Bayesian data analysis*. CRC press, 2004.
- [28] J.J. Gómez-Hernández and X.H. Wen. Multigaussian models: The danger of parsimony. *Statistical Methods & Applications*, 4(2):167–181, 1995.
- [29] J.J. Gómez-Hernández and X.H. Wen. To be or not to be multi-Gaussian? A reflection on stochastic hydrogeology. *Advances in Water Resources*, 21(1):47–61, 1998.
- [30] G.R.P. Van Goor and E.H.F. Vossenaar. Factual report betreffende resultaten dataverzameling in het kader van pov-piping "continue doorlatendheidsprofielen: Verdiepend inzicht in de bodem" opdrachtnummer: 1213-0101-000. Technical Report 1213-0101-000, FUGRO, January 2015.
- [31] Y.A. Hegazy, P.W. Mayne, and S. Rouhani. Geostatistical assessment of spatial variability in piezocone tests. In *Proceedings of Uncertainty in the geological environment: from theory to practice*, New York, 1996. ASCE.
- [32] M.A. Hicks and C. Onisiphorou. Stochastic evaluation of static liquefaction in a predominantly dilative sand fill. *Geotechnique*, 55:123–133, 2005.
- [33] J.A. Hoeting, D. Madigan, A.E. Raftery, and C. T. Volinsky. Bayesian Model Averaging: a tutorial. *Statistical Science*, 14(14):382–417, 1999.
- [34] M. Huber. *Soil variability and its consequences in geotechnical engineering*. PhD thesis, University of Stuttgart, 2013.
- [35] K. M. Irvine, A. I. Gitelman, and J. Hoeting. Spatial designs and properties of spatial correlation: effects on covariance estimation. *Journal of agricultural, biological, and environmental statistics*, 12(4):450–469, 2007.
- [36] E.H. Isaaks and R.M. Srivastava. *Applied geostatistics*, volume 2. Oxford University Press New York, 1989.

- [37] M. B. Jacksa. *The influence of spatial variability on the geotechnical design properties of a stiff, overconsolidated clay*. PhD thesis, The University of Adelaide, 1995.
- [38] A.G. Journel and F. Alabert. Non-gaussian data expansion in the earth sciences. *Terra Nova*, 1(2):123–134, 1989.
- [39] A.G. Journel and C.J. Huijbregts. *Mining geostatistics*. Academic Press, London, 1978.
- [40] W. Kanning. *The weakest link: spatial variability in the piping failure mechanism of dikes*. PhD thesis, TU Delft, 2012.
- [41] C.E. Koltermann and S.M. Gorelick. Heterogeneity in sedimentary deposits: A review of structure-imitating, process-imitating and descriptive approaches. *Water Resources Research*, 32(9):2617–2658, 1996.
- [42] H.B. Mann. Nonparametric tests against trend. *Econometrica: Journal of the Econometric Society*, 2:245–259, 1945.
- [43] B. Matérn, editor. *Spatial variation*, volume 36. Springer Science & Business Media, 2013.
- [44] A.B. McBratney and R. Webster. Choosing functions for semi-variograms of soil properties and fitting them to sampling estimates. *European Journal of Soil Science*, 37(4):617–639, 1986.
- [45] R.A. Olea. Sampling design optimization for spatial functions. *Journal of the international Association for Mathematical Geology*, 16(4):369–392, 1984.
- [46] J. Ortiz and C.V. Deutsch. Calculation of uncertainty in the variogram. *Mathematical Geology*, 34(2):169–183, 2002.
- [47] E. Pardo-Iguzquiza and P. Dowd. Variance–covariance matrix of the experimental variogram: Assessing variogram uncertainty. *Mathematical Geology*, 33(4):397–419, 2001.
- [48] K.-K Phoon, S.-T. Quek, and P. An. Identification of statistically homogeneous oil layers using modified Bartlett statistics. *Journal of Geotechnical and Geoenvironmental Engineering*, 120(7):649–659, 2003.
- [49] K.K. Phoon. *Reliability-Based Design in Geotechnical Engineering - Computations and Applications*. Taylor & Francis, 2008.
- [50] J.S. Piersol. Random data analysis and measurement procedures. *Measurement Science and Technology*, 11:1825, 2000.
- [51] R. Popescu. *Stochastic variability of soil properties: data analysis, digital simulation, effects on system behavior*. PhD thesis, Princeton University, 1995.
- [52] A. Raftery, F. Balabdaoui, T. Gneiting, and M. Polakowski. Using Bayesian Model Averaging to calibrate forecast ensembles. Technical Report 440, Department of statistics, University of Washington, December 2004.
- [53] N. Remy, A. Boucher, and J. Wu. *Applied geostatistics with SGeMS: A user's guide*. Cambridge University Press, 2008.
- [54] Rijkswaterstaat. Handreiking ontwerpen met overstromingskansen, OI2014v3. Technical report, RWS WVL, 2015.
- [55] B.D. Ripley. *Spatial statistics*, volume 575. John Wiley & Sons, 2005.
- [56] L. Sachs. *Angewandte Statistik*. Springer, 2002.

- [57] D. Schulze-Makuch, D. Carlson, D. S. Cherkauer, and P. Malik. Scale dependency of hydraulic conductivity in heterogeneous media. *Groundwater*, 37(6):904–919, 1999.
- [58] Hans Sellmeijer, Juliana López de la Cruz, Vera M van Beek, and Han Knoeff. Fine-tuning of the backward erosion piping model through small-scale, medium-scale and IJkdijk experiments. *European Journal of Environmental and Civil Engineering*, 15(8):1139–1154, 2011.
- [59] W Sichardt. *Das Fassungsvermögen von Rohrbrunnen und seine Bedeutung für die Grundwasserabsenkung, insbesondere für größere Absenkungstiefen*. Springer, 1928.
- [60] S. Thompson, editor. *Sampling*. New York: John Wiley and Sons, 1992.
- [61] P.H.A.J.M. van Gelder. *Stochastic methods for the risk-based design of civil structures*. PhD thesis, Delft University of Technology, 2000.
- [62] E Van Goor, G.; Vossenaar. Resultaten dataverzameling. pov-piping: Continue doorlatendheidsprofielen: Verdiepend inzicht in de bodem. 1213-0101-000. Technical report, Fugro Geoservices, Waterbouw, 2015.
- [63] E.H. Vanmarcke. *Random fields: analysis and synthesis*. MIT Press, 1984.
- [64] E.H. Vanmarcke and M. Grigoriu. Stochastic finite element analysis of simple beams. *Journal of Engineering Mechanics*, 109:1203, 1983.
- [65] VNK2. Van ruwe data tot overstromingsrisico - Handleiding ter bepaling van het overstromingsrisico van dijkringen binnen het project VNK2, Versienummer: 2.5. Technical report, RWS Waterdienst, 2013.
- [66] H. Wackernagel. *Multivariate geostatistics: an introduction with applications*. Springer Verlag, 2003.
- [67] J.F. Wang, A Stein, B.-B. Gao, and Y. Ge. A review of spatial sampling. *Spatial Statistics*, 2:1–14, 2012.
- [68] R. Webster and M.A. Oliver. *Geostatistics for environmental scientists*. John Wiley & Sons Inc., 2007.
- [69] D. Wickremesinghe and R.G. Campanella. Scale of fluctuation as a descriptor of soil variability. In *Proceedings of Conference on Probabilistic Methods in Geotech. Engrg*, pages 233–239, 1993.
- [70] D.S. Wickremesinghe. *Statistical characterisation of soil profile using in situ tests*. PhD thesis, University of British Columbia, 1989.
- [71] A Wiersma, Vonhögen, M. de Kleine, R. Hoogendoorn, S. Gruijters, D. Maljers, and V. Marges. Rapportage bepaling ondergrondparameters piping VNK2, 1203622-000-BGS-0004. Technical report, Deltares, 2011.
- [72] S.Y. Wong. *Stochastic Characterization and Reliability of Saturated Soils*. PhD thesis, Ph. D. Thesis, Manchester Centre for Civil and Construction Engineering, University of Manchester, England, 2004.
- [73] Z.J. Zhang and M.T. Tumay. Statistical to fuzzy approach toward CPT soil classification. *Journal of Geotechnical and Geoenvironmental Engineering*, 125(3):179–186, 1999.

## A Introduction to statistics

### A.1 Moments of a distribution function

Every distribution function can be characterized by different moments listed below.

First moment of distribution & mean value

$$\mu = \int_{-\infty}^{\infty} x f(x) dx = E[X] \quad (0.8)$$

Second moment of distribution & variance

$$\sigma^2 = \int_{-\infty}^{\infty} (x - \mu)^2 f(x) dx = E[(X - \mu)^2] \quad (0.9)$$

Coefficient of variation

$$COV = \frac{\sigma}{\mu} \quad (0.10)$$

Third moment of distribution & skewness

$$\gamma_1 = \frac{1}{\sigma^3} \int_{-\infty}^{\infty} (x - \mu)^3 f(x) dx = \frac{\mu^3}{\sigma^3} = \frac{E[(X - \mu)^3]}{\sigma^3} \quad (0.11)$$

Fourth moment of distribution & excess kurtosis

$$\gamma_{2,excess} = \frac{1}{\sigma^4} \int_{-\infty}^{\infty} (x - \mu)^4 f(x) dx - 3 = \frac{\mu^4}{\sigma^4} - 3 = \frac{E[(X - \mu)^4]}{\sigma^4} - 3 \quad (0.12)$$

### A.2 Distribution functions

Looking into statistical textbooks like Sachs [56] or Abramovich & Stegun [1], one can find a vast number of different probability distribution functions. According to Remy et al. [53], a distribution function should account for all information available; it provides all that is needed to quantify the uncertainty about the actual outcome of the variable  $x$ .

For example:

- probability intervals can be derived as

$$\text{Prob}\{Z \in (a, b)\} = F(b) - F(a) = \int_a^b f(z) dz. \quad (0.13)$$

- quantile values can be derived such as the 0.10 quantile or the 1st decile:

$$q_{0.10} = F^{-1}(0.10) = z - \text{outcome value such that } \text{Prob}(Z \leq q_{0.10}) = 0.10 \quad (0.14)$$

Phoon [49] as well as Baecher & Christian [4] point out the normal and the lognormal distribution function as widespread probability distribution functions in geotechnical engineering, which are explained in detail afterwards.

## A.2.1 Normal distribution function

The location of the distribution function is controlled by the mean value  $\mu$  the shape is defined by the variance  $\sigma^2$ . A normal distribution with  $\mathcal{N}(\mu=0, \sigma^2=1)$  is called the standard normal. Function  $f(x)$  is unimodal and symmetric around the point  $x = \mu$ , which is at the same time the mode (peak value of the distribution function that occurs most frequently), the median (middle value and location parameter separating the lower and upper half of the distribution) and the mean of the distribution. The inflection points of the curve occur one standard deviation away from the mean (i.e. at  $x = \mu - \sigma$  and  $x = \mu + \sigma$ ). The  $n$ -th derivative is given by  $\Phi^{(n)}(x) = (-1)^n H_n(x) \Phi(x)$ , where  $H_n(x)$  is the Hermite polynomial of order  $n$ .

$$f(x; \mu, \sigma^2) = \frac{1}{\sigma \sqrt{2\pi}} \exp\left(-\frac{(x-\mu)^2}{2\sigma^2}\right) = \frac{1}{\sigma} \Phi\left(\frac{x-\mu}{\sigma}\right) \quad (0.15)$$

The cumulative distribution function (CDF) describes probability of a random variable falling in the interval  $(-\infty, x]$ . The CDF of the standard normal distribution  $\Phi$  can be computed as an integral of the probability density function:

$$\Phi(x) = \frac{1}{\sqrt{2\pi}} \int_{-\infty}^x f(x; \mu, \sigma^2) = \frac{1}{\sigma \sqrt{2\pi}} \exp\left(-\frac{(x-\mu)^2}{2\sigma^2}\right) = \frac{1}{\sigma} \Phi\left(\frac{x-\mu}{\sigma}\right) \quad (0.15)$$

$$F(x; \mu, \sigma) = \Phi\left(\frac{x-\mu}{\sigma}\right) \quad (0.16)$$

## A.2.2 Lognormal distribution function

In probability theory, a log-normal distribution is a continuous probability distribution of a random variable whose logarithm is normally distributed. If  $X$  is a random variable with a normal distribution, then  $Y = \exp(X)$  has a lognormal distribution; likewise, if  $Y$  is log-normally distributed, then  $X = \log(Y)$  is normally distributed.

A variable might be modelled as log-normal if it can be thought of as the multiplicative product of many independent random variables each of which is positive. In a lognormal distribution  $X$ , the parameters denoted  $\mu$  and  $\sigma$  are the mean and standard deviation, respectively, of the variable's natural logarithm (by definition, the variable's logarithm is normally distributed), which means using  $Z$  as a standard normal variable.

$$X = e^{\mu + \sigma Z} \quad (0.17)$$

On a non-logarithmised scale,  $\mu$  and  $\sigma$  can be called the location parameter and the scale parameter respectively. The probability density function of a lognormal distribution is as shown in the following equation.

$$f_x(x; \mu, \sigma) = \frac{1}{x \sigma \sqrt{2\pi}} \exp\left(-\frac{(\ln x - \mu)^2}{2\sigma^2}\right) \quad x > 0 \quad (0.18)$$

The cumulative distribution function of a lognormal distribution is

$$F_x(x; \mu, \sigma) = \Phi\left(\frac{\ln x - \mu}{\sigma}\right) \quad (3.1)$$

### A.3 Multivariate normal distribution

The multivariate normal distribution of a  $k$ -dimensional random vector  $\mathbf{z} = [Z_1, Z_2, \dots, Z_k]$  of the random variables  $Z$  can be written in the following notation:

$$\mathbf{z} = \mathcal{N}_k(\boldsymbol{\mu}, \mathbf{COV}_{ZZ}) \quad (0.19)$$

with a  $k$  - dimensional mean vector

$$\boldsymbol{\mu} = [E[Z_1], E[Z_2], \dots, E[Z_k]] \quad (0.19)$$

and a  $k \times k$  covariance matrix

$$\mathbf{COV}_{ZZ} = \left[ \mathbf{COV}[Z_i, Z_j] \right], i=1, 2, \dots, k; j=1, 2, \dots, k \quad (0.19)$$

The main diagonal gives the variance and the off-diagonals are symmetrical covariances. The covariance matrix is not singular and definite. In case of a singular covariance matrix, the corresponding distribution has no density.

The probability density function  $f(\mathbf{z})$  can be written in the following form.

$$f(\mathbf{z}) = (2\pi)^{-k/2} |\mathbf{COV}_{ZZ}|^{-1/2} \exp[-1/2 (\mathbf{z} - \boldsymbol{\mu})^T \mathbf{COV}_{ZZ}^{-1} (\mathbf{z} - \boldsymbol{\mu})] \quad (0.19)$$

According to Sachs [56], no analytical expression exists for den cumulative density function.

Table A.1 Summary of the lognormal distribution

support	$x \in (0, +\infty)$
mean	$e^{\mu + \sigma^2/2}$
median	$e^\mu$
mode	$e^{\mu - \sigma^2}$
variance	$e^{\sigma^2} - 1 e^{2\mu + \sigma^2}$
skewness	$e^{\sigma^2} + 2\sqrt{e^{\sigma^2} - 1}$
excess kurtosis	$e^{4\sigma^2} + 2e^{3\sigma^2} + 3e^{2\sigma^2} - 6$

Table A.2. Summary of the normal distribution

support	$x \in \mu + \text{span}(\boldsymbol{\Sigma}) \subseteq \mathbf{R}^k$
mean	$\mu$
median	$\mu$
mode	$\mu$
variance	$\boldsymbol{\Sigma}$



## B Mathematical description of spatial correlation

This appendix provides a brief introduction into the mathematical description of spatial variability.

### B.1 Introduction

Soils are geological materials formed by weathering processes and, save for residual soils, transported by physical means to their present locations. They have been subjected to various stresses, pore fluids, and physical and chemical changes. Thus, it is hardly surprising that the physical properties of soils vary from place to place within resulting deposits. Scatter observed in soil data comes both from this spatial variability and from errors in testing. By assuming a statistically homogeneous continuum without a trend, this can be mathematically described in a smooth way by using random variables and random functions. In comparison to this, a deterministic variable can just model one outcome; this outcome is either known or unknown leaving no flexibility for uncertainty. Conversely, a *random variable* is an independent variable that can take a series of possible outcomes, each with a certain probability or frequency of occurrence. A random variable is typically denoted with the capital letter  $Z$  and its possible outcomes are denoted with the corresponding small case letter  $z_i$ ,  $i = 1, \dots, n$ . Most applications of geostatistics involve mapping, which is the joint consideration of variables at several locations in space and/or time. For this reason, random functions can be used to describe the joint spatial distribution of variables. A *random function*  $Z(\mathbf{X})$  is a set of dependent random variables, each marked with a coordinate vector  $x$ . The variable  $\mathbf{X} = (x, y, z)$  can involve space coordinates, but also both space and time as e.g. atmospheric pressure, in which case  $\mathbf{X} = (x, y, z, t)$ , which is rather unusual in geotechnical engineering in comparison to other sciences like earth sciences or meteorology [14, 15].

Using well known means of univariate statistics, one can describe these measurements using a mean value  $\mu$  and the standard deviation  $\sigma$ , a coefficient of variation  $COV = \sigma/\mu$  and a probability density function, as described in Appendix A.3. Univariate statistics is not able to describe the spatial structure of the data.

As stated by several authors [6, 14, 28, 29, 38], the simplest way of describing spatial variability is to choose the *multi-Gaussian* way. Within the multi-Gaussian approach, a random process or random field can be described by a mean value  $\mu$ , a standard deviation  $\sigma$  and a covariance function  $C$ . For  $n$  pairs of a random variable  $Z$  of two different locations  $\mathbf{X}_i$  and  $\mathbf{X}_j$ , the covariance  $C(\mathbf{X}_i, \mathbf{X}_j)$  of the random function  $Z(\mathbf{X}_i)$  and  $Z(\mathbf{X}_j)$  is given by equation (0.19). Herein,  $E$  denotes the expected value, as described in detail in the Appendix A.3.

$$C(\mathbf{X}_i, \mathbf{X}_j) = E \left[ (Z(\mathbf{X}_i) - E(Z(\mathbf{X}_i))) (Z(\mathbf{X}_j) - E(Z(\mathbf{X}_j))) \right] \quad (0.19)$$

It has to be pointed out that the means of univariate statistics are not influenced by the covariance function. The probability density function can follow e.g. a normal distribution or a lognormal distribution whether or not the investigated data have a spatial correlation. In the case of a multivariate distribution, all random variables are linked through a covariance

matrix, as defined in Appendix A.3. The basic assumptions for the description of spatial variability are as follows:

- STATIONARITY is defined as when the mean value  $\mu$  and the standard deviation  $\sigma$  are constant over the whole domain. Moreover, the covariance  $C(\tau)$  is only dependent on the separation  $\tau$  and not on the absolute position [68].
- HOMOGENEITY is defined as stationarity of the variance statistically spoken [48], which is closely linked to the definition of the stationarity.
- ERGODICITY is also closely related to stationarity. A random process is said to be ergodic, when the moments of the single observable realization in space approach those of the ensemble as the regional bounds expand towards infinity. According to Webster & Oliver [68], it is of mainly theoretical interest rather than of practical value because the regions studied in geotechnical engineering are finite.

## B.2 Variogram approach

According to Phoon [49] and Baecher & Christian [4], the most common method of estimating spatial variability is the variogram. Herein, the statistical moments of the observations (e.g. sample means, variances and covariances) are used as estimators of the corresponding moments of the population being sampled. The variogram approach is a non-parametric approach, which means that no assumptions are needed about the mathematical shape of the autocovariance function; there is only a need to assume that the second moments exist. The moment estimator is consistent and asymptotically unbiased. Therefore, it is a desirable method as stated in [4, 5, 14, 36].

The semivariance  $\gamma(\tau)$  of a random function  $Z(X)$  can be computed using equation (0.20), which is also called the empirical variogram. The lag vector  $\tau$  is generally a vector describing the mutual distance between the points. The lag vector  $\tau$  becomes a scalar  $\tau = |\tau|$  in case of an isotropic variogram. The isotropic variogram describes the spatial correlations as being the same in all directions, for which  $\hat{\gamma}(\tau)$  can be computed only at integral multiples of the sampling interval.

$$\hat{\gamma}(\tau) \equiv \frac{1}{2} E \left[ (Z(\mathbf{X}) - Z(\mathbf{X} + \tau))^2 \right] \approx \frac{1}{2 m(\tau)} \sum_{i=1}^{m(\tau)} (Z(\mathbf{X}_i) - Z(\mathbf{X}_i + \tau))^2 \quad (0.20)$$

The variogram does not require the knowledge of the mean of the random function  $Z(X)$  because the squared difference in equation (0.20) eliminates the mean value. Moreover, small variations are filtered out [14]. It has to be pointed out that the variogram approach describes the spatial dependence as an integral of the whole distribution of parameter values. The spatial correlation of the extreme values of the random function  $Z(X)$  cannot be investigated separately.

### B.2.1 Variogram calculation

The simplest case for calculating the variogram is an equally spaced dataset as shown in Figure B.1 (a). First, the squared differences between neighbouring pairs of values  $z_1$  and  $z_2$ ,  $z_2$  and  $z_3$  are determined for each position and averaged. If there are missing values at some locations, then there will be fewer neighbouring pairs as indicated in Figure B.1 (b).

If data are irregularly scattered then the average semivariance of a particular lag can be derived only by grouping the individual lag distances between pairs of points, as depicted in

Figure B.1 and as shown in equation (0.20). In typical geostatistical literature [7, 21], the classical equation of determination of the semi-variogram is

$$\hat{\gamma}(\tau) = \frac{1}{2N(\tau)} \sum_{(ij) \in R(\tau)} [Z(\mathbf{X}_i) - Z(\mathbf{X}_j)]^2 \quad (0.20)$$

where

$$R(\tau) = \{ \tau - w/2 \leq d_s(u_i, u_j) \leq \tau + w/2 \} \quad (0.20)$$

$d_s(\mathbf{X}_i, \mathbf{X}_j)$  is the spatial distance between the spatial point sets  $\mathbf{X}_i, \mathbf{X}_j$ ,  $N(\tau)$  is the number of pairs in  $R(\tau)$  and  $w$  is the width of the spatial distance class as shown in Figure B.2. The bigger the  $w$  becomes, the smoother is the semi-variogram because this filters out the very high and low values.

The variograms of second-order stationary processes reach upper bounds, at which they remain constant after their initial increases as shown in Figure B.3.

A variogram may reach its sill at a finite lag distance, in which case it has a range, also known as the correlation length; since this is the range at which the autocorrelation becomes 0 (Figure B.3). This separation marks the limit of spatial dependence. Places further apart than this are spatially independent. For practical purposes their effective ranges are usually taken as the lag distances at which they reach 95 % of their sills [14, 21, 39, 66].

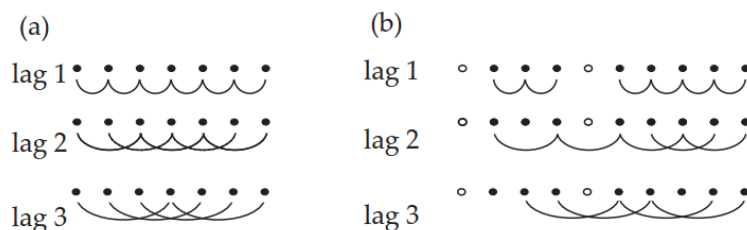


Figure B.1. Comparison for computing a variogram from a regular sampling on a transect (a) with a complete set of data, indicated with • and (b) with missing values indicated by ◦ from Huber [34].

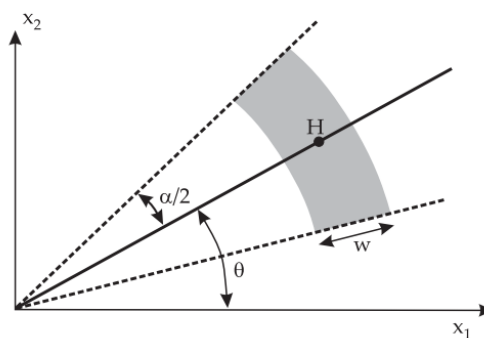


Figure B.2. The geometry for discretizing the lag into bins by distance and direction in two dimensions from [34]

## B.2.2 Theoretical variogram

It is necessary to know the variogram  $\hat{\gamma}(\tau)$  at any value of  $\tau$ , if one wants to use the variogram in terms of geostatistical simulation or interpolation. For this reason it is necessary to fulfil the continuity, the differentiability condition and the conditional positiveness as shown in detail in Chiles & Delfiner [14]. Amongst others, Gascuel-Oudou & Boivin [26] specify several sources of error: firstly only one realization is generally available in nature and it is considered as representative; also errors in the experimental variogram due to sampling and measurement must be considered; secondly, errors may result from the choice of the model and estimation of the theoretical variogram. The semivariogram has to be approximated to be able to simplify further work like e.g. performing a stochastic simulation or interpolation between measurements. For this reason, the behaviour of the variogram model has to be defined at the origin and over the entire range. Different theoretical variogram-models can be classified, according to [190], into models with a sill (bilinear model equation (0.21)), spherical variogram (linear behaviour at the origin, equation (0.22)), exponential variogram (linear behaviour at the origin, (0.23)), Gaussian variogram (parabolic behaviour at the origin, equation (0.24)), models without a sill (power functions, fractal model, logarithmic variogram). Other models like the cubic model, generalized Cauchy models, K-Bessel model, power-law model, pentaspherical model, Matern model or logarithmic model can be found in standard geostatistical textbooks [79, 190, 401, 403].

$$\gamma(\tau) = \begin{cases} \tau / a & \text{for } \tau \leq a \\ a & \text{for } \tau > a \end{cases} \quad (0.21)$$

$$\gamma(\tau) = \begin{cases} c \left\{ \frac{3\tau}{2b} - \frac{1}{2} \left( \frac{\tau}{b} \right)^3 \right\} & \text{for } \tau \leq a \\ c & \text{for } \tau > a \end{cases} \quad (0.22)$$

$$\gamma(\tau) = 1 - \exp\left(-\frac{\tau}{c}\right) \quad (0.23)$$

$$\gamma(\tau) = 1 - \exp\left(-\frac{\tau^2}{d^2}\right) \quad (0.24)$$

To compare different theoretical variogram models, it is necessary to fit theoretical variogram models in a standard way and automatically to the sample variogram in order to avoid judgement errors. In the course of a detailed geostatistical analysis, an automatic fit rarely provides definitive results. Chiles & Delfiner [14] as well as Deutsch & Journel [21] point out that this can be only the first step of a manual fit. Generally, we look for a variogram  $\gamma(\tau_j; \mathbf{b})$  where  $\mathbf{b}$  represents a vector of the parameters of the variogram (e.g. range, sill, nugget effect, ...) of  $n$  available pairs of data. This vector  $\mathbf{b}$  can be evaluated by minimizing the following equations. A compromise between efficiency and simplicity is the weighted least squares, namely the minimization of  $Q(\mathbf{b})$ :

$$Q(\mathbf{b}) = \sum_{j=1}^n w_j^2 \left[ \hat{\gamma}(\tau) - \gamma(\tau_j; \mathbf{b}) \right]^2 \quad (0.24)$$

Herein,  $w$  is the weight, which can be the reciprocal of the number of pairs at each lag, as proposed by Matheron [240] or also the variance at each point, [14, 46]. The variance-covariance matrix  $\mathbf{V}$  in equation (0.24) can be used to calculate the variance of the variogram.

The expression (0.24) tells us that the uncertainty in the variogram at a distance  $\tau$  is the average covariance between the pairs of the pairs used to calculate the variogram for that particular lag  $\tau$  assuming a multivariate Gaussian distribution of the variables.

$$\mathbf{w} = \frac{1}{\sigma_{2\gamma(\tau)}^2} = n(\tau) / \sum_{i=1}^{n(\tau)} \sum_{j=1}^{n(\tau)} V_{ij}(\tau) \quad (0.24)$$

$$\mathbf{V}(\tau) = E \left\{ \left[ Z(\mathbf{X}_i) - Z(\mathbf{X}_i + \tau) \right]^2 \cdot \left[ Z(\mathbf{x}_j) - Z(\mathbf{X}_j + \tau) \right]^2 \right\} - [2 \hat{\gamma}(\tau)]^2$$

Herein,  $\hat{\gamma}(\tau_j)$  is the vector of the empirical variogram,  $\mathbf{V}$  is the variance-covariance matrix of  $\hat{\gamma}(\tau)$ . The calculation of the variance covariance matrix is rather complicated as highlighted by Ortiz & Deutsch [46]. There are different approaches for choosing the weights  $\mathbf{w}$ . Cressie [87] shows that for equally spaced Gaussian variables, the variance of the estimates can be approximated by equation (0.24):

$$\mathbf{w} \approx \frac{N(\tau)}{2[\hat{\gamma}(\tau)]^2} \quad (0.24)$$

where  $\hat{\gamma}(\tau)$  is the value of the theoretical variogram and  $N(\tau)$  is the number of pairs at a mutual distance of  $\tau$ . It is argued by several authors [14, 18, 47] that this estimation is too crude to construct confidence intervals. McBratney & Webster [44] redefined this further:

$$\mathbf{w} \approx \hat{\gamma}^3(\tau) / m(\tau) \hat{\gamma}(\tau)^2 \quad (0.24)$$

where  $\hat{\gamma}(\tau)$  is the observed value of the semivariance at  $\tau$ . This is usually desirable for kriging, though it might be less desirable if the aim is to estimate the spatial scale of variation. The process of fitting must iterate even where all the parameters are linear because the weights in the two schemes depend on the values expected from the model.

### B.2.3 Model selection using the AKAIKE Information criterion

The selection of the most appropriate model is done via the AKAIKE INFORMATION CRITERION. (AIC) [2], which is defined for a finite sample set  $n$ :

$$AIC = 2k - 2 \ln(L) \quad (0.24)$$

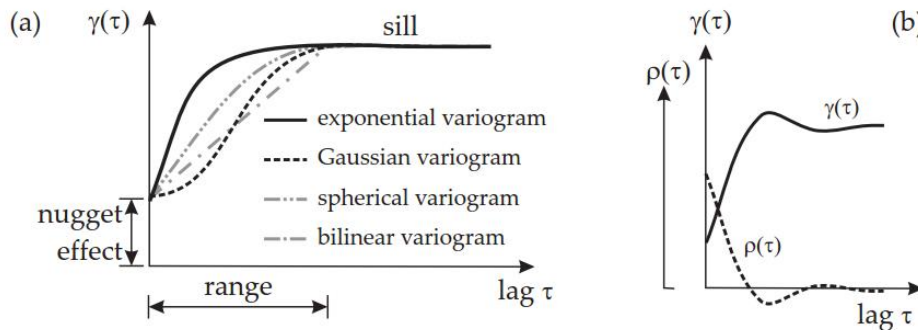


Figure B.3 Theoretical variogram functions (a) and comparison of the semivariance function and autocorrelation function (b)

where  $k$  is the number of parameters in the statistical model, and  $L$  is the maximum value of the likelihood function for the estimated model. The first term is a measure of the quality of fit of a model and the second is a penalty factor for the introduction of additional parameters into the model.  $AIC$  is a measure of the loss of information incurred by fitting an incorrect model to the data. Therefore, given a set of different models for the data, the preferred model is the one with the minimum  $AIC$  value. Hence  $AIC$  not only rewards goodness of fit, but also includes a penalty that is an increasing function of the number of estimated parameters. This penalty discourages overfitting. The preferred model is the one with the lowest  $AIC$  value. Assuming that the model errors are normally and independently distributed, the  $AIC$  can be rewritten for a fitting by least squares. Herein, the residual sum of the squares ( $RSS$ ) are defined:

$$AIC = 2k - n [ \ln( 2\pi RSS / n ) + 1 ]$$

$$RSS = \sum_{i=1}^n \varepsilon_i \quad (0.24)$$

where  $k$  is the number of parameters in the statistical model, and  $L$  is the maximum value of the likelihood function for the estimated model. The first term is a measure of the quality of fit of a model and the second is a penalty factor for the introduction of additional parameters into the model. One can clearly see by looking at equations (0.24) that for a big sample size  $n$  the  $AIC$  is independent of  $n$ . Alternatively, different information criteria amongst others like  $BIC$  or  $KIT$  can be used for small sample sizes or other boundaries, which is described in detail in literature [3, 11, 68].

### B.3 Maximum likelihood method

The Maximum Likelihood (ML) method of estimating the unknown parameters  $\Theta$  is a parametric method assuming that the distribution of the data is known. ML takes the value of  $\hat{\Theta}$  as an estimate of the unknown parameters  $\Theta$  that provides the greatest probability of having measurements  $Z$ , as calculated from the joint probability distribution of the observations conditioned on  $\hat{\Theta}$ . The possible outcomes  $z(X)$  of the random function  $Z(X)$  with mean value  $\bar{z}$  and covariance matrix  $\mathbf{C}_{ZZ}$  are assumed to be described by a  $n$ -dimensional multivariate normal distribution in equation 2.13.

$$f_{\mathbf{z}}(\mathbf{z}) = \frac{1}{\sqrt{(2\pi)^n |\mathbf{C}_{\mathbf{ZZ}}|}} \exp\left[-\frac{1}{2}(\mathbf{z} - \bar{\mathbf{Z}})^T \mathbf{C}_{\mathbf{ZZ}}^{-1} (\mathbf{z} - \bar{\mathbf{Z}})\right] \quad (0.24)$$

The covariance matrix  $\mathbf{C}_{\mathbf{ZZ}}$  contains the values of the auto-covariance function  $C(\mathbf{Z}_i, \mathbf{Z}_j)$  of each possible pair of measurements. Selecting the unknown parameters in a vector  $\Theta = [\bar{Z}, \sigma_r, \theta_h, \theta_v]^T$  the log-likelihood for  $\Theta$  is given in equation (0.24).

$$L(\Theta | \mathbf{z}) = -\frac{n}{2} \ln(2\pi) - \frac{1}{2} \ln |\mathbf{C}_{\mathbf{ZZ}}| - \frac{1}{2} (\mathbf{z} - \bar{\mathbf{Z}})^T \mathbf{C}_{\mathbf{ZZ}}^{-1} (\mathbf{z} - \bar{\mathbf{Z}}) \quad (0.24)$$

By maximizing the likelihood, the optimal parameter set  $\Theta$  can be obtained by standard optimization strategies, for example the simplex method. The advantage of the simplex algorithm is that the results are independent of the initial parameters, hence only depending on data.

De Groot & Baecher [90] state that the maximum likelihood estimator parameters  $\Theta$  are asymptotically jointly normally distributed:

$$\hat{\Theta} \sim \mathcal{N}(\Theta, \mathbf{B}^{-1}) \quad (0.24)$$

where the information matrix  $\mathbf{B}$  can be obtained as

$$\mathbf{B} = \text{diag}(B_{\bar{Z}}, \mathbf{B}_{\Theta}) \quad (0.24)$$

where  $\Theta = [\sigma_r, \theta_h, \theta_v]^T$  is a vector containing the parameters of the theoretical variogram model. The entries of the information matrix are given in [90] as follows:

$$B_{\bar{Z}} = \mathbf{1}^T \mathbf{C}_{\mathbf{ZZ}}^{-1} \mathbf{1} \\ B_{\Theta_{ij}} = \frac{1}{2} \text{tr} \left( \mathbf{C}_{\mathbf{ZZ}}^{-1} \frac{\partial \mathbf{C}_{\mathbf{ZZ}}}{\partial \Theta_i} \mathbf{C}_{\mathbf{ZZ}}^{-1} \frac{\partial \mathbf{C}_{\mathbf{ZZ}}}{\partial \Theta_j} \right) \quad (0.24)$$

where  $\mathbf{1}$  is a unit vector of length  $n$ . Using the information matrix  $\mathbf{B}$ , the accuracy of the obtained parameters is estimated.

#### B.4 On the correlation length

Within the description of spatial variability one has to distinguish between the correlation length and its related model parameters. The definition of the correlation length was introduced by Vanmarcke [63], which is referred to by other authors [5, 12, 24, 32, 37, 51, 72]. They often call it scale of fluctuation.

Vanmarcke [63] defines the correlation length  $\theta$  as distance within which points are significantly correlated (i.e. by more than about 10 %) by the correlation function  $\rho(\tau)$ , which can be e.g. an exponential decaying function. Conversely, two points separated by a distance more than  $\theta$  will be largely uncorrelated.

$$\theta = \int_{-\infty}^{\infty} \rho(\tau) d\tau = 2 \int_0^{\infty} \rho(\tau) d\tau \quad (0.24)$$

The correlation length is defined without the factor of 2 shown to the right-hand side of equation (0.24) especially in the geostatistical literature e.g. Journel & Huijbregts [39]. Another consequence for the application in engineering sciences as well as in earth sciences is that the correlation function is only meaningful for strictly non-negative correlation functions.

### B.5 Uncertainty of the correlation length

In [14, 68], the uncertainty of the correlation length is connected with the application e.g. spatial interpolation or (geostatistical) simulation. Within the concept of interpolation, cross-validation is used to investigate the influence of the correlation length, as described in detail in Webster & Oliver [68].

As mentioned above, different sources like measurement and modelling errors (statistical model, nested structures, ... etc.) cause an uncertainty of the evaluated correlation length. Focusing on the variogram approach, the main source of uncertainty is the definition of the distance and direction classes. In the case of too wide classes, the resulting variogram will be smoothed too much, whereas in the other case the variogram will be too *noisy*. As pointed out above, several authors express the uncertainty of the correlation length via the experimental variogram  $\hat{\gamma}(\tau)$  to calculate the variance and the correlations of the values of the experimental variogram  $\hat{\gamma}(\tau)$ . Herein, they use an approximation of the variance-covariance matrix of the experimental variogram by assuming a normal distribution for the variance-covariance matrix, which is difficult to verify in any application. The variances of  $\hat{\gamma}(\tau)$  can be used as weights for fitting the theoretical variogram to the values of the experimental variogram. This offers also a link to the uncertainty of the correlation length.

In the Maximum Likelihood approach, the assumption of normal distributed variables is governing the whole evaluation of the correlation length. The estimation of the uncertainty of the evaluated spatial correlation is a by-product of the ML procedure as shown in equation (1.14). Via these equations it is possible to estimate the error of the estimated variogram model-parameters and consequently also of the correlation length.

### B.6 Anisotropy of the correlation length

Following the introduction to geostatistics presented in Chiles & Delfiner [14], Deutsch & Journel [21] and Wackernagel [66], one will encounter the anisotropy in the spatial correlation of measurement data. Anisotropy, being defined as the ratio of horizontal  $\theta_{hor}$  and vertical correlation length  $\theta_{ver}$ , can be classified in zonal and horizontal-to-vertical anisotropy.

*Zonal anisotropy* is related to stratification. This implies that the sill value of the horizontal and vertical variogram are different, which can be attributed to different sample distributions. Deutsch [96] points out the importance of the conceptual geological model to describe this in detail. *Horizontal-to-vertical* anisotropy can be related to the geological processes which formed the investigated statistically homogeneous layer. Different anisotropy ratios from literature [5, 14, 21, 20, 34, 39, 41, 72, 66] are summarized in Table B.1. Most of these sources are from geostatistics as well as from petroleum engineering. Therefore, the names of the different categories in table 2.5 come from engineering geology and petroleum engineering. It can be deduced from table 2.5 that the bigger the geological process is the bigger will be the anisotropy ratio  $\theta_{hor}/\theta_{ver}$ . The anisotropy ratios range from  $\theta_{hor}/\theta_{ver} = 10:1$  up to  $1,000:1$ . Therefore, it can be concluded that it is of major importance to set up a conceptual geological model before working on the spatial variability.

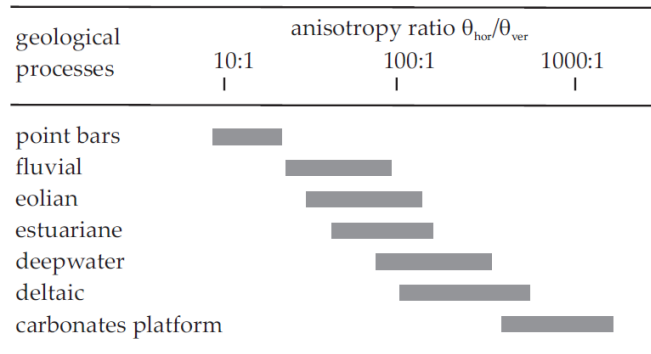


Table B.1. Typical ratios of the horizontal  $\theta_{hor}$  and vertical correlation lengths  $\theta_{ver}$  collected from literature [5, 14, 21, 20, 34, 39, 41, 72, 66].



## C Theoretical background on the evaluation of the vertical spatial correlation

This section provides the theoretical background for the evaluation of the vertical spatial correlation.

To apply the theory to evaluate the spatial variability, one has to check the basic assumptions of this theory in order to use the variogram and the ML approaches. If a trend is not removed from the measurement data, the evaluation of the correlation lengths is more difficult or even impossible. Therefore, a selection of techniques to identify and test measurement data on stationarity and homogeneity are presented in this section.

*Stationarity* can be defined by a constant mean value and variance within the test data. Various authors have proposed techniques for detecting the stationarity of the data. Only some are enlightened in this section. More background can be found in literature like [9, 10, 37].

In the present study we tested the significance of a trend using the Mann-Kendalls'  $\tau$ , which is a smooth way to detect stationarity of measurements within a non-parametric method [42]. The Mann-Kendall test is based on the statistics  $S$ . Each pair of observed values  $y_i, y_j (i > j)$  is inspected to find out whether  $y_i > y_j$  or  $y_i < y_j$ . Let the number of the former type of pairs be  $P$ , and the number of the latter type of pairs be  $M$ . Then  $S$  is defined as

$$S = P - M \quad (0.25)$$

For  $n > 10$ , the sampling distribution of  $S$  is as follows.  $Z$  follows the standard normal distribution, where

$$Z = \begin{cases} (S - 1)\sigma_s & \text{if } S > 0 \\ 0 & \text{if } S = 0 \\ (S + 1)\sigma_s & \text{if } S < 0 \end{cases} \quad (0.26)$$

$$\sigma_s = \sqrt{\frac{n(n-1)(2n+5)}{18}}$$

The null hypothesis that there is no trend is rejected if the computed  $Z$  value is greater than  $Z_{\alpha/2}$  in absolute value. Herein, the significance  $\alpha = 1\%$  is chosen according to [50]. After identifying the trend via the described approaches, the least squares method [8] is used to fit a linear trend to the data as recommended by [4, 49].

After removing the trend of the measurement data by fitting a linear function by least squares, one has to check the data on homogeneity. This can be done by expert judgement; but also statistical can support this judgement on a mathematical basis.

Homogeneity can be defined as stationarity of the variance as presented in [48, 56]. The intra-class correlation coefficient and the Bartlett statistics are used herein for checking the homogeneity of the measurements.

## C.1 Intra-class correlation coefficient

The intra-class correlation coefficient  $RI$  is reported as a useful statistical method for detecting layer boundaries using CPT soundings, Wickremesinghe [69]. The  $RI$  profile is generated by moving two continuous windows containing  $m$  data points each over a measurement profile and computing the following index at the centre of the double window.

$$RI = 1 / \left( 1 + \frac{1}{(m-1)/m + (\hat{\mu}_1 - \hat{\mu}_2)^2 / 2 / (\hat{s}_1^2 + \hat{s}_2^2)} \right) \quad (0.27)$$

Basically, ergodicity of the mean value and the variance within the moving window is assumed. This is only valid for symmetric distributions according to various authors [73]. The critical  $RI$  value  $RI_{crit}$  is estimated according to Hegazy et al. [31]. The boundaries are identified quantitatively at locations where  $RI$  exceeds the empirical relationship of the mean  $\mu_{RI}$  and standard deviation  $\sigma_{RI}$  of the  $RI$  profile:  $RI_{crit} = \mu_{RI} + 1.65 \sigma_{RI}$ ; it is recommended to check the computed results visually and to judge the evaluated soil layer. The critical  $RI_{crit}$  according to Hegazy et al. [31] is slightly higher than the recommendation of Zhang & Tumay [73]  $RI_{crit} = 0.70$ , which is also an empirical rule. Others [31, 73] also point out that the choice of  $RI_{crit}$  does not seem to depend on the underlying correlation structures of the profile, which is also discussed by Phoon et al. [48].

## C.2 Bartlett statistics

This classical test is used to test the equality of multiple sample variances for independent data sets.

This has not to be taken into account in this case study because a normal distribution function can be fitted to the residuals of the CPT/HPT measurements.

For the case of two sample variances,  $s_1^2$  and  $s_2^2$ , the Bartlett test statistic reduces to:

$$B_{stat} = \frac{2.30295(m-1)}{1 + 2/(1(m-1))} \left[ 2 \log s^2 - (\log s_1^2 + \log s_2^2) \right] \quad (0.28)$$

where  $m$  is the number of data points used to evaluate  $s_1^2$  and  $s_2^2$ . The total variance  $s^2$  is defined as:

$$s = \frac{s_1^2 + s_2^2}{2} \quad (0.29)$$

While using the Bartlett statistics, one has to keep in mind that this procedure is very sensitive to non-normally distributed and skewed variables. According to Sachs [56], he implies that in the case of a small deviation from the symmetric normal distribution, the procedure will not offer reliable results. Especially in the presence of a skewness  $\gamma_1 \neq 0$  ( $\text{kN/m}^2$ )<sup>3</sup> and an

excess kurtosis  $\gamma_{2,excess} \neq 0 (\text{kN/m}^2)^4$ , which can be observed very often in the case of measurement data.

A continuous Bartlett statistic profile can be easily generated by moving a sampling window over the simulated soil profile. Campanella et al. [12] as well as Wickremesinghe [70] recommend a window width of approximately the scale of fluctuation in the layer. This is also pointed out by Phoon et al. [48]. This implies an iterative approach. The sampling window is divided into two equal segments and the sample variance  $s_1^2$  and  $s_2^2$  is calculated from data points lying within each segment.

The Bartlett statistic basically indicates the difference between the sample variances in these two adjacent segments. As shown in equation (2.5), the Bartlett statistic is zero, if  $s_1^2$  and  $s_2^2$  are equal. Phoon et al. [48] offer a critical value  $B_{crit}$  under the framework of the *modified Bartlett statistics* taking into account the spatial correlation using an exponential model. Herein,  $I_1 = n/k$  ranges between 5 and 50 and  $I_2 = m/k$  where  $k$  is the number of points in one scale of fluctuation;  $n$  is the total number of points in the entire soil record and  $m$  is the number of points in one sampling window.

$$B_{stat,crit} = (0.23k + 0.71) \log(I_1) + 0.91k + 0.23 \quad (0.30)$$

This critical value  $B_{crit}$  is calculated for every layer to take the different correlation lengths into account. The lowest critical value  $B_{crit}$  is used for the whole CPT profile. In Figure 3.5 the detrended measurement data are used to evaluate the  $RI$  as well as the Bartlett statistics. The width of the sampling window is chosen as big as the correlation length. The critical values  $RI_{crit}$  and  $B_{crit}$  indicate the boundary between both soil layers.

### C.3 Comparison of the intra-class correlation coefficient and the Bartlett statistics

Both concept are described in literature to detect the soil layer boundaries. However, by studying Figure 3.5, one can see that the Bartlett statistics (Figure 3.5 b) shows better agreement with the indicative soil classification (Figure 3.5 d) than the intra class correlation coefficient, which is also reported by Huber [34].

### C.4 Bayesian model averaging

One can clearly see in Figure C.1 and Figure C.2 that the variogram and ML approaches offer comparable results. This can be deduced from the nearly symmetric distribution of the residual values shown in in Figure C.1 and Figure C.2 because there is only a very small skewness of the measurement data. These two probability density functions of the variogram and ML approaches are equally probable and can be merged by using the so called Bayesian model averaging (BMA) scheme [33, 52], which is based on the Bayes' theorem.

The Bayes' theorem updates a subjective, prior probability distribution  $f(\theta)$  with a likelihood function  $L(\theta | z_1, z_2, \dots, z_n)$ , which is the conditional probability function of  $z_1, z_2, \dots, z_n$  e.g. measurement values.

$$f(\theta | z_1, z_2, \dots, z_n) \propto f(\theta) \cdot L(\theta | z_1, z_2, \dots, z_n) \quad (0.31)$$

The resulting posterior pdf  $f(\theta | z_1, z_2, \dots, z_n)$  of the variable of interest  $\theta$  is conditioned on the prior probability  $f(\theta)$  and on the Likelihood function  $L(\theta | z_1, z_2, \dots, z_n)$ , [13, 61, 27].

If  $\theta$  is the quantity of interest, then its posterior distribution given data  $D$  is

$$P(\theta | D) = \sum_{k=1}^K P(\theta | M_k, D) \cdot P(M_k | D) \quad (0.32)$$

This is an average of the posterior distributions under each of the models considered, weighted by their posterior model probability. In equation (0.32)  $M_1, M_2, \dots, M_k$  are the models considered. The posterior probability for the model  $M_k$  is given by

$$P(M_k | D) = \frac{P(D | M_k) \cdot P(M_k)}{\sum_{l=1}^K P(D | M_l) P(M_l)} \quad (0.33)$$

where

$$P(D | M_l) = \int P(D | \theta_k, M_k) P(\theta_k | M_k) d\theta_k \quad (0.34)$$

is the integrated likelihood of model  $M_k$ ,  $\theta_k$  is the vector of parameters of model  $M_k$ ,  $P(\theta_k | M_k)$  is the prior density of  $\theta_k$  under model  $M_k$ , is the likelihood and  $P(M_k)$  is the prior probability that  $M_k$  is the true model under the assumption that one of the models considered is true. All probabilities are implicitly conditional on the set of all models being considered.

Hoeting et al. [33] report that BMA presents several difficulties: the specification of the prior distribution over competing models has to be carried out with attention. Another fundamental task is to choose the models over which the averaging can be performed; one of the most challenging tasks is the evaluation of the integral in equation (0.34). Within [13, 33, 52, 61], it is recommended to use Markov Chain Monte Carlo methods to evaluate this integral for the very general combination of different functions. In the simple case of the combination of two (log)normal distribution functions equation (0.34) can be solved by numerical integration, [61].

The combination of the two distribution functions using BMA is shown in Figure C.1 and Figure C.2. The resulting distribution function has a lower variance as well as a lower mean value of the correlation length. Via BMA all information from the two different models (variogram and ML) have been incorporated and this higher level of information is leading to a significant reduction of the coefficient of variation of the combined pdf. In addition to the probability density functions, also the lower and upper bound of the 95% confidence interval are given, which shall help the reader to get a feeling for the presented results.

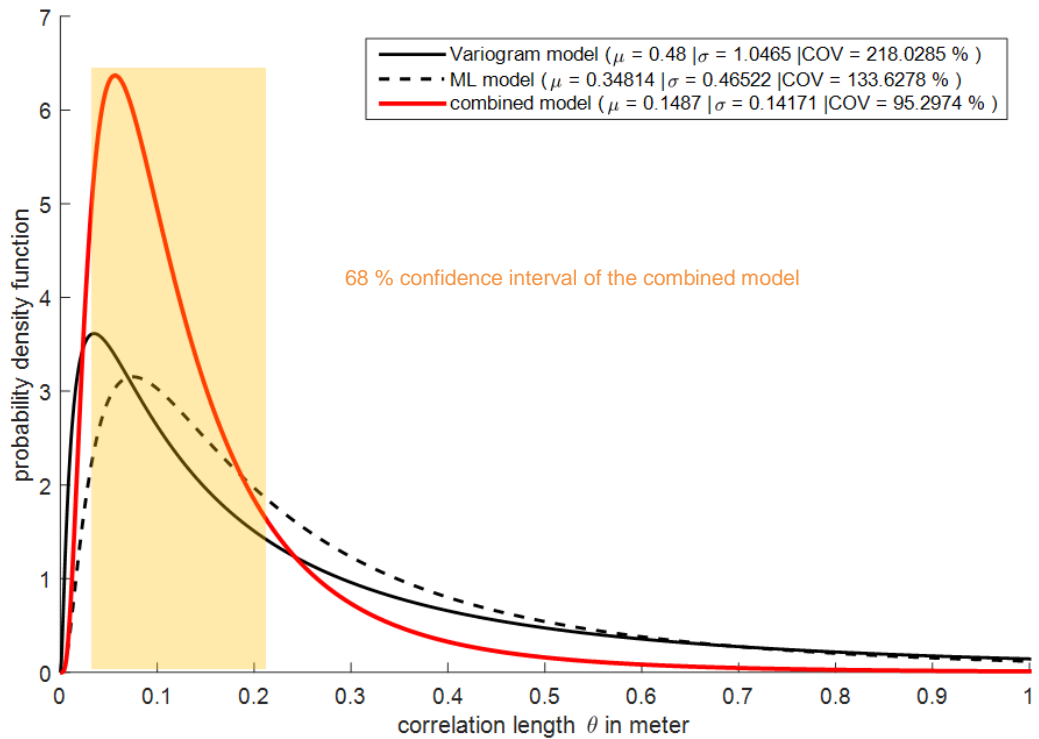


Figure C.1 Vertical correlation length of the CPT cone resistance using the variogram and ML together with the combined results

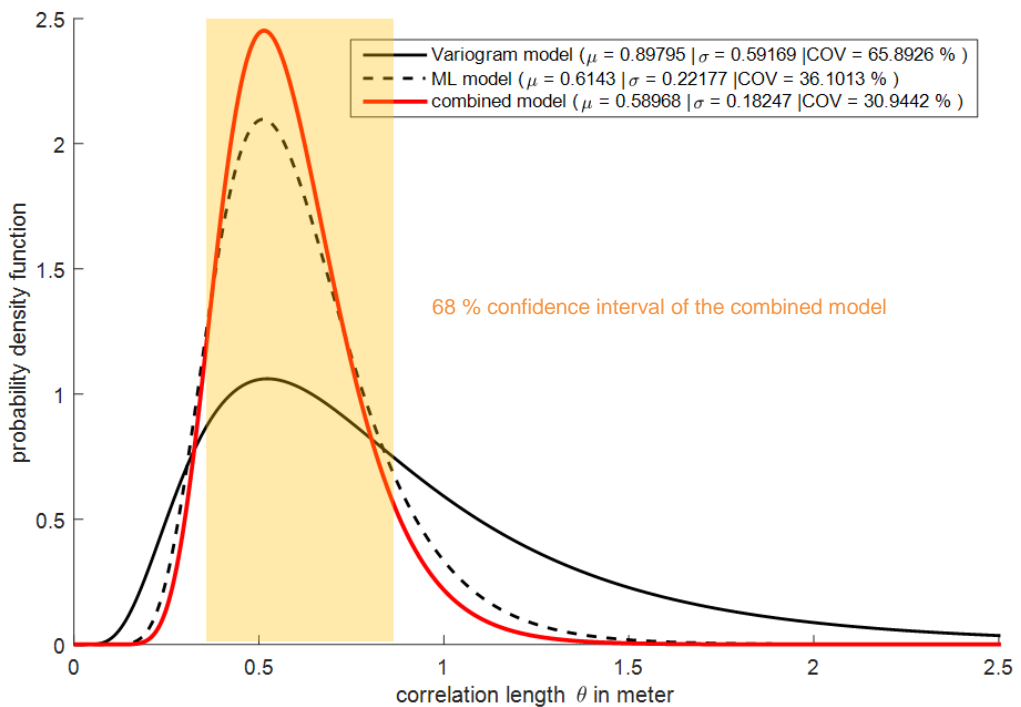


Figure C.2 Vertical correlation length of the Q/P relation from the HPT using the variogram and ML together with the combined results



## D Sampling plans

This appendix summarizes the findings of a literature study on sampling concepts of measurement data, which are spatially correlated.

### D.1 Introduction

Many books are available on sampling theory, and more complete discussions are available in [4, 14, 16, 17, 19, 43, 55, 60]. According to [4], an estimator is a sample statistic that can be used to estimate true population parameters. It can be chosen on different probability density functions, but individual estimators seldom satisfy all the desired criteria simultaneously. An estimate is the realization of a particular estimator for a specific set of sample observations. Estimates are not exact. Uncertainty is reflected in the variance of their distribution about the true parameter value to be estimated. This variance is, in turn, a function of both the sampling plan and the sampled population. By knowing this variance and making assumptions about the distribution shape, confidence limits on true population parameters can be set.

A sampling plan is a program of action for collecting data from a sampled population. Common plans are grouped into many types: for example, simple random, systematic, stratified random, cluster, traverse, line intersects, and so on. Three typical sampling schemes are shown in Figure D.1. In deciding among plans, or in designing a specific program once the type plan has been chosen, one attempts to obtain the highest precision for a fixed sampling cost or the lowest sampling cost for a fixed precision.

### D.2 Common spatial sampling plans

The characteristic property of *simple random sampling* is that individual observations is chosen at random from the sampled population, and each element of the sampled population has an equal probability of being observed.

In *systematic sampling* the first observation is chosen at random, and subsequent observations are chosen periodically throughout the population. For example, grid sampling is a systematic plan.

A heterogeneous population can sometimes be divided into subpopulations that are internally homogeneous. For each homogeneous subpopulation, usually called a stratum precise estimates of stratum characteristics can be obtained by random sampling. Estimates of the total population characteristics can then be made by combining the individual stratum estimates. For certain populations, stratifying before sampling is more efficient than taking samples directly from the total population. Sampling plans that specify a simple random sample in each stratum are called *stratified random sampling plans*.

In *cluster sampling*, aggregates or clusters of elements are selected from the sampled population as units rather than as individual elements, and properties of the clusters are determined. From the properties of the clusters, inferences can be made on the total sampled population. Plans that specify to measure every element within clusters are called single-stage cluster plans, since they specify only one level of sampling; plans that specify that cluster properties be estimated by simple random sampling are called two-stage cluster plans, since they specify two levels of sampling.

The literature addressing statistical aspects of estimating autocovariance functions or variograms from data is not extensive. Most texts on geostatistics quickly pass over the

estimation of the spatial correlation based on intuitive plotting of sample moments and quickly move on to Kriging and other applications of the variogram. The question here is how to design a sampling plan for estimating the spatial correlation. The answer follows the results of Baecher & Christian [4]. They carried out a series of simulation experiments to investigate the properties of maximum likelihood estimators of the spatial correlation being quantified by the correlation length.

In comparing different sampling plans, at least two criteria of optimality might be considered: the quality of the estimates of trend and autocovariance function, and the quality of interpolations using e.g. Kriging.

Olea [45] studied this as well and concluded that for spatial interpolation with known variograms, systematic spatial samples were superior to other sampling plans in the sense of minimizing the variance of interpolations, and that cluster plans fared the worst. However, Baecher & Christian [4] conclude that for estimating the spatial correlation either nested or cluster plans fared better, and gridded plans fared less well. These findings are supported by other researchers as well [35, 67, 68]. Additionally, Webster & Oliver [68] investigated a special type of clustered sampling schemes called hierarchical sampling.

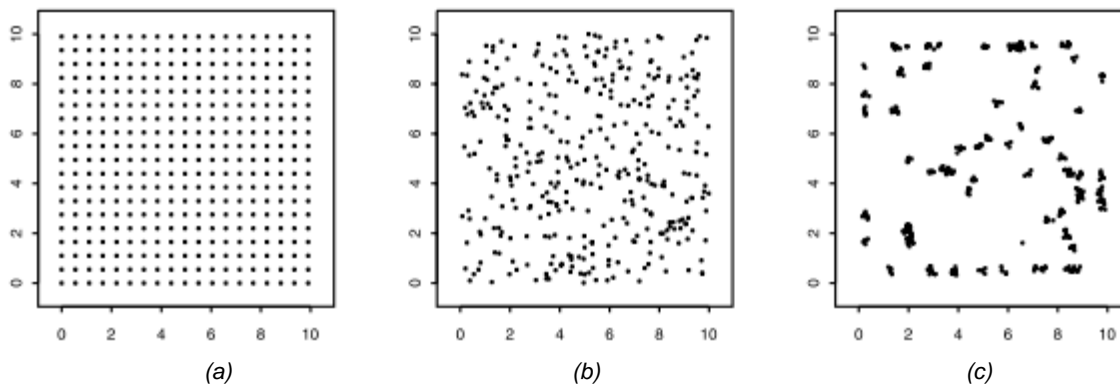


Figure D.1 Examples for a systematic (a), a random (b) and a clustered sampling plan from [68]

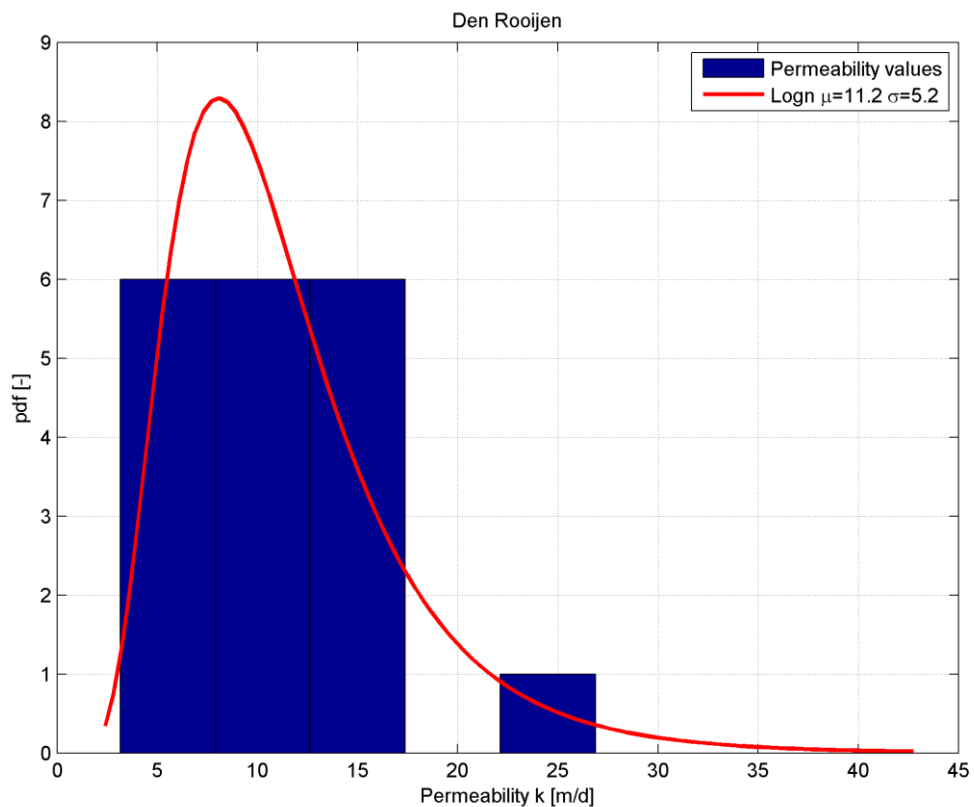
## E Statistical properties and correlation length of the permeability measurements

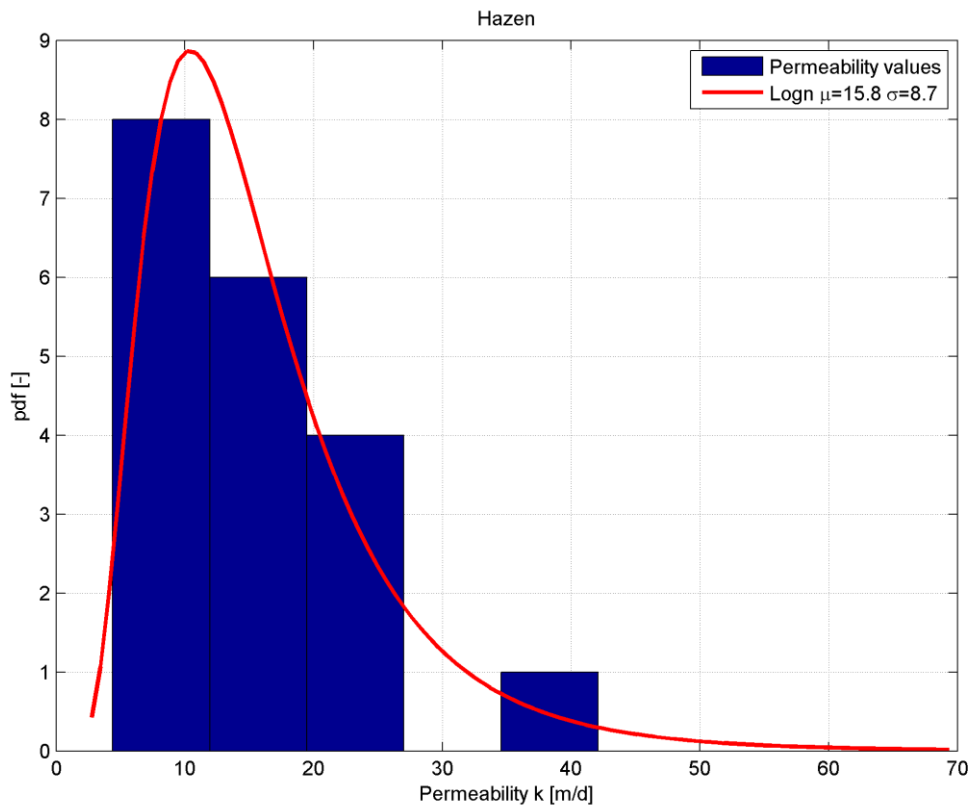
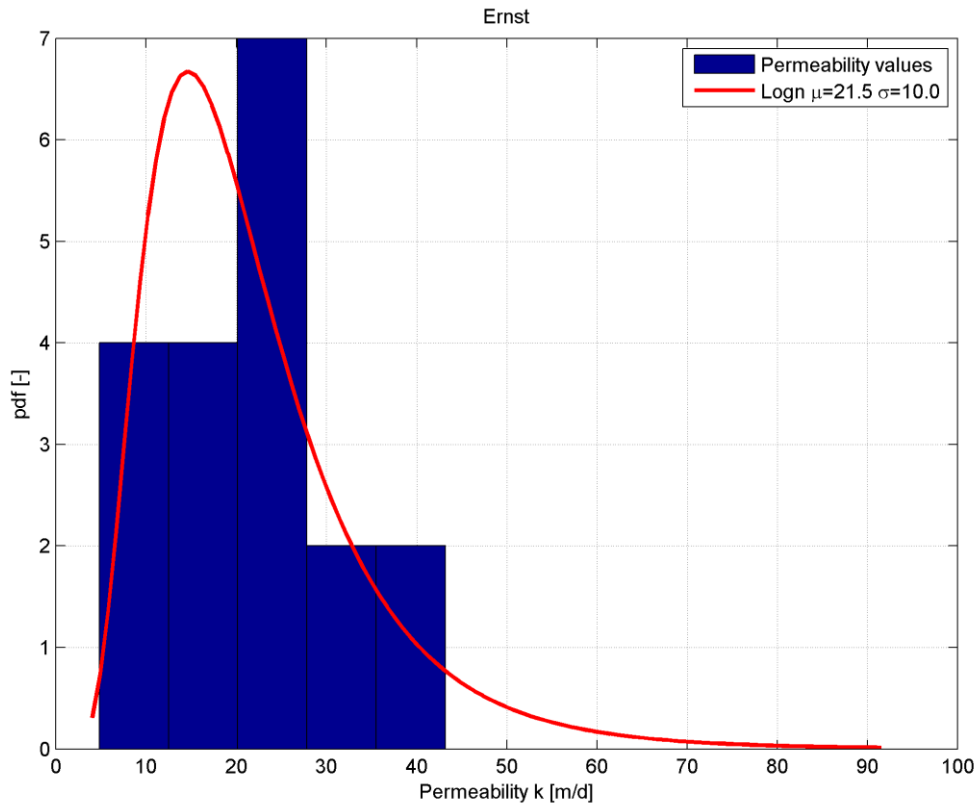
### E.1 Introduction

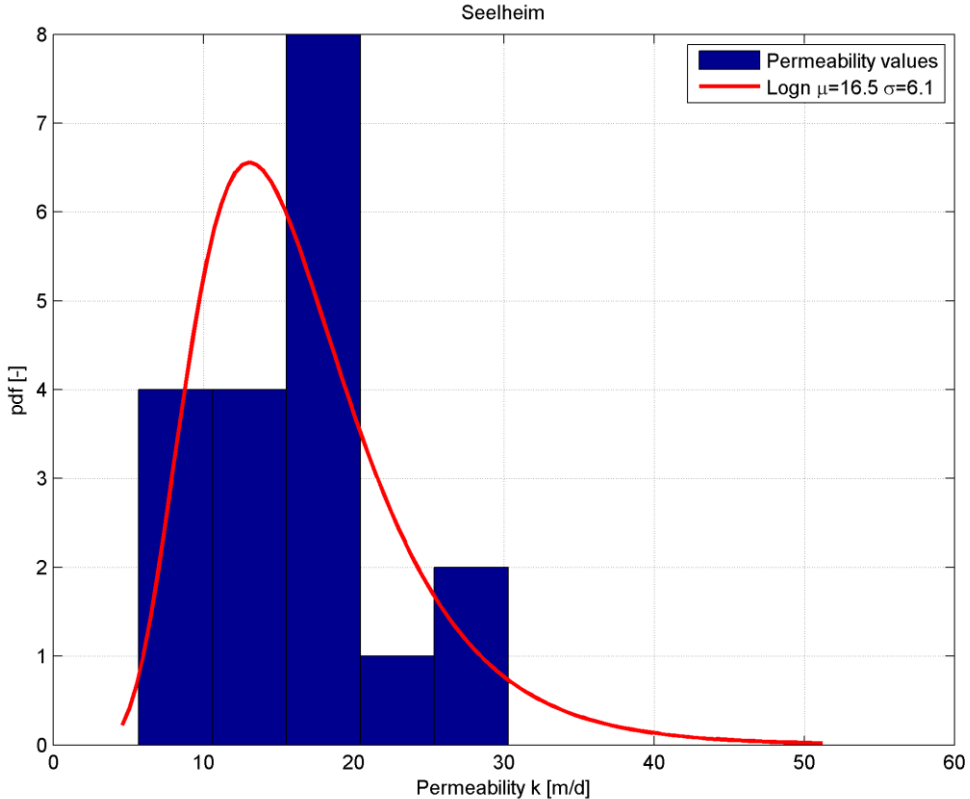
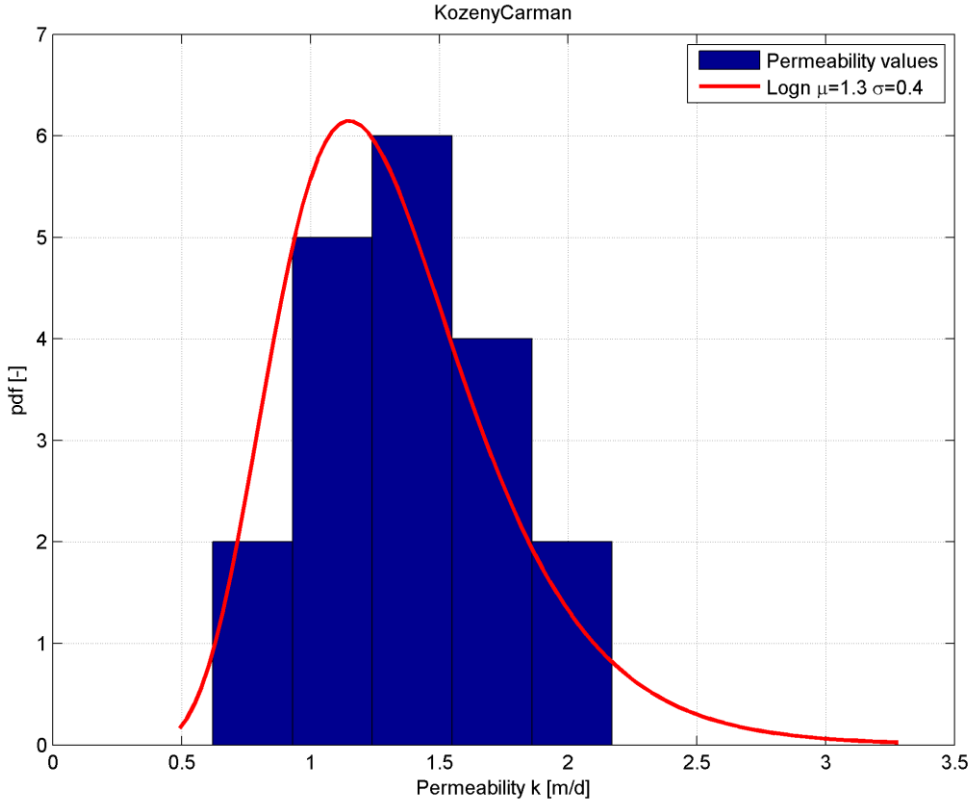
This appendix gives the results of the statistical analysis (mean value, standard deviation, coefficient of variation, horizontal correlation length and coefficient of variation of the horizontal correlation length) as tables and as figures. The Maximum Likelihood is used to estimate mean value, standard deviation and horizontal correlation length.

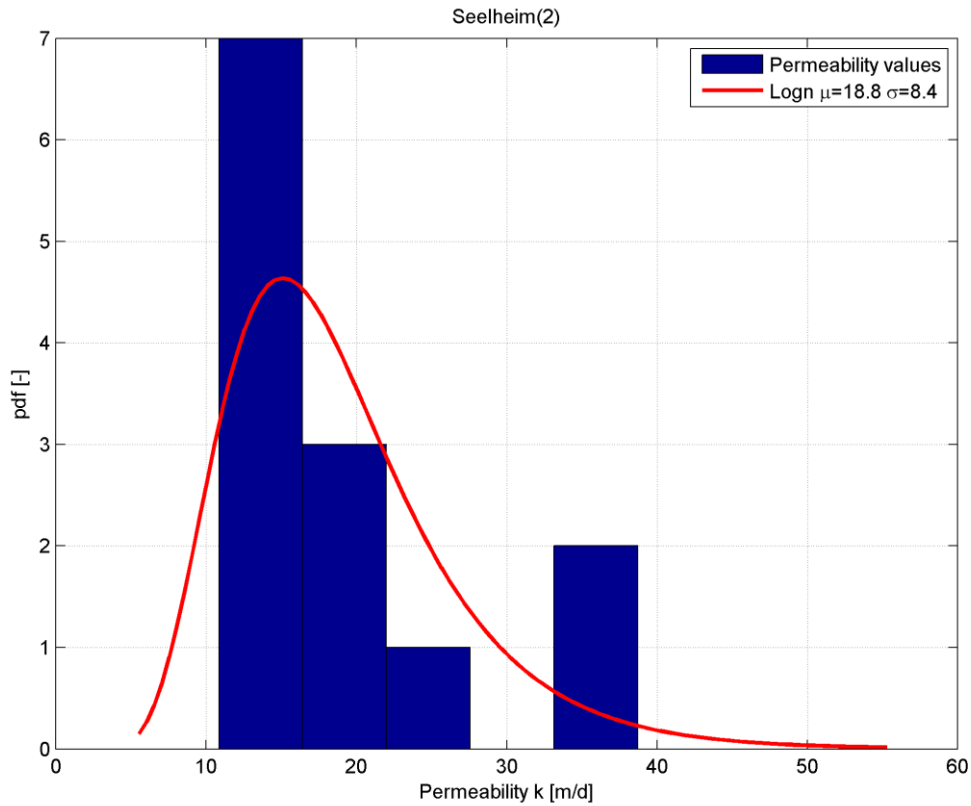
### E.2 Empirical correlations from 20 sieve curves

Permeability	Den Rooijen	Ernst	Hazen	Kozeny-Carman	Seelheim	Seelheim2
$\mu$ [m/day]	11.2	21.5	15.8	1.3	16.5	18.8
$\sigma$ [m/day]	5.2	10.0	8.7	0.4	6.1	8.4
COV	47%	47%	55%	31%	37%	45%
$\theta_h$ in m	137	105	119	(648)	149	113
COV $\theta_h$ [-]	101%	102%	99%	103%	101%	99%









### E.3 HPT results

The 12 HPT measurement results are postprocessed in the following way. After identifying the upper aquifer in the soil profile in a first step, one has to cut off the boundaries on the top and bottom of this aquifer. After this, one can derive the mean value and standard deviation of the permeability, which is approximated by the formulae, given by Fugro [30, 62]. It relates the Q/P ratio to the permeability of the layer using  $k_{HPT} = Q/P * I / C_{hp}$ . Fugro [30, 62] recommends to use  $C_{hpt} = 0.46$  for this special layer. The measurement results of the 12 HPTs are used to derive the mean values and standard deviation of the top aquifer layer, was given in Figure E.1. We used for the derivation of the mean values, standard deviation and horizontal correlation length only the mean values of the permeability of the top aquifer layer. This implies that we neglect the standard deviations in the vertical direction assuming that they are negligible.

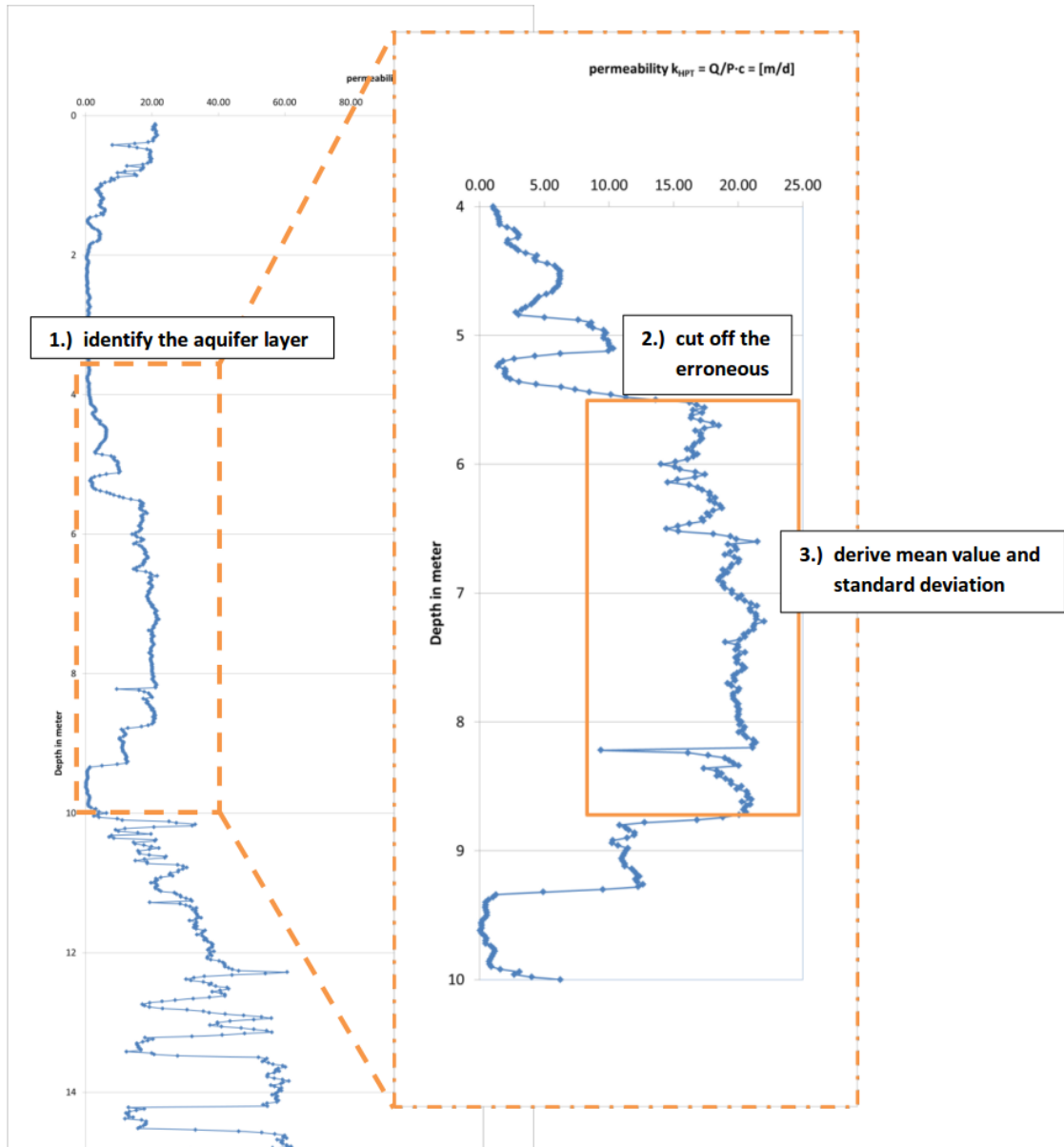
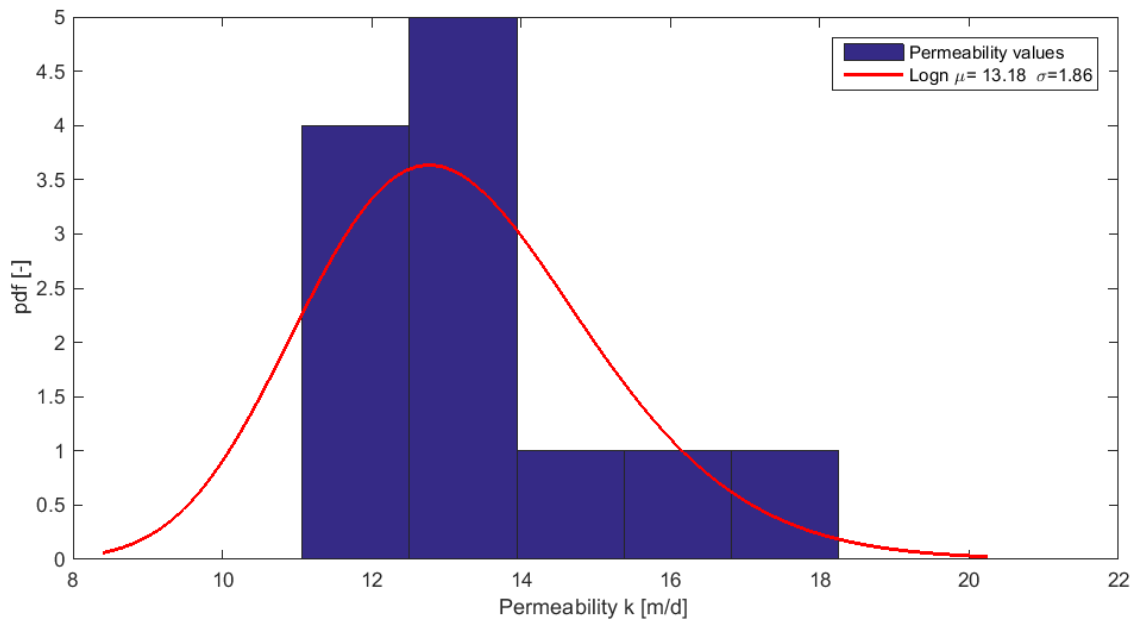


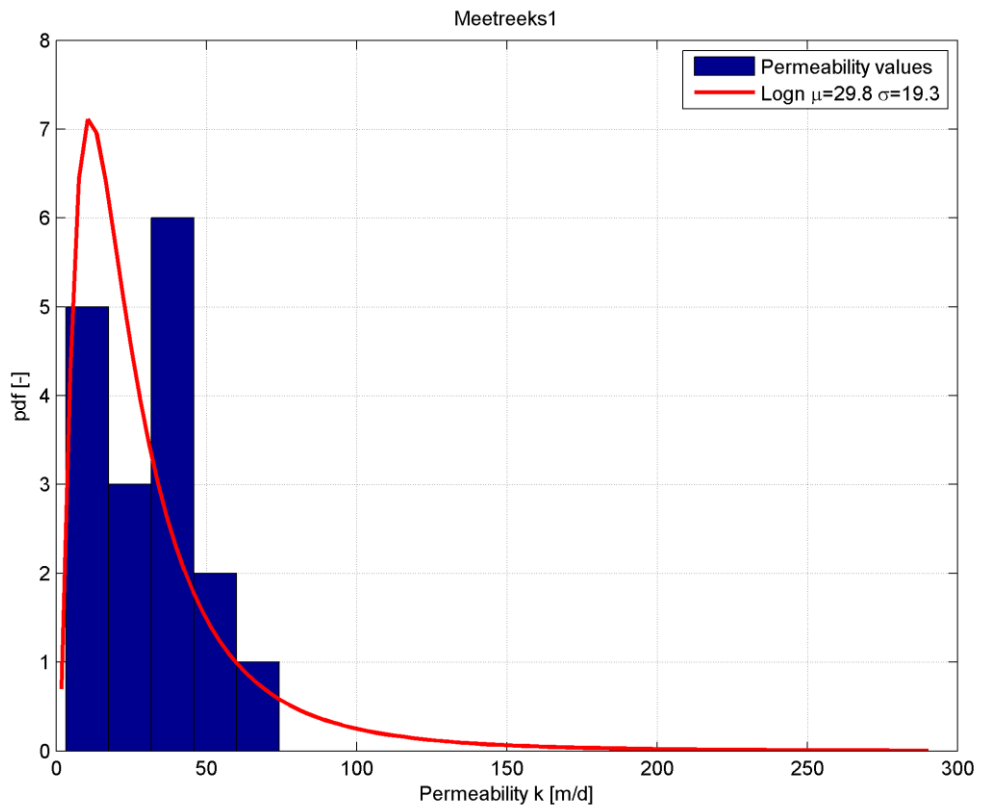
Figure E.1 Schematic Workflow for the evaluation of the HPT permeability

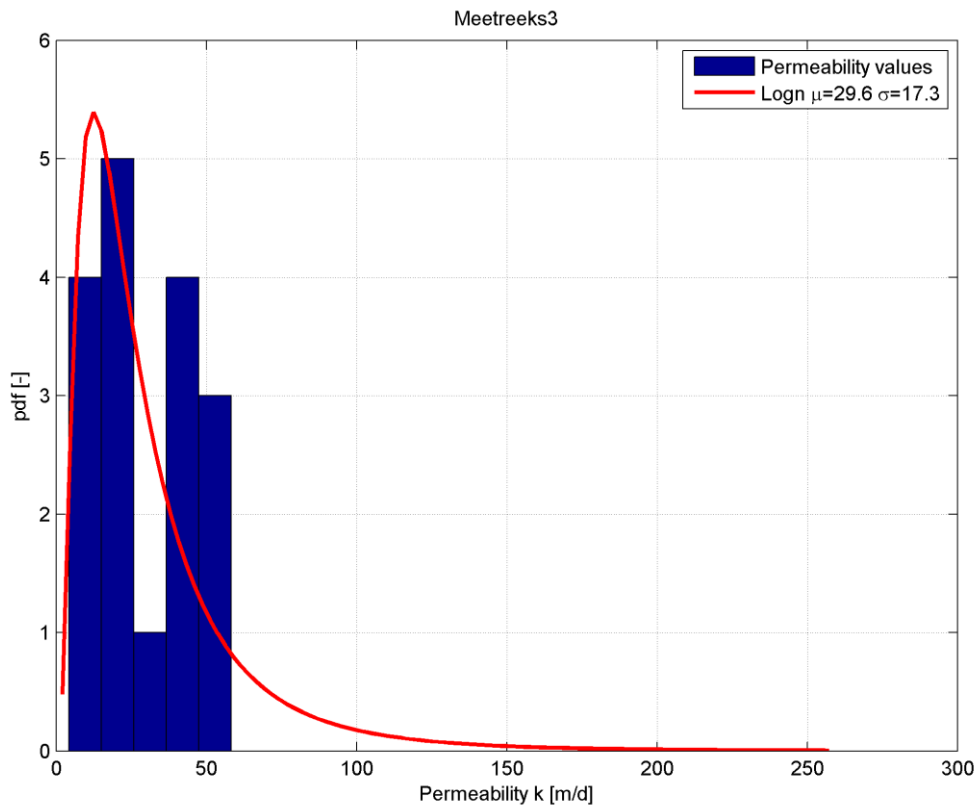
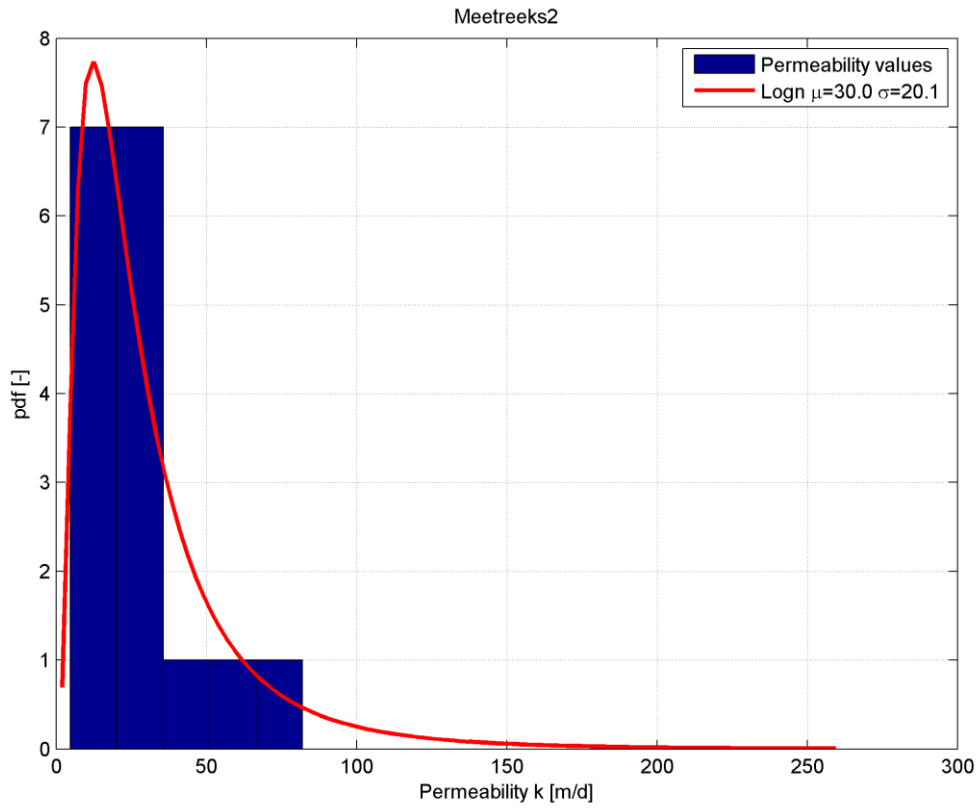
permeability	HPT
$\mu$ [m/day]	13.18
$\sigma$ [m/day]	1.86
COV	14%
$\theta_h$ in m	18.8
COV $\theta_h$ [-]	101%



**E.4 MPT**

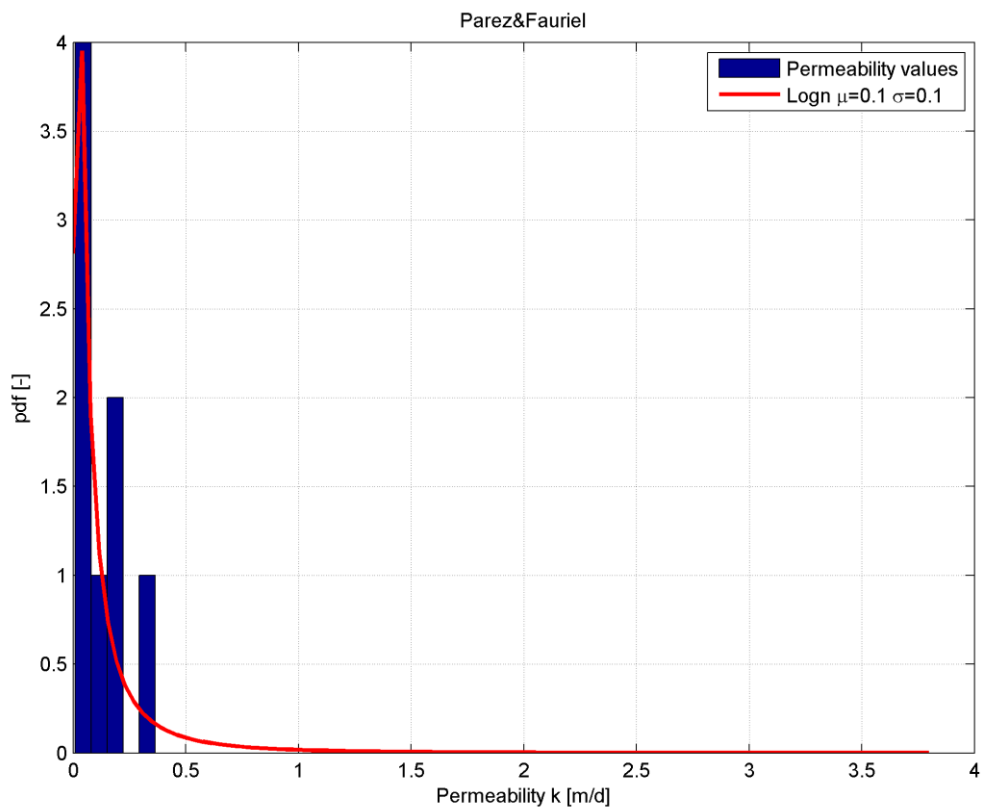
permeability	Meetreks1	Meetreks2	Meetreks3
$\mu$ [m/day]	29.8	30.0	29.6
$\sigma$ [m/day]	19.3	20.1	17.3
COV	65%	67%	59%
$\theta_h$ in m	225	322	216
COV $\theta_h$ [-]	97%	101%	99%

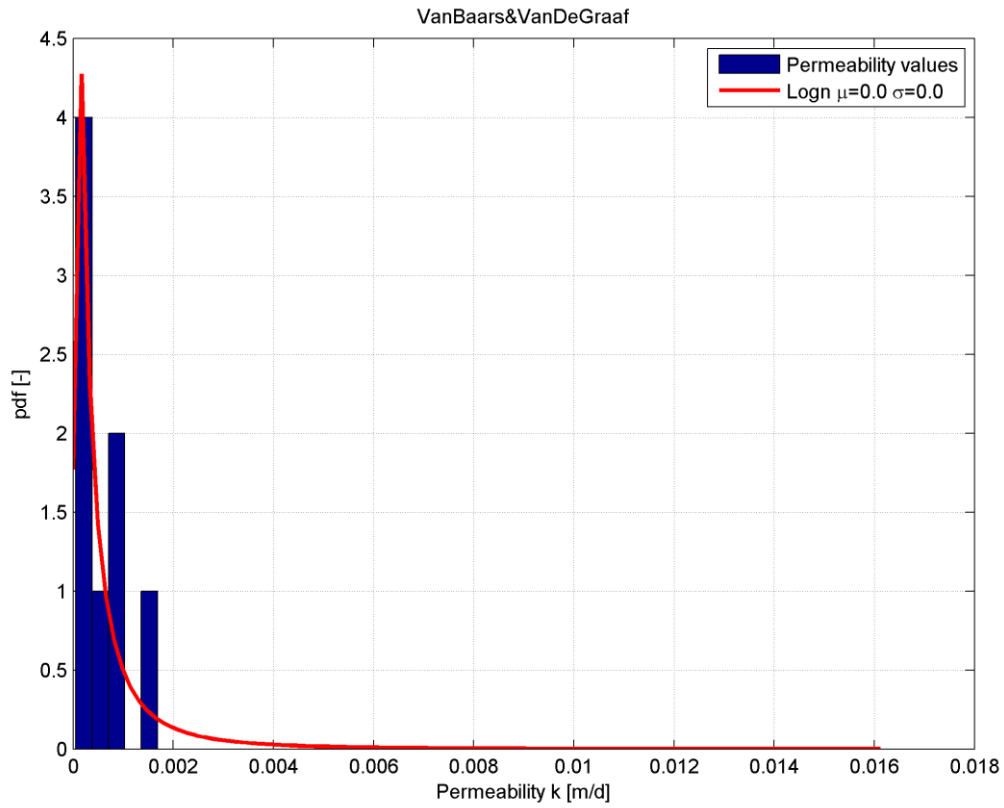




**E.5 Dissipation test**

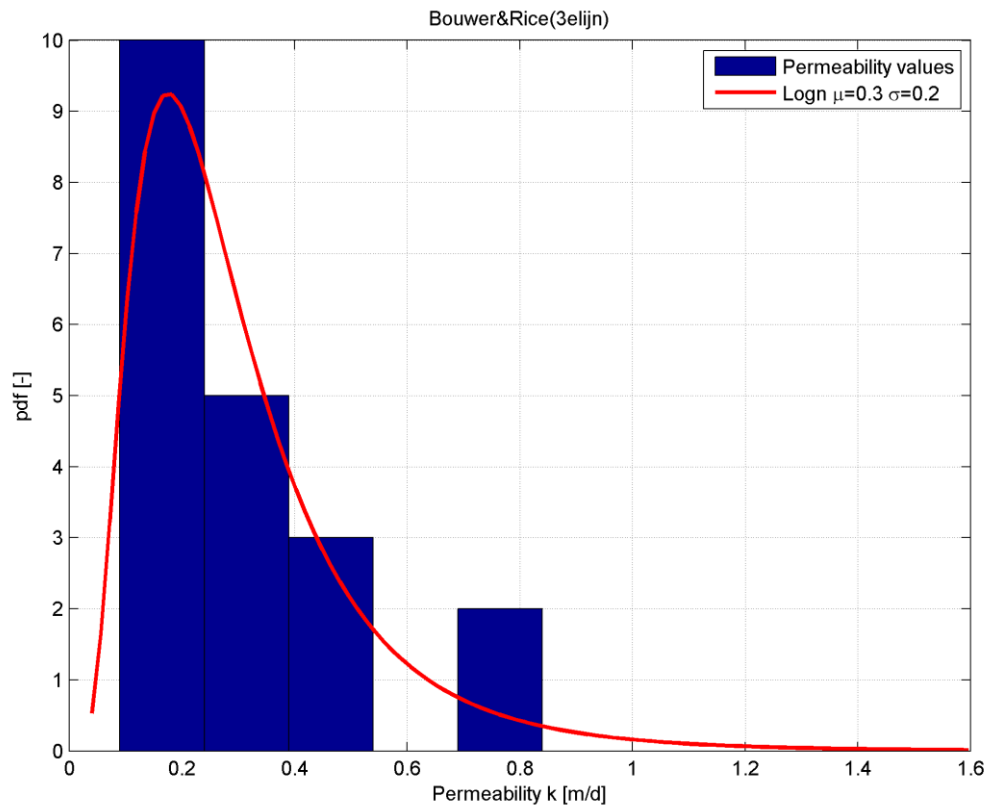
	Parez-Fauriel	Van Baars-Van De Graaf
$\mu$ [m/day]	0.1	0.0
$\sigma$ [m/day]	0.1	0.0
COV	116 %	106 %
$\theta_h$ in m	41	36

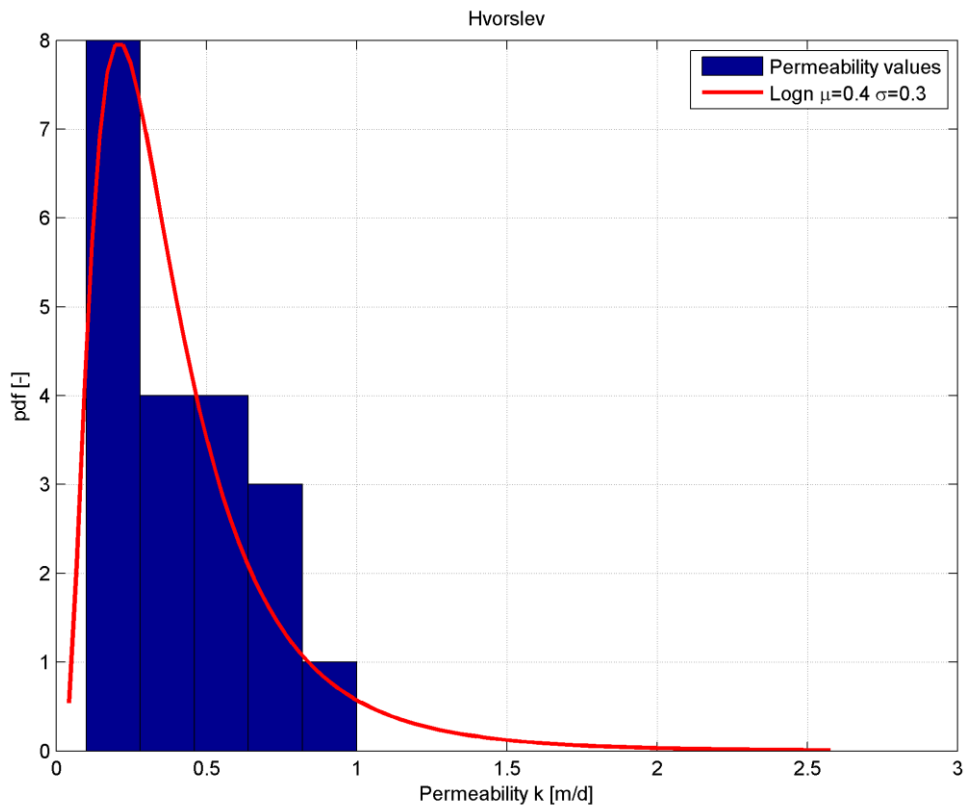
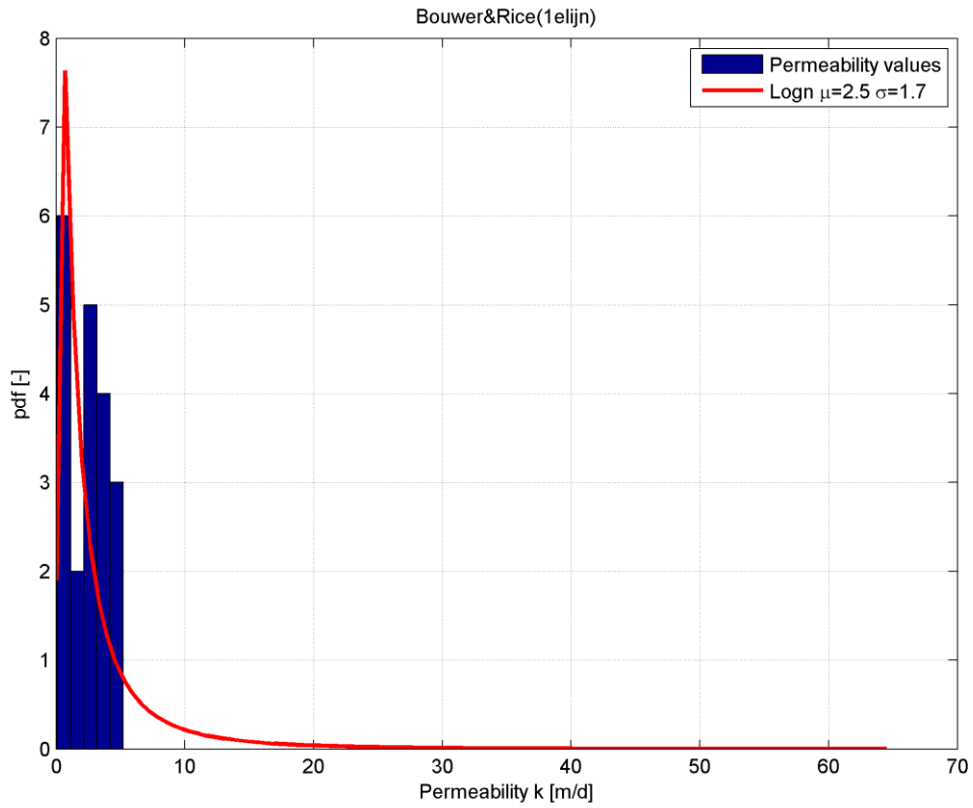




**E.6 Slugtests**

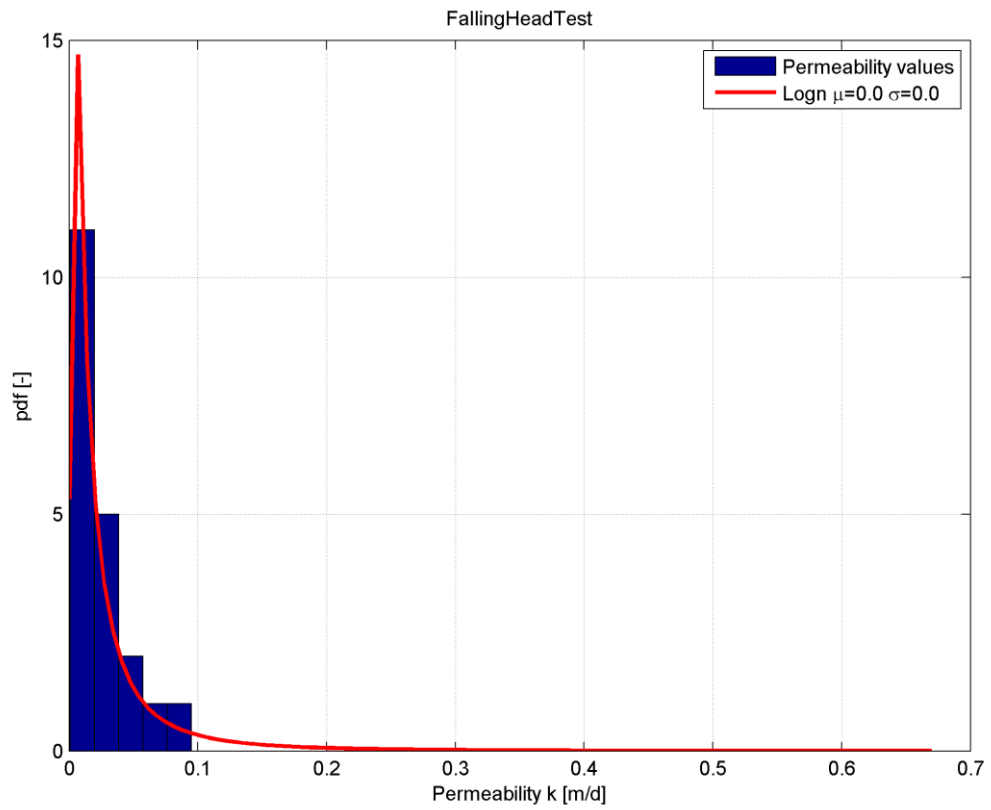
	Bouwer_Rice3lijn	Bouwer_Rice1lijn	Hvorslev
$\mu$ [m/day]	0.3	2.5	0.4
$\sigma$ [m/day]	0.2	1.7	0.3
COV	67%	67%	64%
$\theta_h$ in m	81	69	79
COV $\theta_h$ [-]	101%	102%	101%





### E.7 Falling Head Test

Falling_Head_test	
$\mu$ [m/day]	0.0228
$\sigma$ [m/day]	0.0231
COV	101%
$\theta_h$ in m	31
COV $\theta_h$ [-]	97%





## F Background on Piping

This section provides an overview of the limit state, which we investigate using semi-probabilistic and full probabilistic methods within this report.

Piping, concerns backward internal erosion under dikes with pre-dominantly horizontal seepage paths. Two calculation methods are used: Sellmeijer original and Sellmeijer revised. [58] The limit state function is given in equation (0.35).

$$Z_p = m_p H_c - (h_{river} - h_{exit} - r_c d) \quad (0.35)$$

Piping models are based on average gradients between the entry and exit point. Together with the seepage length  $L$ , this leads to a critical head difference  $H_c$  [m], given by equations (0.37) (Sellmeijer (2006)) and (0.38) (Sellmeijer 2011) which can be compared with the actual head difference.

$$\frac{H_c}{L} = \alpha c \frac{\gamma_{sub.particles}}{\gamma_{water}} \tan(\theta_{sellmeijer.original}) (0.68 - 0.1 \cdot \ln(c)) \quad (0.36)$$

$$\alpha = \left(\frac{D}{L}\right)^{\frac{0.28}{2.8} - 1}, \quad c = \eta d_{70} \left(\frac{1}{\kappa L}\right)^{\frac{1}{3}}, \quad \kappa = \frac{v_{water}}{g} k$$

Sellmeijer (2006) 
$$\frac{H_c}{L} = F_{resistance} F_{scale} F_{geometry} \quad (0.37)$$

Sellmeijer (2011) 
$$F_{resistance} = \eta \frac{\gamma_{sub.particles}}{\gamma_{water}} \tan \theta_{sellmeijer.revised}$$

$$F_{scale} = \frac{d_{70,m}}{\sqrt[3]{\kappa L}} \left(\frac{d_{70}}{d_{70,m}}\right)^{0.39}, \quad \kappa = \frac{v_{water}}{g} k \quad (0.38)$$

$$F_{geometry} = 0.91 \left(\frac{D}{L}\right)^{\frac{0.28}{2.8} + 0.04 - 1}$$

The variables in the limit state equation are given in Table F.1. The values for probabilistic analyses are derived from the VNK-2 project [65]. For semi-probabilistic calculations, the characteristic value for each parameter is used according to the percentile. Per subsoil schematization, multiple values or distributions can be present.

Table F.1

Symbol	Unit	Description	Uplift	Heave	Piping	Distribution type	Values from VNK-2 [65]	Usual characteristic value
$m_u$	-	Model factor for uplift	x			log	$\mu$ 1.0 , $\sigma$ 0.10	1
$\gamma_{sat,cover}$	[kN/m <sup>3</sup> ]	Saturated volumetric weight of the cover layer (blanket)	x			norm	$\mu$ 14.0 , $\sigma$ 1.54	5%
$r_{exit}$	-	Damping factor at exit	x	x		log	$\mu$ 0.7 , $\sigma$ 0.07	5%
$i_{c,h}$	-	Critical heave gradient		x		log	$\mu$ 0.7 , $\sigma$ 0.10	0.5
$d$	[m]	Total thickness of the cover layer	x	x	x	log	$\mu$ 1.25 , $\sigma$ 0.19	5%
$h_{exit}$	[m+NAP]	Phreatic level at the exit point	x	x	x	norm	$\mu$ 0.7 , $\sigma$ 0.10	5%
$m_p$	-	Model factor for piping			x	log	$\mu$ 1.0 , $\sigma$ 0.12	1
$h$	[m+NAP]	Outside water level	x	x	x	Hydra-Ring		Design water level
$r_c$	-	Reduction factor			x	-	0.3	-
$L$	[m]	Seepage length, from entry point to exit point			x	log	$\mu$ 69.0 , $\sigma$ 0.69	5%
$\gamma_{sub,particles}$	[kN/m <sup>3</sup> ]	Submerged volumetric weight of sand particles			x	norm	$\mu$ 16.5 , $\sigma$ 0.17	16.5
$\eta$	-	White's drag coefficient			x	-	0.25	-
$d_{70}$	[m]	70%-quantile of the grain size distribution of the piping-sensitive layer			x	log	$\mu$ 2E-4 , $\sigma$ 2E-5	5%
$k$	[m/s]	Darcy permeability			x	log	$\mu$ 2.3E-4 , $\sigma$ 2.4E-4 $\mu$ 5.0E-4 , $\sigma$ 4.8E-4 $\mu$ 3.1E-4 , $\sigma$ 2.0E-4	95%
$\nu_{water}$	[m <sup>2</sup> /s]	Kinematic viscosity of water			x	-	$1.33 \times 10^{-6}$	-
$g$	[m/s <sup>2</sup> ]	Gravitational constant			x	-	9.81	-
$D$	[m]	Thickness of aquifer			x	log	$\mu$ 3.55 , $\sigma$ 0.58 $\mu$ 14.5 , $\sigma$ 5.1 $\mu$ 42.3 , $\sigma$ 5.3	95%
$d_{70,m}$	[m]	Mean value of the $d_{70}$ in small scale tests			x	-	$2.08 \times 10^{-4}$	-
$\theta_{sellmeijer.revised}$	[°]	Bedding angle of sand grains for the revised Sellmeijer rule (Sellmeijer 2011)			x	-	37	-
$\theta_{sellmeijer.original}$	[°]	Bedding angle of sand grains for the original Sellmeijer rule			x	-	43	-

## G Bayesian evaluation procedure for characteristic values

### G.1 Calculation of the characteristic values for normal and lognormal distributed data

The sequel steps describe the calculation of the determination of characteristic values for normally and log-normally distributed random variables.

#### G.1.1 Variables with Normal distribution

If a random variable is normally distributed with mean  $\mu$  and standard deviation  $\sigma$ , then the characteristic value of this variable, based on the 5%-quantile, is equal to:

$$\text{characteristic value} = \mu - 1.65\sigma \quad (0.39)$$

and, based on the 95%-quantile, it is equal to:

$$\text{characteristic value} = \mu + 1.65\sigma \quad (0.40)$$

#### G.1.2 Variables with Log-normal distribution

If a random variable is log-normally distributed with mean  $\mu$  and standard deviation  $\sigma$ , then the characteristic value of this variables, based on the 5%-quantile, is derived as follows:

$$\sigma_M^2 = \ln \left[ 1 + \left( \frac{\sigma}{\mu} \right)^2 \right] \quad (0.41)$$

$$\mu_M = \ln \mu - \frac{1}{2} \cdot \sigma_M^2 \quad (0.42)$$

$$\text{characteristic value} = \exp(\mu_M - 1.65 \cdot \sigma_M) \quad (0.43)$$

and, based on the 95%-quantile, it is equal to:

$$\text{characteristic value} = \exp(\mu_M + 1.65 \cdot \sigma_M) \quad (0.44)$$

### G.2 Theoretical background on Bayesian updating

Bayesian inference is a method of statistical inference in which Bayes' theorem is used to update the probability for a hypothesis as evidence is acquired.

Statistically spoken, Bayesian inference derives the posterior probability as a consequence of two antecedents, a prior probability and a "likelihood function" derived from a statistical model for the observed data. Bayesian inference computes the posterior probability according to Bayes' theorem:

$$P(H | E) = \frac{P(E | H) \cdot P(H)}{P(E)} \quad (0.45)$$

Herein, “|” denotes a conditional probability; more specifically, it means given.  $H$  stands for any hypothesis whose probability may be affected by data (called evidence below). Often there are competing hypotheses, from which one chooses the most probable.  $E$  stands for the evidence and corresponds to new data that were not used in computing the prior probability.

- $P(H)$  the prior probability, is the probability of  $H$  before  $E$  is observed. This prior probability is described by the mean value  $M$  and the standard deviation  $\tau$ .
- $P(E/H)$  is the likelihood function, which is the probability of observing  $E$  given  $H$ . This likelihood function is described by the mean value  $\mu$  and  $\sigma$ .
- $P(E)$  is termed the marginal likelihood; it can be seen as a scaling factor, which ensures that the resulting pdf of the product of  $P(E/H)$  and  $P(H)$  is 1.
- $P(H/E)$ , the posterior probability, is the probability of  $H$  given  $E$ , i.e., after  $E$  is observed. This tells us what we want to know: the probability of a hypothesis *given* the observed evidence. The mean value and standard deviation of the posterior probability can be calculated by the following equations.

$$\mu_{posterior} = \frac{\sigma M + n \tau^2 \mu}{n \tau^2 + \sigma^2} \quad (0.46)$$

$$\sigma_{posterior} = \sqrt{\frac{\sigma^2 \tau^2}{n \tau^2 + \sigma^2}} \quad (0.47)$$

### G.3 Calculation of the characteristic values using Bayesian Updating

At first the lognormal distribution parameters are transformed into distribution parameters of the underlying normal distribution: from lognormal distribution to the underlying normal distribution parameters  $\mu_{\ln x}$  and  $\sigma_{\ln x}$ :

$$\begin{aligned} \mu_{\ln x} &= \ln(\mu_x) - \frac{1}{2} \sigma_{\ln x}^2 \\ \sigma_{\ln x} &= \sqrt{\ln\left(1 + \frac{\sigma_x^2}{\mu_x^2}\right)} \end{aligned} \quad (0.48)$$

Then the Bayes theorem is applied on this underlying normal distribution and transformed into lognormal parameters  $\mu_x$  and  $\sigma_x$ :

$$\begin{aligned} \mu_x &= \exp\left(\mu_{\ln x} + \frac{1}{2} \sigma_{\ln x}^2\right) \\ \sigma_x &= \sqrt{\frac{\mu_{\ln x}^2}{\exp(\sigma_{\ln x}^2) - 1}} \end{aligned} \quad (0.49)$$

## H Extract Handreiking ontwerpen met overstromingskansen

OI2014-v3, Juli 2015, Rijkswaterstaat Water, Verkeer en Leefomgeving, Chapter 4 Piping



Rijkswaterstaat  
Ministerie van Infrastructuur en Milieu

### 4 Piping

Tot op heden worden bij het faalmechanisme *piping* voor dijken zonder verticale elementen (zoals kwelschermen) slechts het opbarsten van de binnendijkse deklaag en terugschrijdende (interne) erosie in de watervoerende zandlaag beschouwd. In het WT12017 wordt ook het deelfaalmechanisme heave opgenomen voor dijken met een deklaag aan de landzijde. Als gevolg van nieuwe inzichten omtrent de fluïdisatie van het zand op het moment van opbarsten van de deklaag is er nog een discussie lopende omtrent de te hanteren waarde voor de kritieke gradiënt. Daarom wordt heave in deze versie van het OI2014 vooralsnog niet meegenomen.

#### Omgang met piping

De weerstand tegen het deelfaalmechanisme piping dient te worden bepaald met het aangepaste rekenmodel van Sellmeijer [Förster et al, 2012]. Dit rekenmodel kan worden toegepast met een analytische formule of in een eindige elementen model, waarin ook tijdsafhankelijkheid en lokale heterogeniteiten meegenomen kunnen worden. Bij het bepalen van de benodigde kwelweglengte dienen de volgende veiligheidsfactoren te worden toegepast op het kritieke verval:

$\gamma_{mp}$  Partiële factor voor de model- en parameteronzekerheid van het deelfaalmechanisme piping (sterktefactor), deze is voor het OI2014 afhankelijk van de gestelde betrouwbaarheidseis. Deze factor vervangt de partiële weerstandsfactor  $\gamma_n$  uit [Deltares, 2012].

$\gamma_b$  Partiële factor voor de onzekerheid over de ondergrondopbouw en de water(over)spanningen (schematiseringfactor) bij het deelfaalmechanisme piping.

#### Sterktefactor voor piping

De geëiste betrouwbaarheidsindex ( $\beta_{eis,dsn}$ ) voor een doorsnede volgt uit de faalkanseis per doorsnede volgens:

$$\beta_{eis,dsn} = -\Phi^{-1}(P_{eis,dsn}) \quad (4.1)$$

Hierin is  $\Phi^{-1}$  de inverse van de standaardnormale verdeling.

In een studie voor het WT12011 zijn veiligheidsfactoren voor het aangepaste rekenmodel van Sellmeijer bepaald [Lopez de la Cruz et al., 2010]. Daarbij is rekening gehouden met maximaal toelaatbare overstromingskansen van 1/1.250 per jaar in het rivierengebied. Gelet op de normspecificaties moeten de veiligheidsfactoren ook bij strengere overstromingskansnormen voldoende veiligheid bieden. Op basis van de berekeningsresultaten uit Lopez de la Cruz et al. [2010] wordt de volgende veiligheidsfactor voorgesteld:

$$\gamma_{mp} = 0,8\beta_{eis,dsn} - 2,4 \quad \text{waarbij } 1,2 \leq \gamma_{mp} \quad (4.2)$$

waarin

$\gamma_{mp}$  Sterktefactor voor het deelfaalmechanisme piping (-)  
 $\beta_{eis,dsn}$  Geëiste betrouwbaarheidsindex voor een doorsnede (-)

In bijlage A is een overzicht gegeven van de aan te houden waarde van de sterktefactor  $\gamma_{mp}$  per dijktraject. Opgemerkt wordt dat momenteel gewerkt wordt aan een

nieuwe kalibratiestudie ten behoeve van WTI 2017. Bovenstaande formule kan dus nog wijzigen en moet gezien worden als het best beschikbare. De kalibratiestudie is naar verwachting eind 2015 gereed. De voorlopige resultaten uit deze kalibratiestudie vertonen een regionaal sterk wisselend beeld. Vooral voor situaties zonder afdekkend pakket of een dun afdekkend pakket rondom het IJsselmeer, het Markermeer, in de Vechtdelta en de IJsseldelta wordt geadviseerd rekening te houden met de gevoeligheid voor een hogere factor. Voor het bovenrivierengebied en het Wadengebied lijkt formule 4.2 passend en voor het benedenrivierengebied en langs de Westerschelde te streng. Voor het benedenrivierengebied en langs de Westerschelde wordt geadviseerd rekening te houden met de gevoeligheid voor een lagere factor.

#### Schematiseringsfactor

Voor de bepaling van de schematiseringfactor zijn er geen wijzingen ten opzichte van de vigerende methodiek uit het *Technisch Rapport Grondmechanisch Schematiseren* (TRGS) [Calle, 2011].

#### Omgang met opbarsten

Overeenkomstig Eurocode 9997-1 [NEN, 2012] dient voor het ontwerp bij een toets op opbarsten in principe een factor op de belastingen te worden toegepast conform de waarden in Tabel 6. De eindtoets dient te voldoen aan een waarde 1,0. Dit betreft een overall-toetsing, waarbij géén schematiseringsfactor hoeft worden toegepast.

**Tabel 6: Partiële factoren op belastingen ( $\gamma_F$ )**

Belasting	Symbol	Waarde
Blijvend		
Ongunstig <sup>a</sup>	$\gamma_{G;dst}$	1,0
Gunstig <sup>b</sup>	$\gamma_{G;std}$	0,9
Veranderlijk		
Ongunstig <sup>a</sup>	$\gamma_{Q;dst}$	1,2 of 1,5
<sup>a</sup> Aandrijvend		
<sup>b</sup> Weerstandbiedend		

Op het gewicht van de grond dient dus een factor 0,9 te worden toegepast, op het permanente deel van de waterdruk een factor 1,0 en alleen op het variabele deel van de waterdruk een factor 1,2 of 1,5. De formulering uit de Eurocode is afgeleid voor opbarstsituaties bij bouwputten, waar metingen doorgaans ontbreken. Binnen dit ontwerpinstrumentarium kan met een waarde van 1,2 worden gerekend voor het variabele deel van de waterdruk indien er metingen beschikbaar zijn bij een historische hoogwaterstand, volgens:

$$\frac{\text{gronddruk}}{\text{waterdruk}} = \frac{0,9(\gamma_{nat} - \gamma_w)d_x}{1,0\gamma_w(\varphi_{z,x,HHW} - h_{p,x}) + 1,2\gamma_w(\varphi_{z,x,MHW} - \varphi_{z,x,HHW})} \geq 1,0 \quad (4.4)$$

waarin

$d_x$  dikte deklaag in de opbarstzone (m)

$h_{p,x}$  polderpeil in de opbarstzone, waarbij  $h_p$  gelijk aan of hoger is dan het maaiveld ter plaatse<sup>3</sup> (m NAP)

<sup>3</sup> Onder maatgevende omstandigheden zal de kwelstroom dusdanig kunnen zijn dat nabij opbarsten met een verzaagde situatie rekening gehouden dient te worden (zoals ook vermeld in het Technisch Rapport Zandmeevoerende Wellen (TAW, 1999)).



Rijkswaterstaat  
Ministerie van Infrastructuur en Milieu

$\gamma_{nat}$	nat volumegewicht (kN/m <sup>3</sup> )
$\gamma_w$	volumegewicht van water (kN/m <sup>3</sup> )
$\phi_{z,x,MHW}$	stijghoogte in de opbarstzone in de watervoerende laag bij maatgevende omstandigheden (m NAP)
$\phi_{z,x,HHW}$	stijghoogte in de opbarstzone in de watervoerende laag bij het historische hoogwater waarbij metingen beschikbaar zijn (m NAP)

Voor het gewicht van de deklaag die uit meerdere lagen bestaat kan uiteraard worden uitgegaan van een sommatie van de gewichten van de onderscheiden grondlagen.

Indien geen metingen aanwezig zijn, dient een factor van 1,5 op het variabele deel van de waterdruk te worden aangehouden. Dit is te schrijven als:

$$\frac{\text{gronddruk}}{\text{waterdruk}} = \frac{0,9(\gamma_{nat} - \gamma_w)d_x}{1,0\gamma_w(\phi_{z,x,GHW} - h_{p,x}) + 1,5\gamma_w(\phi_{z,x,MHW} - \phi_{z,x,GHW})} \geq 1,0 \quad (4.3)$$

met in aanvulling op de eerder gebruikte symbolen:

$\phi_{z,x,GHW}$	stijghoogte in de opbarstzone in de watervoerende laag bij het gemiddelde jaarlijkse hoogwater (m NAP)
------------------	--

In een specifieke situatie mag de gunstigste van beide formuleringen worden gebruikt.

Opgemerkt wordt dat bij een kleine demping,  $\phi_{z,x,MHW}$  niet veel kleiner is dan MHW ( $\phi_{z,x=0,MHW}$ ). Het kan voorkomen dat als gevolg van de partiële veiligheidsfactoren de stijghoogte met veiligheid (ofwel: de rekenwaarde van de stijghoogte) hoger is dan MHW. In die gevallen geldt:

$$\frac{\text{gronddruk}}{\text{waterdruk}} = \frac{0,9(\gamma_{nat} - \gamma_w)d_x}{\gamma_w(\phi_{z,x=0,MHW} - h_{p,x})} \geq 1,0 \quad (4.5)$$

Het is zeer aan te bevelen om metingen uit te voeren om gebruik te kunnen maken van een gunstige partiële veiligheidsfactor en het ontwerp niet onnodig conservatief te maken.

**Let op:** Het OI2014 is een generiek ingestoken handreiking, waar beargumenteerd van kan worden afgeweken. Mogelijk leidt het toepassen van het OI2014 tot een bovenmatig conservatief ontwerp. De gebruiker dient zich dan ook te realiseren dat door lokaal maatwerk optimalisatie van het ontwerp vaak mogelijk is.

Met name bij een relatief groot kwelwegtekort is het aan te bevelen om in te zetten maatregelen die het optreden van piping uitsluiten. Ook kunnen beheermaatregelen in combinatie met fysieke maatregelen wellicht een doelmatige oplossing bieden.

Indien uit het ontwerp blijkt dat de te treffen maatregelen voor piping sterk afwijken van hetgeen bij een dergelijke waterkering verwacht mag worden, verdient het de aanbeveling om een verdiepingsslag te maken en/of een expert te raadplegen. Het Kennisplatform Risicobenadering (kpr@rws.nl) kan daarbij ondersteunen.